ALMA MATER STUDIORUM
UNIVERSITÀ DI BOLOGNA

DEPARTMENT OF PHYSICS AND ASTRONOMY "A. RIGHI"

SECOND CYCLE DEGREE

PHYSICS

Adiabatic manipulation of longitudinal beam distributions in the presence of energy damping and random perturbations

Supervisor
Prof. Armando Bazzani

Co-supervisor
Dr. Federico Capoani
Dr. Massimo Giovannozzi

Defended by
Emanuele Nori

Graduation Session 12/2025
Academic Year 2024/2025

You can't connect the dots looking forward; you can only connect them looking backwards. So you have to trust that the dots will somehow connect in your future. You have to trust in something — your gut, destiny, life, karma, whatever. Because believing that the dots will connect down the road will give you the confidence to follow your heart even when it leads you off the well worn path; and that will make all the difference.

Steve Jobs

Abstract

In recent years, non-linear beam dynamics has been promoted as a means to perform novel manipulations of hadron beams in circular accelerators. This is made possible because of the adiabatic trapping and transport phenomena in phase space for Hamiltonian systems. The extension of the non-linear beam manipulations to circular lepton accelerators has been recently considered, but a rigorous theoretical framework to extend adiabatic theory to stochastically perturbed Hamiltonian systems is still lacking. This project represents a first step in this direction, aiming at analysing the effect of energy damping and random perturbation on adiabatic manipulations. This goal is achieved by studying simple models relevant for beam dynamics, incorporating both analytical and numerical investigations.

Contents

Introduction

The study of beam dynamics in particle accelerators has made significant progress in recent decades, enabling the design and operation of increasingly sophisticated machines. A central aspect of this progress concerns the understanding of non-linear effects that play a decisive role in the manipulation and stability of the beam. In particular, the analysis of resonances and stable structures in phase space shows how such mechanisms can be exploited, in order to control longitudinal and transverse beam distribution.

Although these techniques are well established in the case of hadron beams ([12], [15]), their extension to the lepton case raises new and still open questions. In lepton accelerators, the beam dynamics cannot be treated as a purely conservative system: the presence of dissipative mechanisms due to energy damping, together with fluctuations arising from quantum excitation, significantly modify the underlying dynamics. This requires the development of theoretical and numerical tools that describe a Hamiltonian framework with the addition of energy damping and stochastic perturbations.

This thesis project is framed within this context. In particular, the goal is to investigate the possibility of extending adiabatic manipulation techniques to lepton machines. The adopted approach relies on simplified models of longitudinal dynamics, which are tested through numerical simulations to understand the role of dissipation and noise in resonance trapping and transport in phase space.

Lepton accelerators

The analysis will be performed using parameters of real lepton machines, such as the *Advanced Light Source* (**ALS**) in Berkeley, California, and the *Future Circular Collider* in the case of lepton beams (**FCC-*ee***).

ALS

The ALS at the Lawrence Berkeley National Laboratory is a third-generation synchrotron light source designed to produce intense and highly coherent soft x-rays ([1]). It operates with ultra-relativistic electrons in different beam energy ranges, going from $1.0\,\mathrm{GeV}$ to $1.9\,\mathrm{GeV}$ depending on the scope of the research. Indeed, the produced light is used

for research in different fields, such as molecular dynamics, 3D biological imaging, etc. Currently, it is operating at an upgraded version called *ALS-U*, which is meant to enhance brightness and coherence by more than two orders of magnitude ([2]).

FCC-*ee*

The FCC is a next-generation accelerator project proposed at CERN, which is designed to be built inside a tunnel $91\,\mathrm{km}$ long. Among its planned operating modes, the FCC-*ee* represents the high-luminosity electron–positron collider stage, which will be operated at beam energies ranging from $42.6\,\mathrm{GeV}$ (Z optics) up to $182.5\,\mathrm{GeV}$ ($t\bar{t}$ optics). The FCC-*ee* is conceived as a "precision machine", namely, it will be used as a high-luminosity Higgs, top, and electroweak factory ([9]). The second stage, FCC-*hh*, will serve as "discovery machine", namely, it will be dedicated to find new physics beyond the Standard Model, operating as a high-energy proton–proton collider with centre-of-mass energies up to $100\,\mathrm{TeV}$.

Top-up injection in the FCC-*ee*

The FCC-*ee* is designed as a double-ring collider with separate beam pipes for electrons and positrons. Since leptons are strongly affected by energy damping as a result of the emission of synchrotron radiation, the injection of new particles to keep a constant current is needed. In particular, a steady and very high value of luminosity must be kept throughout machine operations: the top-up injection represents an optimal solution in this sense.

The injection comes from a full-energy booster synchrotron, located within the same $91\,\mathrm{km}$ tunnel as the collider itself, and is integrated in a single technical straight section in PB, as shown in Fig. 1.

In early lepton colliders, the beam current was required to drop significantly before the beam was pushed out for a new injection. This procedure was already in use for hadron accelerators, but it was very time-consuming to obtain stable collisions again, and the luminosity production was not efficient.

The first known use of top-up injection dates back to the '1980s, under the name of *top-up-and-Coast* mode [30], employed in the Positron-Electron Project (*PEP*) at SLAC, Stanford [28]. Nevertheless, this was still an early-stage version, since the detectors were turned off during injection, meaning no gain in terms of integrated luminosity. However, it was a considerable savings in time. The modern version of the top-up injection first appeared at the beginning of 21*st* century at *KEKB* and *PEP-II*, paving the way to its ordinary use also for modern light sources.

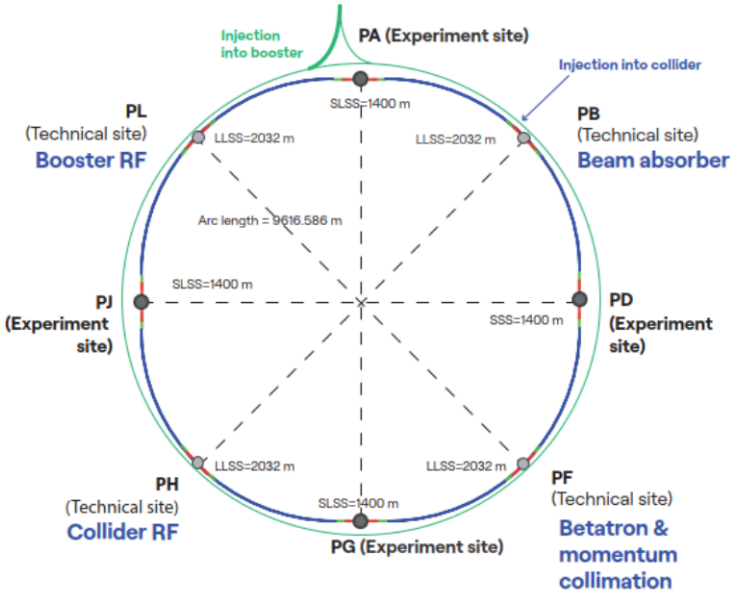

Figure 1: FCC-*ee* layout (Fig. from [9].

Structure of the work

The present thesis is divided into two main parts. The first one, which consists of Chapter One and Chapter Two, is intended to provide all the mathematical and physical aspects to understand the idea and construction of the considered model.

In **Chapter One**, the main concepts related to beam dynamics are presented. A general introduction on particle accelerators precedes the analytical framework at issue, where the coordinate system and the Hamiltonian function for a relativistic particle is shown. Then, we will go in detail on the two types of motion that can be studied in beam dynamics, namely the transversal and the longitudinal one. The equations of motion for the two cases will be derived, together with some deeper insights for the longitudinal case. In particular, we will see how an external modulation affects the system evolution, besides some early considerations about stochastic effects in lepton accelerators.

Then, **Chapter Two** provides an extensive overview of various topics from dynamical systems, such as the Hamiltonian description for the construction of a model in beam dynamics. In this, Hamilton's equations of motion, canonical transformations, and the Liouville theorem are some examples. Then, for the study of periodic systems, the action-angle coordinates are introduced, as well as the concept of integrable systems and the Poincaré section. Afterward, some results from perturbation theory are presented, in order to lay the basis for the theory of separatrix crossing. Eventually, the stochastic approach to study the evolution of particle distributions is presented, to-

gether with the statistical interpretation of resonance trapping for stochastic systems.

The second part of this work will instead focus on the model under analysis, giving its physical motivation and structure in **Chapter Three**.

Then, in **Chapter Four**, the different algorithms exploited in the simulations are presented, in addition to the results obtained throughout the whole study. A final comparison will show the main differences between the two models, highlighting the role of damping and stochastic noise on the Hamiltonian framework.

Chapter 1

Fundamentals of Beam Dynamics

1.1 Introduction to particle accelerators

Particle accelerators represent some of the most sophisticated and fascinating scientific instruments ever conceived. They provide a controlled means for investigating the fundamental constituents of matter, to generate high-brightness photon beams for material and biological studies, and to enable a wide range of applications in medicine and industry. Although their design and operation involve highly complex technologies and instrumentation, the underlying dynamics of accelerated particles are mostly based on classical mechanics.

From a fundamental point of view, accelerators are devices that employ *electric fields* to increase the kinetic energy of charged particles and *magnetic fields* to guide and constrain their motion along a specific trajectory. Depending on the spatial configuration and use of these fields, two major categories of accelerators can be identified:

- *Linear accelerators* (**linacs**), in which particles gain energy while travelling along a straight trajectory through a sequence of radio-frequency (RF) cavities;
- *Circular accelerators*, such as **synchrotrons** and **storage rings**, where magnetic dipoles bend the trajectory into a closed orbit, while RF cavities located in straight sections restore the energy lost during each revolution.

In circular accelerators, particles perform an extremely large number of revolutions, thus reaching high energies within a compact geometry. This enabled circular accelerators to be considered as a useful tool for multiple studies in particle physics. The first high-energy machines ever built, such as the Bevatron at the Lawrence Berkeley Laboratory or the Proton Synchrotron at CERN, proved the reliability and effectiveness of these kinds of accelerators as a precise means of investigation.

Today, a great number of particle accelerators are operating all over the world with different goals, among which the Large Hadron Collider (LHC) at CERN represents the diamond tip. It is responsible for the most important recent breakthrough in the field

Figure 1.1: Aerial view of the LHC at CERN (Fig. from [13]). It lies in an underground 27 km tunnel in circumference beneath the France–Switzerland border near Geneva. The four main experiments, i.e. ALICE, CMS, Atlas and LHCb are located along the ring.

of particle physics, namely the discovery of the Higgs boson in 2012 with CMS and Atlas experiments.

This huge success pushes the scientific community to design and develop bigger and higher-energy machines for the next decades, such as the Future Circular Collider (FCC) at CERN and the Circular Electron Positron Collider (CEPC) in China, in a $91\,\mathrm{km}$ and $100\,\mathrm{km}$ tunnels, respectively. To this end, this thesis work is also intended to provide some results that might be useful for the top-up injections, i.e. the designed injection scheme of the FCC-*ee*.

Circular accelerators involve a number of technical challenges and specific design issues that must be carefully addressed. One of the most critical points is the beam stability, which is hindered by the constant energy loss experienced by charged particles due to *synchrotron radiation*. As particles are forced to follow curved trajectories under the action of magnetic fields, they emit electromagnetic radiation tangentially to their path. This effect becomes particularly important for light particles, such as electrons, since the radiated power scales inversely with the fourth power of the particle mass:

$$P \propto \frac{1}{m^4}\,, \tag{1.1.1}$$

for a fixed energy and radius of the ring. Moreover, the quantum nature of this syn-

chrotron emission forces the introduction of stochastic terms in the governing equations and the use of stochastic dynamics to describe the particle motion.

The chapter is conceived as follows. Firstly, the framework of study will be outlined by defining the coordinate system and types of motion which will be involved. Thereafter, we will go in detail to characterise the particle transversal dynamics through the Hills' equations, where the betatron motion will be analysed together with the phase-space description through the Twiss parameters. Then, we will move on to the longitudinal dynamics, which is the core subject of this thesis, reviewing the equations for synchrotron motion and the effect of damping and noise on the system evolution. The analysis mainly follows the content of Ref. [21].

1.2 Coordinate system and equations of motion

The description of particle motion in a circular accelerator is conveniently formulated with respect to a reference trajectory with nominal energy and momentum. Since the geometry of the system exhibits toroidal symmetry, it is natural to express the equations of motion in a curvilinear coordinate system that follows the design orbit. The most widely adopted framework for this purpose is the *Frénet-Serret coordinate system*, which provides an optimal orthonormal basis to describe particle motion.

Let the reference trajectory be parametrised by the curvilinear coordinate s, corresponding to the longitudinal arc length along the closed orbit. In addition, the Cartesian coordinates x and y identify the orthogonal plane with respect to s (see Fig. 1.2 for a graphical representation of the coordinate system).

This coordinate system is needed since we want to obtain an expression for the Hamiltonian of a particle written as a function of these variables.

Before delving into the details, let us point out a couple of concepts which will be used later. First of all, we can distinguish between two kind of motions, which we consider to be approximately independent:

- *longitudinal*, which describes the beam motion along the circular ring;
- *transversal*, which occurs in the plane orthogonal to the longitudinal axis.

Each of these motions is described through different coordinates and equations, which allow one to separately describe the underlying physics under different standpoints.

In the second instance, we can define a useful quantity for transverse motion known as *beam rigidity*. To this end, consider a particle of charge e, mass m and tangent velocity $\mathbf{v}$, being kept in circular motion by a magnetic field $\mathbf{B}$ of constant magnitude. Then,

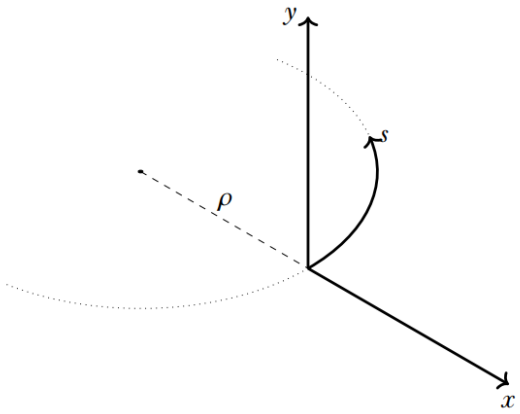

Figure 1.2: Frénet-Serret coordinate system for a particle in a closed circular curve, where ρ is the curvature radius (Fig. from [11]).

the centripetal force is given by the Lorentz force itself:

$$evB = m\frac{v^2}{\rho} \tag{1.2.1}$$

where we considered the hypothesis $\mathbf{v} \perp \mathbf{B}$, and from this expression, we get the relation

$$\rho B = \frac{p}{e}\,, \tag{1.2.2}$$

where we used the classical definition of particle momentum $p = mv$. This relation for $B\rho$ is thus known as *beam rigidity*, which is commonly used to measure the resistance of the beam to the deflection caused by a magnetic field.

Let us now go through the analysis of the system coordinates and equations. First, we map the Frénet-Serret coordinate system to the Cartesian coordinate system (X, Y, Z). Let ρ be the radius of the circular accelerator. The following transformations allow one to express the Cartesian coordinates as a function of the Frénet-Serret variables:

$$X = (x+\rho)\cos\left(\frac{s}{\rho}\right)\,, \quad Y = y\,, \quad Z = (x+\rho)\sin\left(\frac{s}{\rho}\right) \tag{1.2.3}$$

Basically, the Hamiltonian that will be used to describe the motion of a particle in a circular accelerator is the one of a particle subjected to a Lorentz force. Acceleration is provided by the action of an electric field $\mathbf{E}$, while a magnetic field $\mathbf{B}$ bends the particle to keep it in a circular motion.

Consider a relativistic particle of mass m and electric charge e. Its Hamiltonian

reads:

$$\mathcal{H} = e\Phi + \sqrt{m^2c^4 + (c^2\mathbf{p} - e\mathbf{A})^2}\,. \tag{1.2.4}$$

where

$$\mathbf{E} = -\boldsymbol{\nabla}\Phi - \frac{\partial \mathbf{A}}{\partial t} \qquad \mathbf{B} = \boldsymbol{\nabla} \times \mathbf{A}\,. \tag{1.2.5}$$

Φ is the scalar potential, while $\mathbf{A}$ is the vector potential. The corresponding equations of motion read

$$\dot{\mathbf{q}} = \frac{\partial \mathcal{H}}{\partial \mathbf{p}} \qquad \dot{\mathbf{p}} = -\frac{\partial \mathcal{H}}{\partial \mathbf{q}} \tag{1.2.6}$$

where $\mathbf{q} = (x, y, z)$ is the position coordinate and $(\mathbf{q}, \mathbf{p})$ are conjugate phase-space coordinates.

The expressions that we have just found represent the Hamiltonian and the related equations of motion for a particle in a Euclidean space. However, we want to take advantage of the Frénet-Serret coordinates to write the equations in a more suitable reference system for beam dynamics.

Consider the term $(c\mathbf{p} - e\mathbf{A})^2$ in (1.2.4). In order to write this norm through the Frénet-Serret coordinates, we can make use of the metric tensor g_{ij} for this reference system, which is defined as:

$$g_{ij} = \text{diag}\left((1 + x/\rho)^2,\, 1,\, 1\right) \tag{1.2.7}$$

Through this definition, the full expression for the square norm of $(c\mathbf{p} - e\mathbf{A})$ becomes:

$$(c\mathbf{p} - e\mathbf{A})^2 = \frac{(cp_s - eA_s)^2}{(1 + x/\rho)^2} + (cp_x - eA_x)^2 + (cp_y - eA_y)^2 \tag{1.2.8}$$

Thus, the Hamiltonian reads:

$$\mathcal{H} = e\Phi + \sqrt{m^2c^4 + \frac{(cp_s - eA_s)^2}{(1 + x/\rho)^2} + (cp_x - eA_x)^2 + (cp_y - eA_y)^2}\,. \tag{1.2.9}$$

At this point, it is much more convenient to treat the variable s as a time variable, instead of the actual time t. This is a natural choice to study the periodic motion of particles in a circular ring, since it allows synchronising the dynamics with the geometry of the ring, rather than using an absolute value of time t, which is not that informative. In addition, this change of variable allows us to promote the conjugated momentum $-p_s$ to a new Hamiltonian $\tilde{\mathcal{H}}$.

Indeed, by solving Eq. (1.2.9) for p_s we get:

$$\tilde{\mathcal{H}} = -\left(1 - \frac{x}{\rho}\right)\sqrt{\frac{E^2}{c^2} - m^2c^2 - (p_x - eA_x)^2 - (p_y - eA_y)^2} - eA_s \tag{1.2.10}$$

where $E = \mathcal{H} - e\Phi$. From special relativity, the mass-shell relation states that $E^2/c^2 = p^2 + m^2c^2$. Thus:

$$\tilde{\mathcal{H}} = -\left(1 - \frac{x}{\rho}\right)\sqrt{p^2 - (p_x - eA_x)^2 - (p_y - eA_y)^2} - eA_s\,. \tag{1.2.11}$$

We can now consider the additional statement that, in high-energy circular accelerators, particles move almost in parallel with respect to the reference trajectory in the longitudinal axis. That is, $p_x, p_y \ll p_s \approx p$, hence the paraxial[1] approximation can be applied. Using the expansion $\sqrt{1+x} \approx 1 + x/2$, the Hamiltonian simplifies to

$$\tilde{\mathcal{H}} = \left(1 + \frac{x}{\rho}\right)\left[-p + \frac{1}{2p}\left(p_x^2 + p_y^2\right)\right] - eA_s\,. \tag{1.2.12}$$

Here, we considered that along the longitudinal axis there is no contribution of the magnetic field. That is, $A_x = A_y = 0$, i.e., $\mathbf{B} = (B_x, B_y, 0)$.

1.3 Transverse motion

Let us now go through the transverse dynamics of a particle in a circular accelerator, neglecting the effect on the longitudinal plane. From Hamiltonian (1.2.12), the equations of motion of a particle in the transverse plane can be derived as:

$$x' = \left(1 + \frac{x}{\rho}\right)\frac{p_x}{p}\,, \qquad p_x' = \frac{p}{\rho}\left(1 + \frac{x}{\rho}\right) + e\frac{\partial A_s}{\partial x}\,, \tag{1.3.1}$$

$$y' = \left(1 + \frac{x}{\rho}\right)\frac{p_y}{p}\,, \qquad p_y' = e\frac{\partial A_s}{\partial y}\,. \tag{1.3.2}$$

where the prime denotes the derivative with respect to the longitudinal variable s.

We aim now to find an explicit expression both for $\partial A_s/\partial x$ and $\partial A_s/\partial y$, in terms of the Frénet-Serret coordinates. For this purpose, consider the definition of the magnetic field $\mathbf{B}$ through the rotor of the vector potential $\mathbf{A}$, written in the Frénet-Serret

[1] The word "paraxial" comes from the Greek roots *para-* ("near") and *-axis* ("axis"), meaning "near the axis."

coordinates:

$$\boldsymbol{\nabla} \times \mathbf{A} = \frac{\hat{x}}{1 + x/\rho} \frac{\partial A_s}{\partial y} - \frac{\hat{y}}{1 + x/\rho} \frac{\partial A_s}{\partial x} = B_x \hat{x} + B_y \hat{y} \,, \tag{1.3.3}$$

since, as seen before, the only non-zero component of the vector potential is the one along the s axis. This leads to:

$$\frac{\partial A_s}{\partial x} = -\left(1 + \frac{x}{\rho}\right) B_y \qquad \frac{\partial A_s}{\partial y} = \left(1 + \frac{x}{\rho}\right) B_x \,. \tag{1.3.4}$$

Then, if we substitute these relations in the equations of motion, we get:

$$x' = \left(1 + \frac{x}{\rho}\right) \frac{p_x}{p} \,, \qquad p_x' = \frac{p}{\rho} \left(1 + \frac{x}{\rho}\right) \left[\frac{p}{\rho} - e B_y\right] \,, \tag{1.3.5}$$

$$y' = \left(1 + \frac{x}{\rho}\right) \frac{p_y}{p} \,, \qquad p_y' = e \left(1 + \frac{x}{\rho}\right) B_x \,. \tag{1.3.6}$$

At this point, we can recover the definition of beam rigidity, given by (1.2.2), to rewrite these equations of motion as second-order differential equations.

$$x'' = \frac{1}{\rho} + \frac{x}{\rho^2} + \frac{B_y}{B\rho} \left(1 + \frac{x}{\rho}\right)^2 \,, \tag{1.3.7}$$

$$y'' = \frac{B_x}{B\rho} \left(1 + \frac{x}{\rho}\right)^2 \,. \tag{1.3.8}$$

Neglecting nonlinear terms of the magnetic fields B_x and B_y, we can express these relations as

$$\begin{aligned} x'' + K_x(s) x &= 0 \,, \\ y'' + K_y(s) y &= 0 \,, \end{aligned} \tag{1.3.9}$$

where $K_{x,y}(s)$ is periodic with respect to the length of the accelerator ring:

$$K_{x,y}(s) = K_{x,y}(s + L) \,, \tag{1.3.10}$$

where L is the length of the circumference. The function $K_{x,y}(s)$ takes into account the effect of a linear magnetic field on the particle inside the accelerator. Equations (1.3.9) that we have just derived, considering the periodic condition on the function $K(s)$, are known as *Hill's equations*.

Let us now highlight the dependence of Hill's equations on the longitudinal variable s. From the Floquet theorem, an ansatz of the following form can be proposed for the solution:

$$\begin{cases} x(s) = \sqrt{\varepsilon_x \beta_x(s)}\cos(\psi_x(s) + \psi_{0x}) \\ y(s) = \sqrt{\varepsilon_y \beta_y(s)}\cos(\psi_y(s) + \psi_{0y}) \end{cases} \tag{1.3.11}$$

These two expressions correspond to harmonic oscillators with amplitude $\beta_x(s), \beta_y(s)$ and phase advances $\psi_x(s), \psi_y(s)$, both terms being functions of s. The two pairs of factors $\varepsilon_x, \varepsilon_y$ and ψ_{0x}, ψ_{0y} determine the oscillation amplitude and the initial phase of the oscillator, respectively. They are constant and can be determined through the initial conditions.

By substituting these solutions into the Hill's equations (1.3.9), we then get the following relations:

$$\begin{aligned} &\psi_x'\beta_x' + \psi_x''\beta_x = 0\,, \\ &\psi_y'\beta_y' + \psi_y''\beta_y = 0\,, \\ &\frac{1}{2}\beta_x'' - \frac{1}{4\beta_x}(\beta_x')^2 - \beta_x(\psi_x')^2 + \beta_x K_x(s) = 0\,, \\ &\frac{1}{2}\beta_y'' - \frac{1}{4\beta_y}(\beta_y')^2 - \beta_y(\psi_y')^2 + \beta_y K_y(s) = 0\,. \end{aligned} \tag{1.3.12}$$

The first two equations allow us to find the relation between the amplitude β and the phase advance ψ:

$$\psi_x(s) = c_x \int_0^s \frac{\mathrm{d}\sigma}{\beta_x(\sigma)} \qquad \psi_y(s) = c_y \int_0^s \frac{\mathrm{d}\sigma}{\beta_y(\sigma)}\,, \tag{1.3.13}$$

where c_x, c_y are constant terms. Also, We can observe that for $\psi_x(0) = \psi_y(0) = 0$.

In the literature, β_x and β_y are known as *beta functions* of the accelerator, and they determine the amplitude and the shape of the beam. Indeed, for values of s where $\beta(s)$ is large, the beam exhibits larger transverse amplitudes but smaller angular divergences. In contrast, small values of $\beta(s)$ lead to narrower bunches but more angular spread. This claim can be grasped considering, e.g., the expression for x and the corresponding angle with respect to the s axis, namely $x' = \frac{\mathrm{d}x}{\mathrm{d}s}$. We get:

$$x(s) = \sqrt{\varepsilon_x \beta_x(s)}\cos(\psi_x(s) + \psi_{x0}) \tag{1.3.14}$$

$$x'(s) = \sqrt{\frac{\varepsilon}{\beta_x(s)}}\left(\frac{\beta_x'(s)}{2}\cos(\psi_x(s)) - \sin(\psi_x(s))\right)\,. \tag{1.3.15}$$

If we observe the dependence of x and x' on the function β_x, we can see from the first expression that $x(s) \propto \sqrt{\beta_x(s)}$, while from the second one $x'(s) \propto 1/\sqrt{\beta_x(s)}$. This

means that as we change the value of β_x, the spatial and angular amplitudes exhibit opposite behaviours. Additionally, because of the periodicity of the system with respect to the length L of the accelerator, the functions β_x and β_y can also be considered periodic with the same period. In the second case, the quantities ε_x and ε_y represent the *transversal emittances*, which measure the width of the beam in the horizontal and vertical plane, as mentioned before. We can then define the *betatron tune* of the accelerator as:

$$\nu_x = \frac{\psi_x(L)}{2\pi} \qquad \nu_y = \frac{\psi_y(L)}{2\pi}\,. \tag{1.3.16}$$

This quantity is the 1-turn phase advance, i.e. it measures the number of betatron oscillations per single turn around the accelerator circumference.

Lastly, $\beta(s)$ allows us to define the *alpha function* $\alpha(s)$, that is:

$$\alpha = -\frac{1}{2}\beta'(s)\,, \tag{1.3.17}$$

whose sign tells whether the beam envelope is shrinking ($\alpha < 0$) or expanding ($\alpha > 0$).

1.3.1 Courant-Snyder formalism and Twiss parameters

The relations derived above naturally lead to the Courant–Snyder formulation, which provides a compact and elegant framework for the description of the transverse dynamics of charged particles in an accelerator. This formalism rephrases Hill's equations in terms of a set of invariant quantities and optical parameters, known as *Twiss parameters*, which fully characterise the evolution of the beam envelope and phase-space ellipse along the lattice[2]. Through this approach, the oscillatory motion of individual particles can be represented geometrically by an ellipse in the (x, x') or (y, y') phase-space, whose shape and orientation are determined by the Twiss parameters themselves. In what follows, we shall introduce the Courant–Snyder invariant, derive the corresponding envelope equations, and discuss the physical meaning of the Twiss parameters in the context of beam optics.

To describe the motion in phase space, it is convenient to introduce the so-called *Twiss parameters* $\alpha(s)$, $\beta(s)$, and $\gamma(s)$. The function $\gamma(s)$ can be obtained as a function of α and β, which we already introduced, as:

$$\gamma(s) = \frac{1 + \alpha^2(s)}{\beta(s)}\,. \tag{1.3.18}$$

and it is related to the divergence of the beam.

[2] In accelerator physics, the term "lattice" refers to the periodic arrangement of magnetic and accelerating elements that defines the beam optics along the machine.

Due to its periodic nature, one can describe the motion through a different pair of coordinates, which accounts for the amplitude and the angular position of particles. In this sense, we can set the canonical pair (y, p_y) by defining:

$$p_y = \beta_y \frac{dy}{ds} - \frac{1}{2}\frac{d\beta_y}{ds}\, y. \tag{1.3.19}$$

This definition ensures that the phase-space trajectory becomes circular in the (y, p_y) plane, as will be clear in a moment. Substituting the expression for $y(s)$ into Eq. (1.3.19), and recalling that

$$\frac{dy}{ds} = a\left[\frac{\beta_y'}{2\sqrt{\beta_y}}\cos(\psi_y + \xi_s) - \frac{1}{\sqrt{\beta_y}}\sin(\psi_y + \xi_s)\right], \tag{1.3.20}$$

we obtain:

$$\begin{aligned} p_y &= \beta_y \frac{dy}{ds} - \frac{1}{2}\beta_y' y \\ &= a\left[\frac{\beta_y'}{2}\sqrt{\beta_y}\cos(\psi_y + \xi_s) - \sqrt{\beta_y}\sin(\psi_y + \xi_s)\right] - a\frac{\beta_y'}{2}\sqrt{\beta_y}\cos(\psi_y + \xi_s)\,, \end{aligned} \tag{1.3.21}$$

which simplifies to

$$p_y = -a\sqrt{\beta_y(s)}\sin(\psi_y(s) + \xi_s). \tag{1.3.22}$$

Now, we can see that the trajectory of a single particle in the (y, p_y) plane therefore describes a circle of radius $a\sqrt{\beta_y(s)}$:

$$y^2 + p_y^2 = a^2\beta_y(s)\,. \tag{1.3.23}$$

We can thus define the *Courant-Snyder ellipse* as:

$$C(y, y') = \frac{y^2 + p_y^2}{\beta_y(s)} = \gamma_y y^2 + 2\alpha_y y y' + \beta_y y'^2 = a^2 \equiv \epsilon\,, \tag{1.3.24}$$

while ϵ is called *Courant-Snyder invariant*. The Twiss parameters are related as in Eq. (1.3.18).

Substituting the solutions for y and p_y into Eq. (1.3.24), one finds the following:

$$C(y, y') = \frac{1}{\beta_y}\left[a^2\beta_y\cos^2\psi_y + a^2\beta_y\sin^2\psi_y\right] \tag{1.3.25}$$

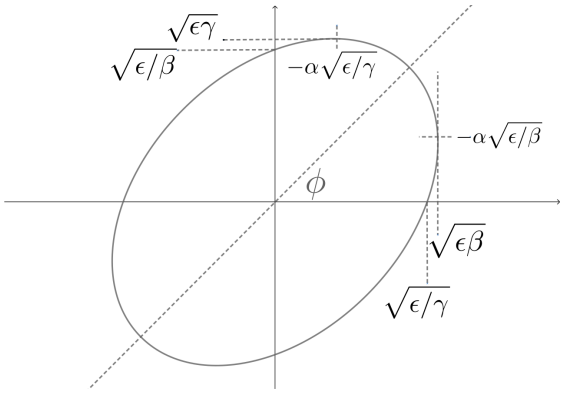

Figure 1.3: The Courant-Snyder ellipse in the (y, y') phase-space. The area enclosed by the ellipse is equal to $\pi\epsilon$, where ϵ is the beam emittance. The Twiss parameters α, β, and γ determine the orientation and aspect ratio of the ellipse.

Hence, the area enclosed by this ellipse in the (y, y') phase plane is equal to

$$A = \pi\epsilon\,. \tag{1.3.26}$$

Since $a^2 = \epsilon$, we can express $y(s)$ as

$$y(s) = \sqrt{\epsilon_y \beta_y(s)}\cos\psi_y(s)\,, \tag{1.3.27}$$

Note that the Courant-Snyder invariant, which is a property of a single particle, should not be confused with the beam emittance, which is defined relative to a distribution of particles in the phase space. Nevertheless, we will see their connection in a moment.

1.3.2 Statistical properties and beam emittance

In beam dynamics, a particle ensemble is often described by a normalised phase-space distribution function $\rho(y, y')$, where y denotes the transverse displacement and y' its angular deviation. To characterise the beam's shape and quality, we first compute its statistical moments.

The *first moments* give the mean position and mean angle:

$$\langle y\rangle = \iint y\,\rho(y,y')\,\mathrm{d}y\,\mathrm{d}y' \qquad \langle y'\rangle = \iint y'\,\rho(y,y')\,\mathrm{d}y\,\mathrm{d}y'. \tag{1.3.28}$$

However, the mean values alone do not describe the spatial and angular spread of the beam. This information is contained in the *second moments*, namely the variances:

$$\sigma_y^2 = \iint (y-\langle y\rangle)^2\rho(y,y')\,\mathrm{d}y\,\mathrm{d}y', \qquad \sigma_{y'}^2 = \iint (y'-\langle y'\rangle)^2\rho(y,y')\,\mathrm{d}y\,\mathrm{d}y'. \tag{1.3.29}$$

In addition, we can measure the correlation between the beam position and the angular deviation through the *covariance*:

$$\sigma_{yy'} = \iint (y - \langle y \rangle)(y' - \langle y' \rangle)\, \rho(y, y')\, dy\, dy'. \tag{1.3.30}$$

Now, starting from these three second-order moments that we have just defined, we can quantify the phase-space area occupied by the beam, through the *root-mean-square (rms) beam emittance*:

$$\varepsilon_{\mathrm{rms}} = \sqrt{\sigma_y^2 \sigma_{y'}^2 - \sigma_{yy'}^2} = \sigma_y \sigma_{y'} \sqrt{1 - r^2}, \tag{1.3.31}$$

where r is the correlation coefficient between y and y', namely

$$r = \frac{\sigma_{yy'}}{\sigma_y \sigma_{y'}}\,. \tag{1.3.32}$$

The rms emittance, which is also known as *geometrical emittance*, thus acts as a bridge between the statistical description of the beam and the single-particle emittance derived from betatron motion.

To visualise this concept, consider an ideal beam where the particles are uniformly distributed inside an ellipse defined by the following:

$$\frac{y^2}{a^2} + \frac{y'^2}{b^2} = 1. \tag{1.3.33}$$

The area enclosed by this ellipse is:

$$A = \pi a b\,. \tag{1.3.34}$$

It can be shown that this area is related to the rms beam emittance by:

$$A = 4\pi\, \varepsilon_{\mathrm{rms}}\,. \tag{1.3.35}$$

For this reason, it is common in accelerator physics to define the *full emittance* as:

$$\varepsilon = 4\, \varepsilon_{\mathrm{rms}}\,, \tag{1.3.36}$$

so that the corresponding phase-space ellipse has area $\pi\varepsilon$. This definition has the advantage that $\varepsilon_{\mathrm{rms}}$ remains invariant under linear transformations (such as rotations in phase space).

However, in real accelerators, the motion of each particle is governed by Hill's equation, and the ensemble of particles lies along a *Courant–Snyder ellipse* described by Eq.

(1.3.24). By relating this form to the statistical moments via an appropriate phase-space rotation, one obtains the following relationships connecting the beam sizes to the optical functions of the accelerator:

$$\varepsilon_{\mathrm{rms}} = \frac{\sigma_y^2}{\beta} = \frac{\sigma_{y'}^2}{\gamma}, \qquad r = -\frac{\alpha}{\sqrt{\beta\gamma}}. \tag{1.3.37}$$

These expressions can be summarised through the *covariance matrix* Σ and the *Twiss matrix* Ω:

$$\begin{pmatrix} \sigma_y^2 & \sigma_{yy'} \\ \sigma_{yy'} & \sigma_{y'}^2 \end{pmatrix} = \varepsilon_{\mathrm{rms}} \begin{pmatrix} \beta & -\alpha \\ -\alpha & \gamma \end{pmatrix}. \tag{1.3.38}$$

One can also see that it is possible to derive the rms beam emittance ε_{rms} by computing

$$\varepsilon_{rms} = \sqrt{\det \Sigma} \tag{1.3.39}$$

which is in perfect agreement with (1.3.38), since due to (1.3.18), the Twiss matrix has a unit determinant.

1.4 Longitudinal motion

So far, we have analysed the transverse motion of particles inside an accelerator, where the beam evolution is governed by the focusing structure of the lattice and described in terms of the betatron functions and the Twiss parameters. We now turn our attention to the *longitudinal dynamics*, which describes the evolution of the particle motion through the phase of the accelerating field and the particle energy.

While transverse dynamics considers the spatial configuration and the size of the beam envelope, the longitudinal motion takes into account different beam properties, such as the energy spread of its particles, the bunch length, etc. The study of this aspect of beam dynamics then allows one to understand how the particle parameters are related to the radio-frequency (RF) accelerating fields, in addition to how they follow stable orbits around the ring.

To formalise this description, longitudinal dynamics is expressed in terms of canonical phase-space variables, usually chosen as the particle phase ϕ with respect to the RF wave and the relative energy deviation $\delta = \frac{1}{\beta}\frac{\Delta E}{E} = \frac{\Delta p}{p}$. Their evolution gives rise to oscillations around a stable particle, known as the *synchronous particle*. These oscillations, called *synchrotron oscillations*, represent the longitudinal counterpart of the betatron motion, and their manipulation and control is key to longitudinal beam stability.

In the following, we will derive the equations governing the longitudinal motion starting from the energy–phase relations, define the concept of synchrotron oscillation frequency, and introduce nonlinear effects such as the creation of stable islands in the (ϕ, δ) phase-space.

1.4.1 Synchrotron equations of motion

In a circular accelerator, the longitudinal motion of charged particles is governed by the interaction with the oscillating electric fields provided by the RF cavities. These fields are responsible for compensating for the energy loss of the particles during their revolution and for maintaining them in stable bunches around the reference trajectory.

Let the longitudinal electric field at an RF gap be expressed as

$$\mathcal{E} = \mathcal{E}_0 \sin\left(\phi_{\mathsf{rf}}(t) + \phi_s\right) \qquad \phi_{\mathsf{rf}} = h\omega_{\mathsf{rev}} t\,, \tag{1.4.1}$$

where $\omega_{\mathsf{rev}} = \beta_{\mathsf{s}} c / R_{\mathsf{s}}$ is the angular revolution frequency of the synchronous particle, $\mathcal{E}_0$ is the amplitude of the accelerating electric field, $\beta_{\mathsf{s}} c$ and R_{s} are its velocity and average orbit radius, respectively, h is the harmonic number, and ϕ_{s} is the synchronous phase with respect to the RF wave.

The synchronous particle is defined as the particle that encounters the RF voltage at the same phase ϕ_{s} during each passage through the cavity gap. Its energy and phase remain constant turn by turn, as it satisfies the synchronous condition

$$\omega_{\mathsf{rf}} = h\omega_{\mathsf{rev}}\,, \tag{1.4.2}$$

where ω_{rf} is the angular frequency of the RF field.

The energy gain per passage through the gap for the synchronous particle is given by

$$\Delta E = e\mathcal{E}_0 \beta_{\mathsf{s}} c \int_{-g/2\beta_{\mathsf{s}}c}^{g/2\beta_{\mathsf{s}}c} \sin\left(h\omega_{\mathsf{rev}} t + \phi_{\mathsf{s}}\right)\, \mathrm{d}t = e\mathcal{E}_0 g T_{\mathsf{tr}} \sin\phi_{\mathsf{s}}\,, \tag{1.4.3}$$

where g is the effective cavity gap width, and T_{tr} is the transit-time factor, which accounts for the fact that the field varies during the time a particle crosses the gap:

$$T = \frac{\sin\left(hg/2L\right)}{hg/2L}\,. \tag{1.4.4}$$

where L is the length of the gap. The effective accelerating voltage seen by the particle is thus

$$V = \mathcal{E}_0 g T\,, \tag{1.4.5}$$

so that the average energy gain per turn for the synchronous particle can be written as

$$\frac{dE_s}{dt} = \frac{\omega_{\text{rev}}}{2\pi} eV \sin\phi_{\text{s}} \,. \tag{1.4.6}$$

Now, let us consider a non-synchronous particle, having small deviations from the reference values of the synchronous one:

$$\begin{cases} \omega = \omega_{\text{rev}} + \Delta\omega \,, \\ \phi = \phi_{\text{s}} + \Delta\phi \,, \\ p = p_s + \Delta p \,, \\ E = E_s + \Delta E \,. \end{cases} \tag{1.4.7}$$

The synchrotron motion, i.e. the dynamics of this off nominal trajectory particle, can be mainly described by the evolution of $\Delta\phi$ and ΔE. These quantities evolve according to the balance between the accelerating RF field and the change in revolution frequency with energy.

Its energy gain per passage through an RF cavity is

$$\Delta E = eV \sin\phi \,, \tag{1.4.8}$$

hence, subtracting the synchronous contribution, one obtains

$$\frac{\mathrm{d}\Delta E}{\mathrm{d}t} = \frac{\omega_{\text{rev}} eV}{2\pi} \left[\sin\phi - \sin\phi_{\text{s}}\right] . \tag{1.4.9}$$

At this point, it is possible to introduce an alternative variable which will be used throughout the entire work, that is:

$$\delta = \frac{\Delta p}{p_{\text{s}}} = \frac{\omega_{\text{rev}}}{E_{\text{s}}\beta_{\text{s}}^2} \left(\frac{\Delta E}{\omega_{\text{rev}}}\right) \tag{1.4.10}$$

Eq. (1.4.9) can then be recast in the following form:

$$\dot{\delta} = \frac{\omega_{\text{rev}} eV}{2\pi E_{\text{s}}\beta_{\text{s}}^2} \left(\sin\phi - \sin\phi_{\text{s}}\right) \,. \tag{1.4.11}$$

Now, let us determine the time evolution of the phase angle ϕ. Considering that the RF phase experienced by a particle depends on its revolution frequency, one can write

$$\dot{\phi} = h\left(\omega_{\text{rf}} - \omega\right) = -h\Delta\omega, \tag{1.4.12}$$

where $\omega_{\mathsf{rf}} = h\omega_{\mathsf{rev}}$ is the RF angular frequency and ω is the revolution frequency of the particle under consideration.

Now, using the relation $(\omega R)/(\omega_{\mathsf{rev}} R_{\mathsf{s}}) = \beta/\beta_{\mathsf{s}}$ and expanding R as a function of the energy deviation, one finds:

$$\frac{\Delta\omega}{\omega_{\mathsf{rev}}} = \frac{\beta R_{\mathsf{s}}}{\beta_{\mathsf{s}} R} - 1 \tag{1.4.13}$$

$$R = R_{\mathsf{s}}(1 + \alpha_0\delta + \alpha_1\delta^2 + \alpha_2\delta^3 + \cdots)$$

$$\alpha_{\mathsf{c}} = \frac{1}{R_{\mathsf{s}}}\frac{\mathrm{d}R}{\mathrm{d}\delta} = \alpha_0 + 2\alpha_1\delta + 3\alpha_2\delta^2 + \cdots \equiv \frac{1}{\gamma_{\mathsf{T}}^2}\,, \tag{1.4.14}$$

where R is the mean radius of a circular accelerator and α_{c} is the *momentum compaction factor*. Higher-order coefficients $\alpha_1, \alpha_2, \ldots$ account for non-linear contributions to orbit length as the energy deviates from the reference value of the synchronous particle.

By combining Eqs. (1.4.13) and (1.4.14), the fractional change in revolution frequency can be written as

$$\frac{\Delta\omega}{\omega_{\mathsf{rev}}} = -\eta(\delta)\,\delta, \tag{1.4.15}$$

where $\eta(\delta)$ is known as the *phase-slip factor*, which expanded in powers of δ becomes

$$\eta(\delta) = \eta_0 + \eta_1\delta + \eta_2\delta^2 + \ldots\,. \tag{1.4.16}$$

The coefficients are then given by

$$\begin{cases} \eta_0 = \alpha_c - \dfrac{1}{\gamma_{\mathsf{s}}^2}\,, \\ \eta_1 = \alpha_1 - 2\alpha_c\dfrac{1}{\gamma_{\mathsf{s}}^2} + \dfrac{3}{2\gamma_{\mathsf{s}}^4}\,, \\ \eta_2 = \alpha_2 - 2\alpha_1\dfrac{1}{\gamma_{\mathsf{s}}^2} + \alpha_c\dfrac{1}{\gamma_{\mathsf{s}}^4} - \dfrac{3}{2\gamma_{\mathsf{s}}^6}\,. \end{cases} \tag{1.4.17}$$

In most of the real accelerators and within our working purposes, the longitudinal dynamics is well described by considering only the first-order term η_0, leading to

$$\frac{\mathrm{d}\phi}{\mathrm{d}t} = h\omega_{\mathsf{rev}}\eta_{\mathsf{s}}\,\delta\,, \tag{1.4.18}$$

where we set $\eta_s = \eta_0$. The slip factor determines whether the particles with higher energy take longer or shorter times to complete a revolution compared to the synchronous particle. In particular, below the transition energy $\gamma_t = 1/\sqrt{\alpha_c}$, $\eta_0 > 0$, which

means that particles with higher energy have a longer revolution period. In contrast, above transition $\eta_0 < 0$, the opposite behaviour occurs.

Therefore, Eqs. (1.4.11) and (1.4.18) are the equations of motion that describe the synchrotron motion of particles around the reference orbit:

$$\dot{\phi} = h\omega_{\text{rev}}\eta_{\text{s}}\,\delta \qquad \dot{\delta} = \frac{\omega_{\text{rev}}eV}{2\pi E_{\text{s}}\beta_{\text{s}}^2}\left(\sin\phi - \sin\phi_{\text{s}}\right)\,. \tag{1.4.19}$$

For small-amplitude oscillations, one can linearise the equations by setting $\phi = \phi_{\text{s}} + \Delta\phi$ with $|\Delta\phi| \ll 1$, and expand the sine term:

$$\sin\phi \simeq \sin\phi_{\text{s}} + \cos\phi_{\text{s}}\,\Delta\phi\,. \tag{1.4.20}$$

Keeping only first-order terms gives

$$\dot{\delta} \simeq K\,\cos\phi_{\text{s}}\,\Delta\phi\,, \qquad K \equiv \frac{\omega_{\text{rev}}eV}{2\pi E_{\text{s}}\beta_{\text{s}}^2}\,. \tag{1.4.21}$$

By differentiating the phase equation with respect to time and substituting the above expression, we obtain

$$\ddot{\Delta\phi} = h\,\omega_{\text{rev}}\,\eta_{\text{s}}\,\dot{\delta} \simeq h\,\omega_{\text{rev}}\,\eta_{\text{s}}\,K\cos\phi_{\text{s}}\,\Delta\phi\,. \tag{1.4.22}$$

This can be rewritten by highlighting the form of a harmonic oscillator differential equation:

$$\ddot{\Delta\phi} + \omega_{\text{s}}^2\,\Delta\phi = 0\,, \tag{1.4.23}$$

where the synchrotron angular frequency is defined as

$$\omega_{\text{s}}^2 = -\,\omega_{\text{rev}}^2\frac{h\,eV\,\eta_{\text{s}}\,\cos\phi_{\text{s}}}{2\pi E_{\text{s}}\beta_{\text{s}}^2}. \tag{1.4.24}$$

In order to produce stable oscillations, meaning that a particle displaced from the nominal trajectory is pulled back toward it, the following condition must be satisfied:

$$\eta_{\text{s}}\cos\phi_{\text{s}} < 0\,. \tag{1.4.25}$$

This ensures that $\omega_{\text{s}}^2 > 0$ and the solution of Eq. (1.4.23) is oscillatory. Hence, we can express the synchrotron frequency as

$$\omega_{\text{s}} = \omega_{\text{rev}}\sqrt{\frac{h\,eV\,|\eta_{\text{s}}\cos\phi_{\text{s}}|}{2\pi E_{\text{s}}\beta_{\text{s}}^2}}\,. \tag{1.4.26}$$

Therefore, in the small-amplitude approximation, the longitudinal motion of an off-momentum particle consists of stable synchrotron oscillations around the synchronous particle with frequency ω_{s}.

1.4.2 Synchrotron Hamiltonian and Fixed Points

The longitudinal equations of motion derived in the previous section can be obtained starting from the Hamiltonian formalism as well. For a particle that undergoes small deviations in phase and energy with respect to the synchronous one, the Hamiltonian can be written in the form

$$\begin{aligned}\mathcal{H}(\phi,\delta) &= K(\delta) + U(\phi) \\ &= \frac{1}{2} h \eta_{\mathsf{s}} \omega_{\mathsf{rev}} \delta^2 + \frac{\omega_{\mathsf{rev}} eV}{2\pi E_{\mathsf{s}} \beta_{\mathsf{s}}^2} \left[\cos\phi - \cos\phi_{\mathsf{s}} + (\phi - \phi_{\mathsf{s}}) \sin\phi_{\mathsf{s}}\right] ,\end{aligned} \tag{1.4.27}$$

where we used the canonical conjugate variables (ϕ, δ) introduced before.

The Hamiltonian formulation also allows us to identify the equilibrium configurations of the system. These correspond to fixed points in phase-space, namely those pairs of coordinates (ϕ, δ) which remain constant in time. In order to find them, we have to consider the stationary solutions of the equations of motion, i.e. the points in phase-space where both Eqs. (1.4.19) vanish. Clearly, they can also be derived from the Hamiltonian (1.4.27):

$$\dot{\phi} = \frac{\partial \mathcal{H}}{\partial \delta} = h \eta_{\mathsf{s}} \omega_{\mathsf{rev}}\, \delta = 0 \tag{1.4.28}$$

$$\dot{\delta} = -\frac{\partial \mathcal{H}}{\partial \phi} = \frac{\omega_{\mathsf{rev}} eV}{2\pi E_{\mathsf{s}} \beta_{\mathsf{s}}^2} \left(\sin\phi - \sin\phi_{\mathsf{s}}\right) = 0 \,. \tag{1.4.29}$$

These conditions admit the following solutions:

$$\delta = 0 \qquad \sin\phi = \sin\phi_{\mathsf{s}} \,, \tag{1.4.30}$$

from which we find:

$$\mathsf{FP}_1 = (\phi_{\mathsf{s}} \,,\, 0) \,, \qquad \mathsf{FP}_2 = (\pi - \phi_{\mathsf{s}} \,,\, 0) \,. \tag{1.4.31}$$

The nature of these fixed points, i.e. whether they are stable or unstable, is determined by the local curvature of the potential term $U(\phi)$. This can be found through the second derivative $U''(\phi)$ computed at the fixed points, namely:

$$\left.\frac{\partial^2 U}{\partial \phi^2}\right|_{\phi=\phi_{\mathsf{FP}}} = -\frac{\omega_{\mathsf{rev}} eV}{2\pi E_{\mathsf{s}} \beta_{\mathsf{s}}^2} \cos\phi_{\mathsf{FP}} . \tag{1.4.32}$$

A fixed point corresponds to a minimum of the potential, that is, it is stable if the curvature of $U(\phi)$ is positive. This condition holds if

$$\eta_{\mathsf{s}} \cos \phi_{\mathsf{FP}} < 0 \,. \tag{1.4.33}$$

In contrast, it is unstable when $\eta_{\mathsf{s}} \cos \phi_{\mathsf{FP}} > 0$. Hence

- the *stable fixed point* (SFP) is located at $\phi = \phi_{\mathsf{s}}$, corresponding to the synchronous particle;
- the *unstable fixed point* (UFP) lies at $\phi = \pi - \phi_{\mathsf{s}}$.

In the (ϕ, δ) phase plane, these two points define the topology of the Hamiltonian flow. The SFP corresponds to the centre of the synchrotron oscillations, around which bounded trajectories form closed orbits (the RF bucket). On the other hand, the UFP identifies the separatrix, namely the trajectory that splits the phase-space into regions of bounded and unbounded motion.

1.4.3 RF phase modulation

In real accelerators, the motion of particles is subjected to perturbations of different nature. Indeed, fluctuations in the RF system, mechanical vibrations, or electrical noise introduce small but systematic perturbations in the accelerating field. Among these effects, modulation of the RF phase plays a particularly important role, as it directly interferes with the synchronism condition between particles and the accelerating voltage. Such a modulation can arise from a variety of physical mechanisms, including phase noise in the RF cavities, feedback imperfections, and so on.

Depending on the characteristic frequency of the perturbation, these fluctuations act on different timescales. For instance, high-frequency components are typically associated with random thermal fluctuations, while low-frequency ones arise from slow drifts in the power supply or ground motion. When the modulation frequency lies close to the synchrotron particles' frequency, a resonant coupling may occur, leading to a distortion of the longitudinal phase-space structure. This might become a source of instability, causing losses in the circulating beam.

In the following, we will focus on the case of a single-frequency sinusoidal RF phase modulation. The manipulation of such an external effect represents the main technique upon which the present study is conducted. Due to the small amplitude of the modulation with respect to the characteristic scales of the original system, its effect can be consistently described within the formalism of perturbation theory.

In light of the above, consider a modulation of the RF phase of the form $a\omega_{\mathrm{m}} \sin(\omega_{\mathsf{m}} t + \psi_0)$, where $\omega_{\mathsf{m}} = \nu_{\mathsf{m}} \omega_{\mathsf{s}}$ and ν_{m} is the tune of the modulation. The new Hamiltonian, consid-

ering the effect of the modulation, reads:

$$\begin{aligned}\mathcal{H}(\phi,\delta,t) = &\frac{1}{2}h\eta_{\mathrm{s}}\omega_{\mathrm{rev}}\delta^2 + a\omega_{\mathrm{m}}\cos(\omega_{\mathrm{m}}t+\psi_0)\delta + \\ &+ \frac{\omega_{\mathrm{rev}}eV}{2\pi E_{\mathrm{s}}\beta_{\mathrm{s}}^2}\left[\cos\phi - \cos\phi_{\mathrm{s}} + (\phi-\phi_{\mathrm{s}})\sin\phi_{\mathrm{s}}\right] .\end{aligned} \tag{1.4.34}$$

The equation of motion for $\dot{\phi}$ changes accordingly, as:

$$\dot{\phi} = h\eta_{\mathrm{s}}\omega_{\mathrm{rev}}\delta + a\omega_{\mathrm{m}}\cos(\omega_{\mathrm{m}}t+\psi_0) , \tag{1.4.35}$$

It should be noted that, due to the presence of the time-dependent term, the Hamiltonian in Eq. (1.4.34) is no longer an autonomous function of the canonical variables. As a consequence, the total energy of the system is not conserved, since the external modulation continuously injects and extracts energy from the longitudinal motion.

The introduction of an external modulation also modifies the concept of equilibrium. In the unperturbed case, the fixed points $(\phi_{\mathsf{FP}}, \delta_{\mathsf{FP}})$ satisfy the stationary conditions $\dot{\phi} = \dot{\delta} = 0$. When the modulation term is present, these points are no longer static. Instead, the time-dependence causes them to oscillate in phase with the driving frequency, so that the concept of fixed point is not well-defined anymore. Hence, the fixed points of the unperturbed system are replaced by *periodic orbits* in the (ϕ, δ) plane, which can be properly analysed by means of Poincaré sections, as will be shown in the next chapter.

1.4.4 Radiation damping and stochastic effects

In lepton circular accelerators, the emission of synchrotron radiation plays a fundamental role in the evolution of the beam dynamics. This is due to the light masses of leptons, such as electrons, which emit a remarkable amount of radiation according to:

$$P \propto \frac{1}{m^4} , \tag{1.4.36}$$

where P is the radiated power of synchrotron losses and m is the mass of the particle. Each particle loses a small amount of energy through radiation at every turn, and this loss is compensated on average by the accelerating RF system. The resulting energy exchange gives rise to a dissipative mechanism known as *radiation damping*, which progressively reduces the amplitude of synchrotron oscillations and drives the beam toward the reference orbit.

To quantify the scale of this effect, consider an electron and a proton, circulating with the same energy E and the same bending radius R. The ratio of the total radiated

power is given by:

$$\frac{P_e}{P_p} = \left(\frac{m_p}{m_e}\right)^4 \approx (1836)^4 \approx 1.14 \times 10^{13}. \tag{1.4.37}$$

This implies that an electron radiates power ten trillion times more than a proton under the same conditions.

A real context example can be made considering the Advanced Light Source (ALS) at Lawrence Berkeley National Laboratory, whose parameters will be used to test the model considered later on.

The ALS storage ring operates with an electron beam of $E = 1.5\,\mathrm{GeV}$ and has a bending radius of $\rho = 4.01\,\mathrm{m}$. Using the formula for synchrotron radiation losses in an isomagnetic[3] ring, the energy lost per turn by a single electron is:

$$U_0 = C_\gamma \frac{\beta^3 E^4}{\rho} \tag{1.4.38}$$

where $C_\gamma = 8.85 \times 10^{-5}\,\mathrm{m\,GeV^{-3}}$. For an energy of $1.5\,\mathrm{GeV}$, electrons are ultra-relativistic, i.e. $\beta \approx 1$. This yields a numerical value of $\sim 111\,\mathrm{keV}$.

Given the total energy of the electron, this represents a fractional loss of $\Delta E/E \sim 0.007\ \%$ at each revolution. Since the revolution frequency of electrons in ALS is of the order of MHz, the beam would be completely lost in seconds due to synchrotron emission[4].

Yet, in addition to the energy compensation given by the RF system, we have to consider an additional effect which provides energy kicks to the beam, which is the presence of stochastic fluctuations due to the quantum nature of synchrotron radiation emission. This occurs naturally in addition to the radiation emission and contributes to providing a natural equilibrium emittance after the system has stabilised.

Combining these two effects, namely radiation damping and stochastic fluctuations, the equation of motion for $\dot{\delta}$ can be rewritten by adding their contribution, as:

$$\dot{\delta} = \frac{\omega_{\mathrm{rev}} eV}{2\pi E_{\mathrm{s}} \beta_{\mathrm{s}}^2} \left(\sin\phi - \sin\phi_{\mathrm{s}}\right) - \gamma\delta + D\,\xi(t) \tag{1.4.39}$$

where γ is the damping decrement rate and D is the diffusion coefficient. $\xi(t)$, instead, represents a Gaussian white noise process, namely a discrete Gaussian variable with:

$$\langle \xi(t) \rangle = 0 \quad \text{and} \quad \langle \xi(t)\xi(t') \rangle = \delta(t - t') \tag{1.4.40}$$

[3] An isomagnetic ring has constant magnetic field strength in all dipoles.

[4] Actually, since $U_0 \propto E^4$, the loss of energy per turn decreases with time, but the example still holds.

From the point of view of dynamical systems theory, Eq. (1.4.39) is a Langevin equation in the Stratonovich sense, and the white-noise $\xi(t)$ is the derivative of a Wiener process W, i.e. $\xi(t) = \mathrm{d}W/\mathrm{d}t$. This characterisation allows us to study the dynamics through the stochastic differential equations (SDE) formalism, including the use of the Fokker-Planck equation for a distribution of particles.

Chapter 2

Elements of the theory of Dynamical Systems

In this chapter, the main results from the theory of Dynamical Systems are presented. The analysis begins by retrieving some fundamental aspects of Hamiltonian mechanics, such as canonical transformations, action-angle variables, and adiabatic invariants. Then, perturbation theory for Hamiltonian systems is presented, in addition to some insights in the presence of resonances. In order to further develop this concept, we consider the particular case of a time-dependent perturbation, which is treated through the theory of separatrix crossing. Eventually, we take into account systems affected by stochastic effects, which lead to a different description with respect to the Hamiltonian case. In this framework, the reaction-rate theory is presented that studies the possibility of a separatrix crossing in the presence of stochastic noise.

2.1 Hamiltonian mechanics

The content provided in this section is inspired mainly by Refs. [8, 11, 20].

Consider a dynamical system in $\mathbb{R}^{2n}$ defined by the set of coordinates $(\mathbf{q}(t), \mathbf{p}(t))$ and the time-dependent function $\mathcal{H}(\mathbf{p}, \mathbf{q}, t)$, where $\mathbf{p} = (p_1, \dots, p_n)$ and $\mathbf{q} = (q_1, \dots, q_n)$. The system is said to be Hamiltonian if the evolution equations can be written in the form:

$$\dot{\mathbf{q}} = \frac{\partial \mathcal{H}}{\partial \mathbf{p}} \qquad \dot{\mathbf{p}} = -\frac{\partial \mathcal{H}}{\partial \mathbf{q}} \,. \tag{2.1.1}$$

These are called *Hamilton's canonical equations of motion*, and $\mathcal{H}$ is the *Hamiltonian*. The equations of motion are associated with the 1-form

$$\omega = \mathbf{p} \cdot \mathrm{d}\mathbf{q} - \mathcal{H}\, \mathrm{d}t \ , \tag{2.1.2}$$

in the extended phase space, which defines the geometrical structure of the phase flow of a Hamiltonian system by using the concept of rotor lines. Moreover, it allows one to outline Hamilton's Variational Principle, namely the integral

$$\mathcal{S} = \int_{\mathbf{q}_0}^{\mathbf{q}_1} (\mathbf{p} \cdot \mathrm{d}\mathbf{q} - \mathcal{H}\, \mathrm{d}t) = \int_{t_0}^{t_1} (\mathbf{p} \cdot \dot{\mathbf{q}} - \mathcal{H})\, dt, \tag{2.1.3}$$

where $\mathcal{S}$ is the *action* and the integral is taken between two points $\mathbf{q}_0 = \mathbf{q}(t_0)$ and $\mathbf{q}_1 = \mathbf{q}(t_1)$ of the trajectory.

Vice versa, equations (2.1.1) can be obtained by imposing the stationary condition $\delta\mathcal{S} = 0$, which represents the Principle of Least Action written in the Hamiltonian formalism.

2.1.1 Canonical transformations

The Hamiltonian formulation provides a powerful framework for studying physical systems, especially in nonlinear regimes. Its strength comes mainly from the perturbation theory based on the canonical transformations of the phase space variables q and p, which preserve the canonical structure of the equations. This framework gives much freedom: momenta and positions can be swapped freely. This is the main difference from the Lagrangian formulation of Mechanics, where positions and velocities play very distinct roles. This invariance discloses a deep geometric structure of the phase space, called *symplectic*, which also has applications in accelerator physics. For example, one has to use *symplectic schemes* for the numerical integration of the Hamilton equations to preserve the symplectic character of the dynamics.

Consider two pairs of canonical coordinates $(\mathbf{q}, \mathbf{p})$ and $(\mathbf{Q}, \mathbf{P})$ connected by a canonical transformation $(\mathbf{q}, \mathbf{p}) \rightarrow (\mathbf{Q}, \mathbf{P})$ and a Hamiltonian $\mathcal{H}(\mathbf{q}, \mathbf{p})$. Then we can find a function $\mathcal{H}'(\mathbf{Q}, \mathbf{P})$ for which

$$\dot{\mathbf{Q}} = \frac{\partial \mathcal{H}'}{\partial \mathbf{P}} \qquad \dot{\mathbf{P}} = -\frac{\partial \mathcal{H}'}{\partial \mathbf{Q}}\,. \tag{2.1.4}$$

Since $(\mathbf{Q}, \mathbf{P})$ are canonical, they must satisfy the Principle of Least Action:

$$\delta \int_{\mathbf{Q}_0}^{\mathbf{Q}_1} (\mathbf{P} \cdot \mathrm{d}\mathbf{Q} - \mathcal{H}'\, \mathrm{d}t) = 0\,. \tag{2.1.5}$$

In order for the two principles in $(\mathbf{q}, \mathbf{p})$ and $(\mathbf{Q}, \mathbf{P})$ to be equivalent, their integrand must differ at most for the exact differential of an arbitrary function $\mathcal{G}$:

$$\mathbf{p}\mathrm{d}\mathbf{q} - \mathcal{H}\mathrm{d}t = \mathbf{P}\mathrm{d}\mathbf{Q} - \mathcal{H}'\mathrm{d}t + \mathrm{d}\mathcal{G} \tag{2.1.6}$$

since $\mathrm{d}\mathcal{G}$ is zero when evaluated at the integration limits. $\mathcal{G}$ is called *generating function*, or *generatrix*, and completely defines the transformation:

$$\dot{\mathbf{p}} = \frac{\partial \mathcal{G}}{\partial \mathbf{q}} \qquad \dot{\mathbf{q}} = -\frac{\partial \mathcal{G}}{\partial \mathbf{Q}} \qquad \mathcal{H}' = \mathcal{H} + \frac{\partial \mathcal{G}}{\partial t} \tag{2.1.7}$$

In particular, this kind of generating function $\mathcal{G}(\mathbf{q}, \mathbf{Q})$ is said to be of the *first kind*. Based on the variables it depends on, a generating function can also be of the *second*, *third*, and *fourth kind*. More about these can be found in Ref. [20].

A handy way to prove that a transformation is canonical is through *Poisson brackets*.

Let $(\mathbf{q}, \mathbf{p}) \rightarrow (\mathbf{Q}, \mathbf{P})$ be a transformation of coordinates. The transformation is canonical if the following Poisson fundamental relations are fulfilled:

$$\{Q_i, Q_j\}_{\mathbf{pq}} = 0\,, \qquad \{P_i, P_j\}_{\mathbf{pq}} = 0\,, \qquad \{Q_i, P_j\}_{\mathbf{pq}} = \delta_{ij}\,. \tag{2.1.8}$$

where the derivation is made with respect to $\mathbf{p}$ and $\mathbf{q}$.

It is possible to prove that the phase flow of a Hamiltonian system is a canonical transformation itself. By introducing the Lie operator

$$D_H F = \{F, H\}$$

the phase flow can be written in the form of the Lie transformation

$$q(t) = \exp\left(tD_H\right) q(0) \qquad p(t) = \exp\left(tD_H\right) p(0) \tag{2.1.9}$$

We have the property

$$\exp(tD_H) F(x) = F\left(\exp(tD_H) x\right)$$

for any function $F(q, p)$. The application of this result to the fundamental Poisson brackets proves that the transformation (2.1.9) is symplectic. In numerical simulations, this result is of great importance for the development of symplectic integrators, as cited before, which are algorithms that make the system evolve while preserving the Hamiltonian structure. From a geometrical point of view, this is encoded in *Liouville's theorem*.

2.1.2 Liouville theorem

Consider the case of a fully evolving system of n particles through $2n$ coordinates (q_i, p_i). Each pair $(q_i(t), p_i(t))$ represents the state of the ith particle at time t, while a collection of consecutive states forms the *phase trajectory* of the particle in the phase space. The product

$$\mathrm{d}\Gamma = \mathrm{d}q_1 \wedge \ldots \wedge \mathrm{d}q_n \wedge \mathrm{d}p_1 \wedge \ldots \wedge \mathrm{d}p_n \tag{2.1.10}$$

can be considered as a *volume element* in the phase space. As a consequence, the integral $\int \mathrm{d}\Gamma$ gives the volume of the region traced by the particles phase-space trajectory.

We can now state Liouville's theorem, which says that the volume is invariant under canonical transformations. That is to say:

$$\int \mathrm{d}\zeta(q_i, p_i) = \int \mathrm{d}Z(Q_i, P_i) \qquad \forall i, i = 1, \ldots, n \tag{2.1.11}$$

where $(\mathbf{q}, \mathbf{p}) \to (\mathbf{Q}, \mathbf{P})$ is canonical.

Analytically, changing coordinates involves the Jacobian of the transformation, thus the theorem is proven simply by showing that the Jacobian itself is equal to the unit.

Let us write the Jacobian of the canonical transformation as

$$\mathrm{d}Z = \left| \det \frac{\partial Z_i}{\partial \zeta_j} \right| \mathrm{d}\zeta \tag{2.1.12}$$

and consider the following set of coordinates:

$$\tilde{\zeta}_i = (q_i, P_i) \tag{2.1.13}$$

The Jacobian reads

$$\det \frac{\partial Z_i / \partial \tilde{\zeta}_k}{\partial \zeta_j / \partial \tilde{\zeta}_k} = \frac{\det \partial Z_i / \partial \tilde{\zeta}_j}{\det \partial \zeta_i / \partial \tilde{\zeta}_j} \tag{2.1.14}$$

By definition, Z and ζ share the coordinate P_i, so the corresponding terms in the derivative yield a constant. The same happens for the q_i coordinate. This leads to:

$$\det \frac{\partial Z_i}{\partial \tilde{\zeta}_j} = \det \frac{\partial Q_i}{\partial q_j} \,, \qquad \det \frac{\partial \zeta_i}{\partial \tilde{\zeta}_j} = \det \frac{\partial p_i}{\partial P_j} \,. \tag{2.1.15}$$

Now, through the generating function $\mathcal{F}(q, P)$, the two expressions can be rewritten as

$$\frac{\partial Q_i}{\partial q_j} = \frac{\partial}{\partial q_j} \left(\frac{\partial \mathcal{F}}{\partial P_i} \right) = \frac{\partial^2 \mathcal{F}}{\partial q_j \partial P_i} \,, \tag{2.1.16}$$

$$\frac{\partial p_i}{\partial P_j} = \frac{\partial}{\partial P_j} \left(\frac{\partial \mathcal{F}}{\partial q_i} \right) = \frac{\partial^2 \mathcal{F}}{\partial P_j \partial q_i} \tag{2.1.17}$$

Since the two determinants reduce to matrices of mixed second derivatives of the same generating function $\mathcal{F}(q, P)$, we have

$$\frac{\partial Q_i}{\partial q_j} = \frac{\partial^2 \mathcal{F}}{\partial q_j \partial P_i}, \qquad \frac{\partial p_i}{\partial P_j} = \frac{\partial^2 \mathcal{F}}{\partial P_j \partial q_i}. \tag{2.1.18}$$

Since mixed partial derivatives commute,

$$\frac{\partial^2 \mathcal{F}}{\partial q_j \partial P_i} = \frac{\partial^2 \mathcal{F}}{\partial P_i \partial q_j}, \tag{2.1.19}$$

the two matrices are transposes of one another and therefore have equal determinants. It follows that

$$\frac{\det\left(\partial Q_i / \partial q_j\right)}{\det\left(\partial p_i / \partial P_j\right)} = 1. \tag{2.1.20}$$

Hence, the Jacobian of a canonical transformation is unity and the phase-space volume element is preserved.

As will be discussed later, Liouville's theorem is of crucial importance to justify the possible applications of this thesis work. Indeed, top-up injection can be realised under specific conditions, and the present theorem lays the groundwork for it.

2.2 Action-angle variables

In order to introduce the action-angle variables, we need to define the framework in which we can fully exploit them. To this end, one can say that action-angle variables are found to be the most effective in integrable systems.

Consider a Hamiltonian system with n degrees of freedom. The system is said to be *integrable in the Liouville sense* if there exist n independent first integrals[1] $F_1, F_2, \ldots, F_n$ in involution

$$\{F_i, F_j\} = 0 \qquad \forall i, j \tag{2.2.1}$$

and such that the invariant manifold $F_i = f_i$, $i = 1, .., n$ is compact. The fact that we can detect n conserved quantities implies a very important result: the motion of the system is confined to a submanifold of much smaller dimensionality than that of its phase space.

Liouville's theorem, which was stated under the general hypothesis of having canonical transformations, can be further exploited in case of integrable systems and becomes better known as *Liouville-Arnold theorem*. The statement is the following.

Consider an Hamiltonian system with n degrees of freedom and n first integrals $I_i = F_i$, namely an integrable system. Then, the level set

$$M_{\mathsf{F}} = \{x : \ I_i(x) = F_i, \ i = 1, \ldots, n\} \tag{2.2.2}$$

[1] A **first integral** is any function of phase-space coordinates that is constant throughout a trajectory.

is invariant.

Most importantly, a couple of corollaries can be drawn:

- if M_f is compact and connected, then it is diffeomorphic to the n-torus $\mathbb{T}^n$;
- if the previous hypothesis is valid, then the motion is *quasi-periodic* on the torus, meaning that it is made of a superposition of periodic motions with incommensurable frequencies.

Within these conditions, since the motion is quasi-periodical on the torus M_f, it is possible to introduce the *Action-Angle* coordinates (I, φ) by a canonical change of variable, such that the action variables are defined by

$$I_i(F) = \frac{1}{2\pi} \oint_{\gamma_i} \sum_k p_k \, \mathrm{d}q_k$$

where γ_i is a base of cycles on the invariant torus, $F_i = \text{const.}$ are first integrals of motion, and the the evolution of the angle variables reduces to

$$\frac{\mathrm{d}\varphi}{\mathrm{d}t} = \omega(I) \qquad \varphi(t) = \varphi(0) + vb\omega(I)t \tag{2.2.3}$$

where ω_i denotes the i-th *frequency* of the system.

Now, if we choose one of the n integrals of motion as the Hamiltonian of our system, e.g. $\mathcal{H} = F_1$, the phase flow with respect to $\mathcal{H}$ is described by the canonical equations

$$\dot{I}_i = 0 \qquad \dot{\varphi}_i = \omega_i(I) = \frac{\partial H}{\partial I_i} \tag{2.2.4}$$

that is explicitly integrable.

Nevertheless, there is no reason to believe in advance that the couple (I, φ) is canonical. However, it turns out that $J_i = J(I_i)$ is a function such that the variables (J_i, φ_i) are canonical. The last pair of coordinates are what we call *action-angle variables*. The phase flow is now described by the new form:

$$\dot{I}_i = 0 \qquad \dot{\varphi}_i = \omega_i(I_1, \ldots, I_n) \, . \tag{2.2.5}$$

Due to their primary importance in the study of integrable systems, the following lines will be devoted to show how to construct the action-angle variables in the simple case of a one degree of freedom system.

2.2.1 Action-angle variables in one-dimensional systems

Consider a $1d$ system described by the Hamiltonian function $h = \mathcal{H}(q,p)$. In order to construct the action-angle variables, we need to find a canonical transformation $(q,p) \to (I,\varphi)$ with $J = I(E)$, and

$$\oint_{\mathcal{H}=E} \mathrm{d}\varphi = 2\pi \,. \tag{2.2.6}$$

where the integral is taken on the level curve $\mathcal{H}(q,p) = E$.

We define the action variable

$$I(E) = \frac{1}{2\pi} \oint_{\mathcal{H}=E} p\,\mathrm{d}q \tag{2.2.7}$$

assuming that $I(E)$ is invertible. We have the relation

$$\frac{\partial I}{\partial E} = \frac{1}{2\pi} \oint_{\mathcal{H}=E} \frac{\partial p}{\partial H}\,\mathrm{d}q = \frac{T(h)}{2\pi}$$

where $T(I)$ is the period, so that

$$\frac{\partial \mathcal{H}}{\partial I} = \omega(I) \tag{2.2.8}$$

defines the frequency of the orbit. Then we look for the transformation generating function $F(I,q)$, such that

$$p = \frac{\partial F}{\partial q} \qquad \varphi = \frac{\partial F}{\partial I} \qquad \mathcal{H}\left(q, p = \frac{\partial F}{\partial q}\right) = h(I) \,. \tag{2.2.9}$$

Thus, the generating function is computed by

$$F(E(J),q) = \int_{\mathcal{H}=E}^{q} p\,\mathrm{d}q \,, \tag{2.2.10}$$

and the angle variable follows

$$\varphi = \int_{\mathcal{H}=E}^{q} \frac{\partial p}{\partial I}\,\mathrm{d}q = \omega(I)t \,,$$

and after one period $\Delta\varphi = \omega(I)T(I) = 2\pi$. To sum up, the final expressions for the action-angle variables in $1d$ systems are:

$$I = \frac{1}{2\pi} \oint p\,\mathrm{d}q \qquad \varphi = \frac{\partial}{\partial I} \int p\,\mathrm{d}p \,. \tag{2.2.11}$$

The generalisation to higher dimensions $\mathbb{R}^{2n}$, uses a cycle basis γ_i of the n-dimensional torus to define the action variables and the variation of the angle variable φ_i on γ_j is given by $2\pi\delta_{ij}$, where δ_{ij} is the Kronecker delta. As a consequence, the action variables J_i are defined as:

$$I_i(k_1, \ldots, k_n) = \frac{1}{2\pi} \oint_{\gamma_i} p_j \, \mathrm{d}q_j \, . \tag{2.2.12}$$

The construction of the action-angle variables for a system of arbitrary dimensions is then delivered.

2.3 Perturbation theory for Hamiltonian systems

As mentioned previously, integrable systems represent a particular class of dynamical systems which are characterised by a certain number of first integrals. These conserved quantities deeply simplify the analysis of the system at issue, since the dynamics can be properly described in much lower-dimensional manifolds through the action-angle variables.

Yet, it is very difficult to find complete integrable systems in physics, since the fulfilment of integrability hypotheses is highly demanding. Hence, perturbation theory represents a very powerful tool to describe quasi-integrable systems, namely systems which can be decomposed in an integrable Hamiltonian part besides additional perturbative terms. In order to obtain a coherent and correct description of the system in first approximation, the perturbative terms have to be much smaller than the integrable part. Thanks to its versatility, perturbation theory represents a go-to technique in many different fields of physics, ranging from celestial mechanics to quantum mechanics to accelerator physics, indeed.

Multiple approaches have been proposed in perturbation theory, among which the *averaging principle* represents the most suitable choice for this work. This technique relies on the hypothesis that the evolution timescale of the perturbation is much smaller than the one of the unperturbed system. When this happens, we can average the perturbations over time in order to separate the system dynamics in *slow* and *fast variables*. This chapter mainly follows the results presented in Refs. [8] and [11].

Consider an integrable Hamiltonian system with n degrees of freedom and Hamiltonian $\mathcal{H}_0$. Since it is integrable, we can define the action-angle variables $\mathbf{I} = (I_1, \ldots, I_n)$ and $\boldsymbol{\varphi} = (\varphi_1, \ldots, \varphi_n)$ for the n invariant tori which can be identified.

For the unperturbed system, the equations of motion reads:

$$\dot{\mathbf{I}} = 0 \qquad \dot{\boldsymbol{\varphi}} = \frac{\partial \mathcal{H}_0}{\partial \mathbf{I}} = \boldsymbol{\omega}(\mathbf{I}) \,, \tag{2.3.1}$$

where $\boldsymbol{\omega} = (\omega_1, \ldots, \omega_n)$ are the frequencies of motion.

Let us now add a second perturbative term $\mathcal{H}_1 = \mathcal{H}_1(\mathbf{I}, \boldsymbol{\varphi}, \varepsilon)$ to the initial Hamiltonian such that $\mathcal{H}_1$ is periodical on φ and $\varepsilon \ll 1$ quantifies the magnitude of the perturbation. The full Hamiltonian of the system will then read:

$$\mathcal{H} = \mathcal{H}_0 + \varepsilon \mathcal{H}_1 \,. \tag{2.3.2}$$

Equations of motion (2.3.1) can now be rewritten using the new Hamiltonian, from which we get

$$\dot{\mathbf{I}} = -\varepsilon \frac{\partial \mathcal{H}_1}{\partial \boldsymbol{\varphi}} \qquad \dot{\boldsymbol{\varphi}} = \boldsymbol{\omega}(\mathbf{I}) + \varepsilon \frac{\partial \mathcal{H}_1}{\partial \mathbf{I}} \,. \tag{2.3.3}$$

It is evident now that the action variable I is no longer constant, in contrast to the case of an unperturbed system. In particular, since $\mathcal{H}_1$ is periodical in the angle variable, the action I slowly oscillates according to the strength ε of the perturbation. Hence, we can identify the action I as a *slow variable* changing with rate $\mathcal{O}(\varepsilon)$, and the angle φ as a *fast variable* changing with rate $\mathcal{O}(1)$. Therefore, on short timescales (order of a few φ periods) the actions are approximately constant while the angles evolve rapidly.

The idea is to replace the perturbation with the average on the angles:

$$\langle \mathcal{H}_1 \rangle (\mathbf{I}) = \frac{1}{(2\pi)^n} \int_0^{2\pi} \cdots \int_0^{2\pi} \mathcal{H}_1(\mathbf{I}, \boldsymbol{\varphi}) \, \mathrm{d}\varphi_1 \ldots \varphi_n \,, \tag{2.3.4}$$

in order to obtain the averaged Hamiltonian:

$$\langle \mathcal{H} \rangle (\mathbf{I}) = \mathcal{H}_0(\mathbf{I}) + \varepsilon \langle \mathcal{H}_1 \rangle (\mathbf{I}) \,. \tag{2.3.5}$$

The averaged system allows us to define a new pair of action-angle variables (J, ψ), whose equations of motion becomes:

$$\dot{\mathbf{J}} = -\varepsilon \frac{\partial \langle \mathcal{H}_1 \rangle}{\partial \boldsymbol{\varphi}} = 0 \qquad \dot{\boldsymbol{\psi}} = \frac{\partial \mathcal{H}_0}{\partial \mathbf{J}} + \varepsilon \frac{\partial \langle \mathcal{H}_1 \rangle}{\partial \mathbf{J}} \,. \tag{2.3.6}$$

Thus, in the averaged system, the new action J is an adiabatic invariant.

The net effect is the cancellation of the rapid oscillations and the emergence of an average drift given by $\langle \mathcal{H}_1 \rangle$ itself. Figure 2.1 provides a visual representation of the dynamics of the variables.

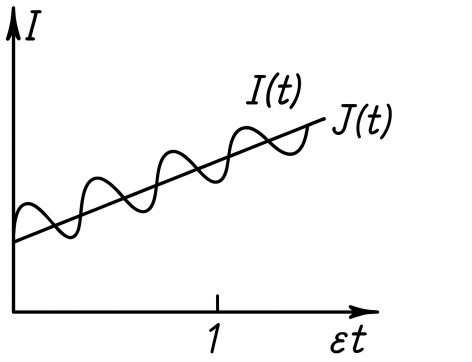

Figure 2.1: Evolution of J and oscillation of I (From [8]).

2.3.1 Resonances

It is important to point out a specific condition for which it is not possible to perform this kind of averaging, that is, in case of *resonance*. To better understand this concept, since $\mathcal{H}_1$ is periodic in $\boldsymbol{\varphi}$, let us write its Fourier expansion as

$$\mathcal{H}_1(\mathbf{I}, \boldsymbol{\varphi}) = \sum_{\mathbf{m}} h_{\mathbf{m}}(\mathbf{I}) e^{i\mathbf{m}\cdot\boldsymbol{\varphi}} \,, \tag{2.3.7}$$

where $\mathbf{m} = (m_1, \ldots, m_n)$ are vectors of integers.

The derivative of the perturbation with respect to the angle variables becomes:

$$\frac{\partial \mathcal{H}_1}{\partial \varphi_j} = \sum_{\mathbf{m}} i m_j h_{\mathbf{m}}(\mathbf{I}) e^{i\mathbf{m}\cdot\boldsymbol{\varphi}} \,. \tag{2.3.8}$$

This expression shows why the action variables oscillate. Indeed, if the angles evolve rapidly according to $\dot{\varphi}_j = \omega_j(\mathbf{I}) + O(\varepsilon)$, then integrating the action equations over time yields:

$$I_j(t) \approx I_j(0) - \varepsilon \int_0^t \frac{\partial \mathcal{H}_1}{\partial \varphi_j}(\mathbf{I}(t'), \boldsymbol{\varphi}(t'))\, \mathrm{d}t' \,. \tag{2.3.9}$$

Each Fourier mode $e^{i\mathbf{m}\cdot\boldsymbol{\varphi}}$ oscillates with characteristic frequency $\mathbf{m}\cdot\boldsymbol{\omega}$, leading to:

$$\int_0^t e^{i\mathbf{m}\cdot\boldsymbol{\varphi}(t')} \mathrm{d}t' \sim \frac{e^{i\mathbf{m}\cdot\boldsymbol{\varphi}(t)}}{i\mathbf{m}\cdot\boldsymbol{\omega}} + \text{constant} \,. \tag{2.3.10}$$

Therefore, the combination of these factors produces bounded oscillations in the action variables, with amplitudes proportional to $\varepsilon/|\mathbf{m}\cdot\boldsymbol{\omega}|$ for each Fourier mode.

Nevertheless, when $\mathbf{m} \cdot \boldsymbol{\omega}(\mathbf{I}) = 0$ for some $\mathbf{m} \neq \mathbf{0}$, a *resonance* occurs. In this case, the corresponding Fourier mode does not oscillate rapidly, and the integral grows linearly with time:

$$\int_0^t e^{i\mathbf{m}\cdot\boldsymbol{\varphi}(t')} \mathrm{d}t' \approx t \cdot e^{i\mathbf{m}\cdot\boldsymbol{\varphi}(0)} + \cdots \tag{2.3.11}$$

These terms, which are called *secular* in perturbation theory, lead to a drift in the action variables, breaking the assumption of slow evolution. Therefore, near a resonance, more sophisticated techniques, such as resonant normal forms or the method of averaging over resonant surfaces, are required.

> **Historical note:** *The adjective "secular", from "saeculum" in Latin, which means "century" or "era", has its roots in 18th-century celestial mechanics. Pierre-Simon Laplace and Joseph-Louis Lagrange observed that certain orbital parameters, such as the precession of Mercury's perihelion, the variation in axial tilt, the precession of the equinoxes and so on, underwent slow, cumulative changes over **saecula**. These variations stood in stark contrast to periodic perturbations that averaged out over shorter intervals. The mathematical signature of such behaviour was a term growing linearly with time in perturbative solutions, which came to be known as a "secular term." The research for secular terms in Uranus' orbit led to the discovery of Neptune in 1846, thanks to the calculations of Urbain Le Verrier and John Couch Adams. This discovery went down in history as the only major planet that has been mathematically located before being directly observed ([31]).*

2.3.2 Poincaré-Birkhoff theorem

A natural way to visualise the effect of resonances in nearly integrable Hamiltonian systems is to reduce the dynamics to a lower–dimensional section of phase space.

For systems with one degree of freedom, the motion occurs on invariant curves parametrised by the action. When a weak periodic perturbation is introduced, it becomes easier to study the *stroboscopic* dynamics, namely the evolution of the system at discrete time intervals equal to the period of the external perturbation. The idea is to "cut" the points trajectories with a hyperplane, the *Poincaré section*, and let the motion be described by these intersection points only. This discrete evolution defines the *Poincaré map*, which captures the essential dynamics while reducing the system's dimension. The fixed points of this map correspond to periodic orbits, whereas invariant curves represent quasi-periodic motion. Figure 2.2 shows this construction.

Near a rational resonance, where the unperturbed frequency $\omega(I)$ satisfies

$$m\omega(I) = n\Omega\,, \tag{2.3.12}$$

the Poincaré map no longer produces smooth invariant tori. Instead, the invariant curve associated with that rational number breaks up into an even chain of alternating stable

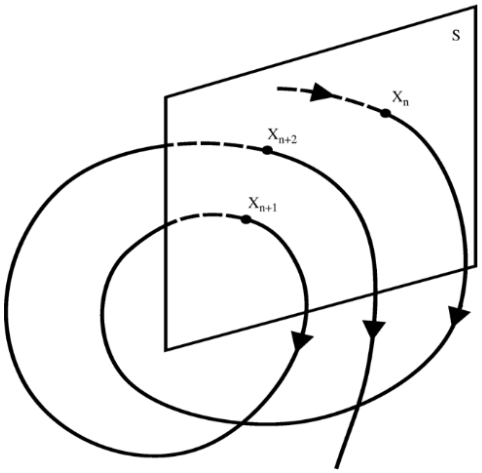

Figure 2.2: Visual representation of the intersection between a trajectory and a Poincaré section S (from [3]). The Poincaré map is the application $\mathcal{P}$ such that $X_{n+k} = \mathcal{P}^k(X_n)$.

(elliptic) and unstable (hyperbolic) fixed points, around which appear small resonant islands in phase space.

Those tori whose associated frequency is irrational with respect to the frequency of the small perturbation tend to survive, despite being slightly deformed (*KAM theorem*).

2.3.3 Adiabatic invariance

Consider a Hamiltonian system with one degree of freedom described by the Hamiltonian function $\mathcal{H} = \mathcal{H}(q, p, \lambda)$. We consider λ to be a slowly-varying parameter with respect to the characteristic time-scale of the system, namely, it varies *adiabatically*. This is equivalent to say:

$$\dot{\lambda} \propto \mu \ll \omega \,, \tag{2.3.13}$$

where μ is the adiabatic parameter and ω is the natural frequency of the system. This condition implies that the relative variation of λ takes much longer to occur than the system evolution. Assuming that $\mathcal{H}(q, p, \lambda) = E$ defines closed curves, one can introduce action-angle variables for any value of the parameter

$$\begin{aligned} I(E, \lambda) &= \oint_{\mathcal{H}=E} p(q, E, \lambda)\, \mathrm{d}q \\ \phi &= \left.\frac{\partial}{\partial I}\right|_q \int_{\mathcal{H}=E}^{q} p(q, E, \lambda)\, \mathrm{d}q \end{aligned} \tag{2.3.14}$$

Let $F(q, I, \lambda)$ be the generating function

$$F(q, I, \lambda) = \int_{\mathcal{H}=E}^{q} p(q, E(I, \lambda), \lambda) \mathrm{d}q$$

We perform the change of variables (2.3.14) in the Hamiltonian system (**??**) and the new Hamiltonian reads

$$\mathcal{H}(I, \lambda) + \mu \left. \frac{\partial F}{\partial \lambda} \right|_{(q,I)} (\theta, I, \lambda) \tag{2.3.15}$$

In the 1DoF cases the adiabatic theory uses the relation

$$\left. \frac{\partial F}{\partial \lambda} \right|_{q,I} = -\frac{1}{\Omega(E, \lambda)} \int^{\theta} \left(\left. \frac{\partial \mathcal{H}}{\partial \lambda} \right|_{q,p} - \left\langle \left. \frac{\partial \mathcal{H}}{\partial \lambda} \right|_{q,p} \right\rangle \right) \mathrm{d}\theta \tag{2.3.16}$$

where $\Omega(E\,\lambda) \simeq O(1)$ is the frequency of the frozen dynamics $\mu = 0$. The relation indicates that the θ-mean value of $\partial F/\partial \lambda$ vanishes. This remark is the basis for the adiabatic invariance of the action variable I, since the only resonance condition is at the separatrix where $\Omega \to 0$. A direct calculation shows that

$$\begin{aligned} I(t+T) - I(t) &= \frac{\mu}{\Omega} \int_{t}^{t+T} \left(\left. \frac{\partial \mathcal{H}}{\partial \lambda} \right|_{q,p} - \left\langle \left. \frac{\partial \mathcal{H}}{\partial \lambda} \right|_{q,p} \right\rangle \right) \mathrm{d}s \\ &= \frac{\mu}{\Omega^2} \int_{0}^{2\pi} \left(\left. \frac{\partial \mathcal{H}}{\partial \lambda} \right|_{q,p} - \left\langle \left. \frac{\partial \mathcal{H}}{\partial \lambda} \right|_{q,p} \right\rangle \right) \mathrm{d}\theta \simeq O\left(\frac{\mu^2}{\Omega^2} \right) , \end{aligned}$$

where we explicitly use the estimate $\Delta I \simeq O(\mu)$ inside the integral. Given a time of order μ^{-1} one can apply the previous estimate fn times with $n = (T\mu)^{-1}$ and we get the adiabatic invariance estimate for the action variables

$$I(t + \mu^{-1}) - I(t) \simeq O\left(\frac{\mu}{\Omega^2} \right) .$$

We observe that the ratio μ/Ω defines the adiabatic parameter since it compares the evolution time scale with the modulation time scale. The use of a perturbative approach allows us to introduce improved adiabatic invariant by performing a change of variables $(\theta, I) \to (\phi, J)$ in the Hamiltonian (2.3.15). This can be performed by a generating function

$$G(\theta, J) = \theta J + \mu G_1(\theta, J, \lambda) ,$$

where the first perturbation order G_1 satisfies the homological equation

$$\Omega(J,\lambda)\frac{\partial G_1}{\partial \theta} + \mu\frac{\partial F}{\partial \lambda} = 0\,.$$

The solution $G_1(\theta, J)$ exists thanks to the relation (2.3.16) and $G_1(J,\theta)$ describes the oscillation of the action variable I. The average value of $G_1(\theta, J)$ is not determined. The new Hamiltonian reads

$$H(J,\phi,\lambda) = \mathcal{H}(J,\lambda) + O\left(\frac{\mu^2}{\Omega^2}\right)\,.$$

It is possible to prove that the new action $J(q,p,\lambda)$ varies by a quantity $O(\mu^2)$ in a time $O(\mu^{-1})$ and is an improved adiabatic invariant.

2.4 Theory of separatrix crossing

In the previous section, we showed that the presence of a resonance between the characteristic frequency of the system and the frequency of an external modulation creates stable regions in the phase space.

We now consider an additional aspect: if the system perturbation is time-dependent, it is possible for particles to cross separatrices and being trapped in these stable regions. This would not be possible in stationary systems, as separatrices represent barriers between different kind of motions, and particles cannot go through them. However, if the perturbation frequency varies adiabatically, capture in a stable island becomes a probabilistic process [24], and the adiabatic invariant undergoes a significant change after capture.

In the following, we outline the theory of separatrix crossing, assuming infinitely slow modulation. This approach has been proposed by A.I. Neishtadt [27], but we follow the derivation presented in the review by J. Henrard (Ref. [17]).

Consider a Hamiltonian $\mathcal{H}(q,p,\lambda)$ depending on a parameter varying slowly λ. Introducing a small dimensionless quantity $\varepsilon \ll 1$, we let the parameter evolve as $\lambda = \varepsilon t$, thus ensuring that its variation occurs on a timescale much longer than the characteristic period of the system. Under this assumption, the dynamics can be treated within the adiabatic approximation.

Consider a phase-space as the one shown in Fig. 2.3. The point C at the centre with coordinates (q_C, p_C) identifies a saddle (hyperbolic) fixed point and, by definition, the collection of points (q,p) such that $\mathcal{H}(q,p) = \mathcal{H}(q_C, p_C)$ identifies the separatrix. Then three different domains can be identified in the phase space: the two lobes G_1 and G_2, and the exterior region G_3. We denote $\Gamma_i = \partial G_i$ and A_i as the area enclosed

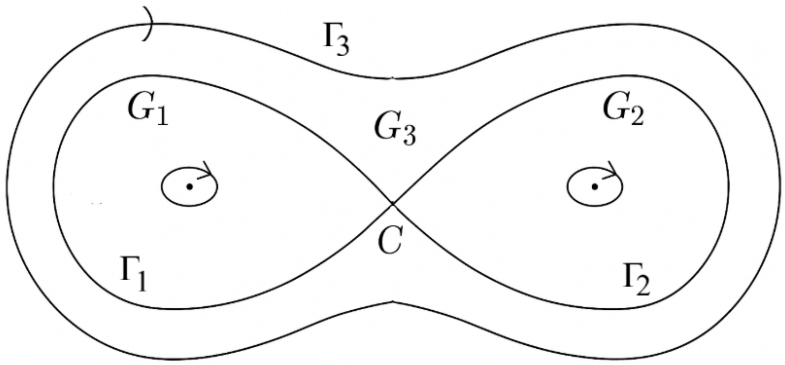

Figure 2.3: Phase-space portrait sketch where the 3 different regions G_1, G_2 and G_3 can be identified (Fig. from [11]).

by each closed curve Γ_i. The scale of the system's energy can be established by adding a suitable constant to the Hamiltonian to set $\mathcal{H}(0,0,\lambda) = 0$, with $\mathcal{H} > 0$ in the outer domain and $\mathcal{H} < 0$ inside G_1 and G_2).

The initial conditions determine in which of the three regions a particle initially moves. Under adiabatic conditions, the parameter λ evolves slowly compared to the characteristic time scale of the system, so that for each value of λ the motion follows the level curves of $\mathcal{H}_\lambda$. In this regime, the area enclosed by the trajectory in phase space, proportional to the action variable, is approximately conserved.

However, when the slow variation of λ causes the geometry of the separatrix to change, a different phenomenon occurs: e.g., if the separatrix shrinks with time, the region that initially contains the trajectory may evolve in such a way that the orbit cannot remain inside it. At this point, the particle is forced to cross the separatrix, passing from one domain to the other. This crossing leads to the breakdown of adiabatic invariance and produces a discrete jump in the value of the action variable, which then settles on a new value.

To describe this process, consider the phase portrait in Fig.2.3. The three dynamical regions G_1, G_2, and G_3 are divided by the separatrix passing through the hyperbolic point (q_C, p_C). As the control parameter λ changes slowly, the enclosed surface of each region evolves accordingly. Suppose, for example, that the lobes G_1 and G_2 expand while λ increases: there will be a specific value $\lambda = \lambda^*$ for which the outer orbit of a particle in G_3 satisfies $A_3(\lambda^*) = 2\pi J_3^*$, which means that its area is equal to that of the separatrix at that instant. time.

The slow time dependence of the system Hamiltonian with respect to $\lambda = \varepsilon t$ can

be treated as a weak perturbation, allowing us to exploit the methods of perturbation theory. By averaging the energy variation over one full revolution around the outer trajectory Γ_3, we obtain

$$\Delta\mathcal{H} = \varepsilon \int_0^T \frac{\partial \mathcal{H}}{\partial \lambda}\Big|_{\lambda^*} \mathrm{d}t = -2\pi\varepsilon \frac{\partial J}{\partial \lambda} = -\varepsilon \frac{\mathrm{d}A_3(\lambda)}{\mathrm{d}\lambda}\,, \tag{2.4.1}$$

where T is the period of the motion along Γ_3. This shows that the Hamiltonian changes by a small quantity proportional to ε per cycle with an error of order $O(\varepsilon^{3/2})$.

At the moment of separatrix crossing, the particle energy $\mathcal{H}^*$ lies in the interval $0 < \mathcal{H}^* < |\Delta\mathcal{H}_3|$, with

$$\Delta\mathcal{H}_3 = \varepsilon \frac{1}{2\pi} \int_{\Gamma_3} p\,\mathrm{d}q = -2\pi\varepsilon \frac{\partial J_3^*}{\partial \lambda}\Big|_{\lambda^*} = -\varepsilon \frac{\mathrm{d}A_3}{\mathrm{d}\lambda}\Big|_{\lambda^*}\,. \tag{2.4.2}$$

Analogously, the variations associated with the inner regions are defined as

$$\Delta\mathcal{H}_1 = -\varepsilon \frac{\mathrm{d}A_1}{d\lambda}\Big|_{\lambda^*}, \qquad \Delta\mathcal{H}_2 = -\varepsilon \frac{\mathrm{d}A_2}{\mathrm{d}\lambda}\Big|_{\lambda^*}. \tag{2.4.3}$$

Since both A_1 and A_2 increase with λ, their derivatives are positive and the corresponding $\Delta\mathcal{H}_i$ are negative. Depending on the value of $\mathcal{H}^*$, there are two possible cases:

- if $0 < \mathcal{H}^* < |\Delta\mathcal{H}_1|$, the trajectory first becomes tangent to Γ_1 and the particle is captured in G_1;
- if $|\Delta\mathcal{H}_1| < \mathcal{H}^* < |\Delta\mathcal{H}_3|$, the crossing occurs through Γ_2, leading to capture in G_2.

Once the particle is captured, its motion becomes bounded within the lobe, performing periodic oscillations along a closed trajectory of constant negative energy $\mathcal{H} < 0$. The trajectory corresponds to a stable orbit that surrounds the centre of the island. The corresponding adiabatic invariant becomes constant again, taking the value $J = A_j(\lambda^*)/(2\pi)$ for the lobe G_j into which the particle has entered. In the adiabatic limit $\varepsilon \to 0$, the post-capture energy approaches 0^-, confirming that the transition occurs exactly at the separatrix.

The exact value of $\mathcal{H}^*$ cannot be predicted deterministically due to the sensitivity to initial action conditions in the limit $\varepsilon \to 0$, and for a ensemble of uniformly distributed initial conditions, the Liouville theorem ensures that $\mathcal{H}^*$ is uniformly distributed in the interval $(0, |\Delta\mathcal{H}_3|)$. The capture in$G_1$ or G_2 is therefore a probabilistic process, and the probability P_i of the transition from G_3 to G_i ($i = 1, 2$) is determined by the relative rate of change of the enclosed areas:

$$P_i = \frac{\Delta\mathcal{H}_i}{\Delta\mathcal{H}_3} = \frac{\mathrm{d}A_i/\mathrm{d}\lambda}{\mathrm{d}A_3/\mathrm{d}\lambda}\Big|_{\lambda=\lambda^*}\,. \tag{2.4.4}$$

These results were obtained considering that the areas of the lobes increase with the parameter λ. More generally, the transition probabilities between regions depend on the relative variations of their areas: if only one lobe gets bigger, capture into that lobe is certain. Hence, the general expression for the transition probability between any two regions G_i and G_j can be written as

$$P_{i\to j} = \max\left\{0, \min\left(\frac{\mathrm{d}A_i/\mathrm{d}\lambda}{\mathrm{d}A_j/\mathrm{d}\lambda}\Big|_{\lambda^*}, 1\right)\right\}, \tag{2.4.5}$$

after capture, under adiabatic conditions, the new action becomes $J = A_j(\lambda^*)/(2\pi)$.

Eventually, an interesting point can be noticed. As we saw, the computation of $\Delta\mathcal{H}$ drags an error of order $O(\varepsilon^{3/2})$. Following the results reported in [25], this implies that a small subset of particles does not follow the prediction given by Eq. (2.4.4). However, the measure of this subset scales as $\sqrt{\varepsilon}$, and thus becomes negligible in the limit of infinitely slow modulation.

2.5 Stochastic dynamics

In many physical systems, the effect of interactions due to collisions when the molecular chaos assumption is satisfied can be described by introducing stochastic effects that simulate a thermal bath. The extension of a Hamiltonian system to include random perturbations uses the results of stochastic dynamical systems and is related to the formulation of stochastic thermodynamics ([29]). In this section, we introduce the mathematical framework used to describe such stochastic dynamics, focusing on how stochastic effects can be incorporated within Hamiltonian theory.

The introduction of a thermal bath for an Hamiltonian system has to consider the fluctuation-dissipation relation that implies the Maxwell-Boltzmann (MB) distribution in the equilibrium state according to the Maximum Entropy Principle. Consider a finite-dimensional phase space with coordinates $x = (q, p) \in \mathbb{R}^{2n}$ and an unperturbed Hamiltonian $\mathcal{H}_0(x)$. The symplectic structure of the phase space allows to write the canonical equations in the form

$$\dot{x} = D_{\mathcal{H}_0} x\,,$$

where we define the Lie operator

$$D_{\mathcal{H}} f = \{f, \mathcal{H}\}\,, \tag{2.5.1}$$

by using the Poisson bracket

$$\{F, G\} = \sum_j \frac{\partial F}{\partial q_j}\frac{\partial G}{\partial p_j} - \frac{\partial F}{\partial p_j}\frac{\partial G}{\partial q_j}\,.$$

We assume that the fluctuation effects are described by $\xi(t$ a stationary stochastic process with zero mean value and a covariance matrix

$$\langle \xi_i(t)\, \xi_j(t+\tau)\rangle = \delta_{ij}\, \phi(\gamma\tau)\,, \qquad \phi(\gamma\tau) \simeq \frac{\gamma}{2} e^{-\gamma|\tau|}\,. \tag{2.5.2}$$

where the quantity γ^{-1} is the correlation scale time of fluctuations that are assumed to be much shorter than the evolution time scale of the unperturbed dynamics $\mathcal{H}_0$. The stochastic dynamics of the Hamiltonian system $\mathcal{H}_0$ in a thermal bath is described by

$$\dot{x} = D_{\mathcal{H}_0} x + \left(-\gamma\{\mathcal{H}_0, \mathcal{H}_1\} + \sqrt{2T\gamma}\xi(t)\right)\, D_{H_1} x\,, \tag{2.5.3}$$

where the interaction Hamiltonian $\mathcal{H}_1(x)$ simulates the dynamics of the interaction with the environment and T is the temperature of the thermal bath. The stochastic equation (2.5.3) generalizes the fluctuation-dissipation relation of Einstein that implies the MB equilibrium distribution for physical systems. Indeed if we compute the dissipation using the average evolution for the Hamiltonian

$$\frac{d\bar{H}_0}{dt} = -\gamma\{H_0, H_1\} D_{H_1}\bar{H}_0 = -\gamma(\{H_0, H_1\})^2$$

and the fluctuation variance

$$\frac{d}{dt}\left\langle (H_0 - \bar{H}_0)^2\right\rangle = 2T\gamma (D_{H_1} H_0)^2 = 2T\gamma(\{H_0, H_1\})^2$$

the ratio between the fluctuation and the dissipation is $2T$. In the case of physical system

$$H_0 = \frac{p^2}{2m} + V(q, \lambda)$$

the choice $H_1 = -\sqrt{m}q$ defines the usual thermal bath for a Boltzmann gas

$$dp = -\frac{\partial V}{\partial q}\, dt + \sqrt{2T\gamma m} dw_t - \gamma p\, dt$$

The arbitrariness in the choice of H_1 understands that the same MB equilibrium highlights to the universality of the MB distribution that allows to describe the equilibrium

stochastic properties of a physical system whose elementary components perform different type of non-linear interactions simulated by the H_1 Hamiltonian.
To study the system (2.5.3) as a diffusion dynamics, we use Stratonovich interpretation to perform the white noise limit $\gamma \to \infty$ for the stochastic noise $\xi(t)$. We recall that Stratonovich interpretation of the stochastic differential equations allows one to perform a perturbation approach to the stochastic Hamiltonian dynamics and to use a covariant description of the motion equation. The interaction Hamiltonian $\mathcal{H}_1$ allows to simulate non-linear interactions between the particle and the environment that define the relaxation process to equilibrium. In the white-noise limit, the Fokker–Planck equation for the probability density $\rho(x,t)$ associated to the stochastic differential equation above reads

$$\frac{\partial \rho}{\partial t} = -\left(D_{\mathcal{H}_0} - \gamma D_{\mathcal{H}_1}\{\mathcal{H}_0, \mathcal{H}_1\}\right)\rho + T\gamma\, D^2_{\mathcal{H}_1}\rho\,. \tag{2.5.4}$$

We look for the equilibrium solution for Eq. 2.5.4 in the form $\rho_{\mathsf{s}}(\mathcal{H}_0)$ and we get the condition

$$\begin{aligned}&\left(-D_{\mathcal{H}_0} + \gamma D_{\mathcal{H}_1}\{\mathcal{H}_0, \mathcal{H}_1\} + T\gamma D^2_{\mathcal{H}_1}\right)\rho_{\mathsf{s}}(\mathcal{H}_0) = \\ &= \gamma D_{\mathcal{H}_1}\left(\{\mathcal{H}_0, \mathcal{H}_1\}\rho_{\mathsf{s}}(\mathcal{H}_0) + T D_{\mathcal{H}_1}\rho_{\mathsf{s}}(\mathcal{H}_0)\right) = 0\,.\end{aligned}$$

Then, if the relation is satisfied

$$\{\mathcal{H}_0, \mathcal{H}_1\}\rho_{\mathsf{s}}(\mathcal{H}_0) + T D_{\mathcal{H}_1}\rho_{\mathsf{s}}(\mathcal{H}_0) = 0\,,$$

we get the stationary solution. Using the property

$$D_{\mathcal{H}_1}\rho_{\mathsf{s}}(\mathcal{H}_0) = \frac{d\rho_{\mathsf{s}}}{d\mathcal{H}_0} D_{\mathcal{H}_1}\mathcal{H}_0\,,$$

it is straightforward to verify that the MB distribution is the equilibrium solution

$$\ln(\rho_{\mathsf{s}}(\mathcal{H}_0)) = -\frac{\mathcal{H}_0}{T} + const. \quad \Rightarrow \quad \rho_{\mathsf{s}}(\mathcal{H}_0) = A(T)\exp\left(-\frac{\mathcal{H}_0(x)}{T}\right)\,. \tag{2.5.5}$$

where $A(T)$ is the partition function

$$A(T) = \int \exp\left(-\frac{\mathcal{H}_0(x)}{T}\right)\mathrm{d}x\,. \tag{2.5.6}$$

In the case of a mechanical system

$$\mathcal{H}_0(q,p) = \frac{p^2}{2m} + V(q)\,,$$

the choice $\mathcal{H}_1 = \sqrt{m}\, q$ defines the usual thermal bath for Eq. (2.5.3)

$$\begin{aligned}\dot{q} &= \frac{p}{m}\,,\\ \dot{p} &= -\frac{\partial V}{\partial q} - \gamma p + \sqrt{2T\gamma m}\,\xi(t)\,.\end{aligned}$$

If we define the current density

$$\mathcal{J} = -\{H_0, H_1\}\rho - T\{\rho, H_1\}\,, \tag{2.5.7}$$

the FP has the continuity form

$$\frac{\partial \rho}{\partial t} = -D_{H_0}\rho - \gamma D_{H_1}\mathcal{J}\,.$$

Introducing the Gibbs' Entropy

$$S(t) = -\int \rho(x,t)\ln\rho(x,t)\,\mathrm{d}x\,, \tag{2.5.8}$$

we compute the entropy production using the solution of the FP equation (2.5.4)

$$\begin{aligned}\frac{dS}{\mathrm{d}t} &= \int [D_{H_0}\rho + \gamma D_{H_1}\mathcal{J}]\ln\rho\,\mathrm{d}x = -\gamma\int \frac{\mathcal{J}}{\rho} D_{H_1}\rho\,\mathrm{d}x\\ &= \frac{\gamma}{T}\int \frac{\mathcal{J}}{\rho}(\mathcal{J} + \{H_0, H_1\}\rho)\,\mathrm{d}x = \frac{\gamma}{T}\int \frac{\mathcal{J}^2}{\rho}\,dx + \frac{\gamma}{T}\int \mathcal{J}\{H_0, H_1\}\,\mathrm{d}x\,.\end{aligned}$$

The parameter γ/T is a scaling factor in entropy production and we distinguish the total entropy production and the dissipated work per unit of time

$$\frac{dS^{\mathrm{tot}}}{\mathrm{d}t} = \frac{\gamma}{T}\int \frac{\mathcal{J}^2}{\rho}\,\mathrm{d}x \qquad W^{\mathrm{dis}} = -\frac{\gamma}{T}\int \mathcal{J}\{H_0, H_1\}\,\mathrm{d}x\,.$$

Since $\mathrm{d}S^{\mathrm{tot}}/\mathrm{d}t \geq 0$ when the density current is $\neq 0$ (i.e. the transformation is not adiabatic), the dissipated work is always non-negative and corresponds to the work performed by the current density which is dissipated and does not contribute to the free-energy change. The adiabatic condition $\mathcal{J} = 0$ during the transformation $\lambda_1 \to \lambda_2$ means that no work performed on (or by) the system is dissipated and contributes to the change in free energy. Due to the definition of thermal bath, $\mathcal{J} = 0$ in the equilibrium state and the total entropy production vanishes since it corresponds to a maximum entropy state. The condition can also be related to the Minimum Entropy Production Principle to characterise the equilibrium state.

2.5.1 Adiabatic Theory for Stochastic Hamiltonians

We consider a stochastic 1D Hamiltonian with a slowly modulated parameter $\lambda = \mu t$

$$\mathcal{H}_0(q,p,\lambda) = \frac{p^2}{2m} + V(q,\lambda)\,, \tag{2.5.9}$$

whose phase space has a bounded region near a stable fixed point. Assuming $\mathcal{H}_1 = -\sqrt{m}q$ we can simulate the effect of a classical thermal bath. We perform the action-angle variables using the covariance properties of the Stratonovich interpretation of Eq. (2.5.3). We have to compute

$$\{\mathcal{H}_0, \mathcal{H}_1\} = -\Omega(I,\lambda)\frac{\partial \mathcal{H}_1}{\partial \theta}(\theta, I, \lambda) = \sqrt{m}\,\frac{\partial \mathcal{H}_0}{\partial p}\bigg|_{q,\lambda}(\theta, I, \lambda)\,,$$

using the properties of the Poisson bracket, and

$$\begin{aligned} D_{\mathcal{H}_1} I &= -\frac{\partial \mathcal{H}_1}{\partial \theta} = \sqrt{m}\,\frac{\partial I}{\partial p}\bigg|_{q,\lambda} = \frac{\sqrt{m}}{\Omega}\frac{\partial \mathcal{H}_0}{\partial p}\,, \\ D_{\mathcal{H}_1}\theta &= \frac{\partial \mathcal{H}_1}{\partial I}\,. \end{aligned}$$

Remark: performing the change of variables in Eq. (2.5.3), λ can be considered a parameter even if $\lambda = \mu t$, but in the computation of the differentials of the new variables, one has to compute the variation with respect to λ. This can be performed maintaining the canonical form by changing the Hamiltonian H_0 according to

$$\mathcal{H}(\theta, I, \lambda) = \mathcal{H}_0(I,\lambda) + \mu\,\frac{\partial F}{\partial \lambda}\bigg|_{q,I}(\theta, I, \lambda)\,,$$

where $F(q, I, \lambda)$ is the generating function for the change in the action-angle of variables.

The stochastic dynamics for the action-angle variables read

$$\begin{aligned} \dot\theta &= \Omega(I,\lambda) + \mu\frac{\partial}{\partial I}\,\frac{\partial F}{\partial \lambda}\bigg|_{q,I} - \gamma\Omega\frac{\partial \mathcal{H}_1}{\partial \theta}\frac{\partial \mathcal{H}_1}{\partial I} + \sqrt{2T\gamma}\frac{\partial \mathcal{H}_1}{\partial I}\xi(t)\,, \\ \dot I &= -\mu\frac{\partial}{\partial \theta}\,\frac{\partial F}{\partial \lambda}\bigg|_{q,I} - \gamma\Omega\left(\frac{\partial H_1}{\partial \theta}\right)^2 - \sqrt{2T\gamma}\frac{\partial \mathcal{H}_1}{\partial \theta}\xi(t)\,. \end{aligned} \tag{2.5.10}$$

where we perform a white noise limit for $\xi(t)$. The existence of a stochastic adiabatic invariance for the action variable is related to the possibility of averaging Eq. (2.5.10)

with respect to the noise realisations and with respect to the angle variable. In the limit of white noise (Stratonovich interpretation) the average action evolution reads

$$\begin{aligned}\langle \Delta I \rangle = &\left[-\mu \frac{\partial}{\partial \theta} \left. \frac{\partial F}{\partial \lambda} \right|_{q,I} - \gamma \Omega \left(\frac{\partial \mathcal{H}_1}{\partial \theta} \right)^2 \right] \Delta t \\ &- \gamma T \left[\frac{\partial^2 \mathcal{H}_1}{\partial \theta^2} \frac{\partial H_1}{\partial I} - \frac{\partial^2 \mathcal{H}_1}{\partial \theta \partial I} \frac{\partial \mathcal{H}_1}{\partial \theta} \right] \Delta t + O(\Delta t^2, \mu^2 \Delta t) \,.\end{aligned}$$

The last term is obtained by the stochastic fluctuations, and it can be written in the form

$$\frac{\partial^2 \mathcal{H}_1}{\partial \theta^2} \frac{\partial \mathcal{H}_1}{\partial I} - \frac{\partial^2 \mathcal{H}_1}{\partial \theta \partial I} \frac{\partial \mathcal{H}_1}{\partial \theta} = \frac{\partial}{\partial \theta} \left[\frac{\partial \mathcal{H}_1}{\partial \theta} \frac{\partial \mathcal{H}_1}{\partial I} \right] - \frac{\partial}{\partial I} \left(\frac{\partial \mathcal{H}_1}{\partial \theta} \right)^2 .$$

The average dynamics for the action can be written in the form

$$\begin{aligned}\langle \Delta I \rangle = &\left[-\mu \frac{\partial}{\partial \theta} \left. \frac{\partial F}{\partial \lambda} \right|_{q,I} - \gamma \Omega \left(\frac{\partial \mathcal{H}_1}{\partial \theta} \right)^2 \right] \Delta t \\ &- \gamma T \left[\frac{\partial}{\partial \theta} \left(\frac{\partial \mathcal{H}_1}{\partial \theta} \frac{\partial \mathcal{H}_1}{\partial I} \right) - \frac{\partial}{\partial I} \left(\frac{\partial \mathcal{H}_1}{\partial \theta} \right)^2 \right] \Delta t + O(\Delta t^2, \mu^2 \Delta t) \,.\end{aligned}$$

Then it is possible to consider the limit of the stochastic process $\bar{I}$ where we also consider the average of the angle variable since the angle is a fast variable and the uniform stationary distribution of the angle can be considered invariant during evolution. The average stochastic process $\bar{I}$ satisfies the stochastic differential equation

$$\begin{aligned}\mathrm{d}\bar{I} = &-\gamma \left[\Omega \left\langle \left(\frac{\partial \mathcal{H}_1}{\partial \theta} \right)^2 \right\rangle_\theta - T \frac{\partial}{\partial I} \left\langle \left(\frac{\partial \mathcal{H}_1}{\partial \theta} \right)^2 \right\rangle_\theta \right] \mathrm{d}t + \\ &+ \sqrt{2T\gamma} \sqrt{\left\langle \left(\frac{\partial \mathcal{H}_1}{\partial \theta} \right)^2 \right\rangle_\theta} \, \mathrm{d}w_t \end{aligned} \tag{2.5.11}$$

This equation holds if the uniform distribution of the angle is preserved in the evolution since the angle variable has a relaxation time faster than the action variable (this can be proven in the limit of small noise). The FP equation for $\bar{\rho}(I,t)$ reads

$$\begin{aligned}\frac{\partial \bar{\rho}}{\partial t} &= \gamma \frac{\partial}{\partial I} \left[\Omega \left\langle \left(\frac{\partial \mathcal{H}_1}{\partial \theta} \right)^2 \right\rangle_\theta - T \frac{\partial}{\partial I} \left\langle \left(\frac{\partial \mathcal{H}_1}{\partial \theta} \right)^2 \right\rangle_\theta \right] \bar{\rho} + \gamma T \frac{\partial^2}{\partial I^2} \left\langle \left(\frac{\partial \mathcal{H}_1}{\partial \theta} \right)^2 \right\rangle_\theta \bar{\rho} \\ &= \gamma \frac{\partial}{\partial I} \left\langle \left(\frac{\partial \mathcal{H}_1}{\partial \theta} \right)^2 \right\rangle_\theta \left[\Omega + T \frac{\partial}{\partial I} \right] \bar{\rho} \,. \end{aligned} \tag{2.5.12}$$

Equation (2.5.12) can describe the evolution of the action distribution far from the separatrix curves where $\Omega \to 0$. In the case of physical systems, (cf. Eqs. (2.5.9) and $\mathcal{H}_1 = -\sqrt{m}q$)

$$\left\langle \left(\frac{\partial H_1}{\partial \theta} \right)^2 \right\rangle_\theta = \frac{1}{\Omega^2} \left\langle \left(\frac{\partial \mathcal{H}_0}{\partial p} \right)^2 \right\rangle_\theta = \frac{1}{\Omega^2} \left\langle \frac{p^2}{m} \right\rangle ,$$

that highlights as we have a singularity when $\Omega \to 0$. Far from the separatrix the $\bar{\rho}(I,t)$ is regular, and for a fixed λ (frozen system) the equilibrium condition reads

$$\left[\Omega + T \frac{\partial}{\partial I} \right] \bar{\rho}_{eq}(I,\lambda) = 0 \quad \Rightarrow \quad \rho_{eq}(I) \propto \exp\left(-\frac{\mathcal{H}_0}{T} \right) ,$$

but we should introduce the boundary condition when I increases. Moreover, the angle dynamics is not fast near the separatrix, and the averaging procedure is not justified.

2.5.2 Adiabatic character of the action distribution

If one considers the evolution of the distribution function $\rho(I,t)$ average on the angle variables we get the conjugated operator of Eq. (2.5.11): i.e the average FP equation (see Eq. (2.5.12))

$$\frac{\partial \bar{\rho}}{\partial t} = \gamma \frac{\partial}{\partial I} \left\langle \left(\frac{\partial \mathcal{H}_1}{\partial \theta} \right)^2 \right\rangle_\theta \left[\Omega(I) \bar{\rho} + T \frac{\partial \bar{\rho}}{\partial I} \right] + O(\mu^2) , \tag{2.5.13}$$

with an error $O(\mu^2)$ that we neglect if $\mu \ll \gamma$. Remark: the dissipation γ^{-1} is a relaxation time scale, so we have to consider the relation between the adiabatic time scale μ^{-1} and the relaxation time scale. The adiabatic assumption $\mu^{-1} \gg \gamma^{-1}$ means that we have the adiabatic approximation for the evolution of the distribution function

$$\Omega \bar{\rho} + T \frac{\partial \bar{\rho}}{\partial I} \simeq 0 \quad \Rightarrow \quad \rho_{\mathrm{ad}}(I,t) = A^{-1}(\mu t) \exp\left(-\frac{\mathcal{H}_0(I,\mu t)}{T} \right) ,$$

and the partition function reads

$$A(\mu t) = \int \exp\left(-\frac{\mathcal{H}_0(I,\mu t)}{T} \right) \mathrm{d}I .$$

Using the partition function $A(\lambda, T)$ we define the Helmholtz Free Energy potential

$$F(\lambda) = -T \ln A(T,\lambda) = -T \ln \int \exp\left(-\frac{\mathcal{H}_0(x,\lambda)}{T} \right) dx$$

which satisfies the relation

$$dF = dE - TdS$$

By definition, we have

$$\frac{dF}{d\lambda} = \int \frac{\partial \mathcal{H}_0}{\partial \lambda}(x,\lambda)\rho_{ad}(x,\lambda)dx \tag{2.5.14}$$

that can be defined as the work performed δW by an infinitesimal change $d\lambda$ in an adiabatic transformation.

In this case, the distribution is independent of the initial condition and the system is in thermal equilibrium. The adiabatic approximation assumes the quasi-stationary condition for the slowly modulated FP equation: the expected error can be computed in a perturbation way, let

$$\rho(I,t) = \rho_{\rm ad}(I,\mu t) + \mu\Delta\rho(I,t) + O(\mu^2)\,.$$

A direct calculation provides

$$\frac{\partial \rho}{\partial t} = \gamma \frac{\partial}{\partial I} D(I)\left[\Omega(I,\lambda)\Delta\rho + T\frac{\partial \Delta\rho}{\partial I}\right] - \mu\frac{\partial \rho_{\rm ad}}{\partial \lambda}\,,$$

where we set

$$D(I) = \left\langle \left(\frac{\partial \mathcal{H}_1}{\partial \theta}\right)^2 \right\rangle_\theta .$$

We observe that by scaling the time we define the adiabatic parameter by the ratio μ/γ and require the condition $\mu/\gamma \ll 1$. Using the relation

$$\begin{aligned}\frac{\partial}{\partial \lambda} A^{-1}(\lambda)\exp\left(-\frac{H_0(I,\lambda)}{T}\right) &= \frac{1}{T}\left[\left.\frac{\partial \mathcal{H}_0}{\partial \lambda}\right|_I - \int \left.\frac{\partial \mathcal{H}_0}{\partial \lambda}\right|_I \rho_{\rm ad}(I,\lambda)\,dI\right]\rho_{\rm ad}(I,\lambda) \\ &= \frac{1}{T}\left[\left.\frac{\partial \mathcal{H}_0}{\partial \lambda}\right|_I - \left\langle \left.\frac{\partial \mathcal{H}_0}{\partial \lambda}\right|_I \right\rangle\right]\rho_{\rm ad}(I,\lambda)\end{aligned}$$

we see that $\partial\rho_{\rm ad}/\partial\lambda$ does not have a component in the kernel of the FP operator. We recall the thermodynamic interpretation of the isotherm transform and recognise in the previous formula the difference between the change of the Helmholtz free energy (2.5.14) and the average work performed during a non-adiabatic transformation of the action $I(t;\xi)$ (but we average over the angle variables assuming that this is the stationary condition). If we introduce the evolution operator

$$\Phi_0^t = \exp\left(t\gamma\frac{\partial}{\partial I}D(I)\left[\Omega(I,\lambda) + T\frac{\partial}{\partial I}\right]\right) = \exp\left(t\gamma\mathcal{L}_{FP}(I)\right)\,,$$

which solves the FP equation (2.5.13) for fixed λ, we formally have

$$\Delta\rho(I,t) = -\mu \int_0^t \Phi_s^t \, ds \left[\frac{\partial \rho_{\rm ad}}{\partial \lambda}(I,\lambda) \right] + O(\mu^2) \,,$$

restricted to the invariant space where the operator is invertible. A direct calculation provides

$$\exp\left(\frac{\mathcal{H}_0}{2T}\right) \mathcal{L}_{FP}(I) \exp\left(-\frac{\mathcal{H}_0}{2T}\right) = T\frac{\partial}{\partial I} D \frac{\partial}{\partial I} + \frac{1}{2}\left[\frac{\partial}{\partial I} D\Omega - \Omega D \frac{\partial}{\partial I}\right] - \frac{\Omega^2}{4T} D \,,$$

that is a self-adjoint operator, and the eigenvalues of the FP operator $\mathcal{L}_{FP}$ are all real and negative except the null one. Then the evolution operator Φ_s^t is a contraction, and we have the estimate

$$\lim_{t\to\infty} \|\Delta\rho(I,t)\| \leq \lambda_{\rm min}^{-1} \left\| \frac{\partial \rho_{\rm ad}}{\partial \lambda} \right\| + O(\mu t) \,,$$

where $\lambda_{\rm min}$ is the Fiedler eigenvalue of the FP operator. If $\lambda_{min} = O(1)$ the previous results implies that $\Delta\rho$ is bounded $O(1)$ for a time $t \propto \mu^{-1}$ and the adiabatic stationary distribution approximates the real distribution with an error $O(\mu)$: i.e. it is an adiabatic invariant for the stochastic dynamics. This result does not hold near a separatrix curve and during the phenomenon of separatrix crossing the distribution changes.

When the phase space is divided into different regions by the separatrix curves, the previous results apply to each region separately but one has to assume that the transition rate among the regions is much smaller than the modulation time scale otherwise the particles can be escape from the resonance and the trapping is not effective. The transition rate among different resonance regions can be estimated by using the Kramer's Theory of transition rate.

2.5.3 Reaction-rate theory

We have just seen how we can use stochastic differential equations to describe the evolution of systems subjected to random effects caused by their interaction with the environment. An interesting model in this context, which is common in many diverse fields such as molecular physics, optics (see, e.g., Ref. [22]), is the double-well model, namely a system with two potential wells divided by a potential barrier.

Within this configuration, consider a particle that is trapped inside one of the two wells. In a purely deterministic system, the only possibility the particle has to escape is to have an energy that exceeds the height of the barrier. This is not true in stochastic systems, since the presence of noise can cause the particle to escape due to random energy kicks. Therefore, one might consider measuring the stability properties of the

wells as a function of dissipation and noise, such as the rate of transition between the wells, the average trapping time, the trapping efficiency, and so on. This kind of analysis has been performed by H. Kramers in 1940, within its article on the Brownian motion modelling of chemical reactions (Ref. [19]). The present chapter is thought to reconstruct the Kramers' reaction rate theory, taking advantage also of the review in [16], in addition to the original article.

Let us consider a one-dimensional system characterised by a potential function $U(x)$ with a local minimum at x_a and a local maximum at x_b, separated by a height barrier $\Delta U = U(x_\mathsf{b}) - U(x_\mathsf{a})$. In addition, denote by $\omega_\mathsf{a} = \sqrt{U''(x_\mathsf{a})}$ the frequency at the bottom of the well and by $\omega_\mathsf{b} = \sqrt{|U''(x_\mathsf{b})|}$ the characteristic frequency at the top of the barrier.

The Langevin equations describing the motion of a particle of unit mass, subject to damping γ and stochastic noise $\xi(t)$, are

$$\dot{q} = p\,, \qquad \dot{p} = -U'(x) - \gamma p + \sqrt{2T\gamma}\xi(t)\,, \tag{2.5.15}$$

where $\xi(t)$ is white noise: $\langle \xi(t) \rangle = 0$ and $\langle \xi(t)\, \xi(t+\tau) \rangle = \delta(\tau)$. The associated FP equation for the probability density $\rho(q,p,t)$ reads

$$\frac{\partial \rho}{\partial t} = -p\,\frac{\partial \rho}{\partial q} + \frac{\partial}{\partial p}\left(U'(q)\rho + \gamma p \rho\right) + \gamma T\,\frac{\partial^2 \rho}{\partial p^2}\,. \tag{2.5.16}$$

This equation describes the probability flow in the two-dimensional phase space (q,p), where the last term represents the diffusion induced by the stochastic force, while the middle term accounts for the deterministic and dissipative drift.

In the limit of strong damping $\gamma \gg \omega_\mathsf{b}$, the momentum relaxes much faster than the coordinate q, so that p can be considered as a fast variable. For this reason, we can obtain the Smoluchowski equation by computing the marginal probability density $f(q,t)$ of p, as:

$$\frac{\partial f}{\partial t} = \frac{\partial}{\partial q}\left[U'(q)\, f + T\,\frac{\partial f}{\partial q}\right]\,. \tag{2.5.17}$$

where time t is rescaled by γ. In the opposite regime of weak damping $\gamma \ll \omega_\mathsf{b}$, the evolution is governed by slow diffusion in the energy space, and the relevant stochastic variable becomes energy E, whose dynamics can be described by the Fokker–Planck equation for the energy distribution $\rho(E,t)$. In both cases, one looks for a quasi-stationary solution that represents the steady probability current J that escapes the potential well.

Assuming that the system is close to the local equilibrium in the well, the stationary solution can be written as $\rho_\mathsf{s}(q,p) \propto \exp(-U(q)/\sigma^2)$, and a small probability flux J across the barrier can be obtained by matching the local equilibrium solution with the

outgoing current at q_{b}. The escape rate k is defined as the ratio between the flux across the barrier and the population inside the well:

$$k = \frac{J}{N_{\mathsf{a}}}\,, \qquad N_{\mathsf{a}} = \int_{\mathsf{well}} f(q)\,\mathrm{d}q\,. \tag{2.5.18}$$

In the steady-state regime, J is constant and represents the net rate of transitions from the metastable state q_{a} to the region beyond the barrier.

Under these assumptions, we can derive different asymptotic forms of the rate depending on the damping regime. In the full intermediate–friction regime, the escape rate is given by the Kramers formula:

$$k = \frac{\lambda_+}{\omega_{\mathsf{b}}}\frac{\omega_{\mathsf{a}}}{2\pi}\exp\!\left(-\frac{\Delta U}{T}\right), \tag{2.5.19}$$

and

$$\lambda_+ = \frac{1}{2}\left[\gamma + \sqrt{\gamma^2 + 4\omega_{\mathsf{b}}^2}\right] \tag{2.5.20}$$

is the positive eigenvalue associated with the linearised dynamics near the top of the barrier. This expression can be rewritten in equivalent form

$$k = \frac{\left(\frac{\gamma^2}{4} + \omega_{\mathsf{b}}^2\right)^{1/2} - \frac{\gamma}{2}}{\omega_{\mathsf{b}}}\,\frac{\omega_{\mathsf{a}}}{2\pi\,\omega_{\mathsf{b}}}\exp\!\left(-\frac{\Delta U}{T}\right). \tag{2.5.21}$$

Based on the damping regime, one can find a simpler expression for the overdamped and underdamped limits.

In the overdamped limit, the escape is limited by the diffusion across the potential barrier, yielding

$$k_{\mathsf{over}} = \frac{\omega_{\mathsf{a}}}{2\pi}\,\frac{\omega_{\mathsf{b}}}{\gamma}\,\exp\!\left(-\frac{\Delta U}{T}\right), \tag{2.5.22}$$

where factor $\omega_{\mathsf{a}}\omega_{\mathsf{b}}/(2\pi\gamma)$ depends on the curvature of the potential at the minimum and at the saddle point, while the exponential term accounts for the Boltzmann factor associated with the activation over the barrier. In the underdamped regime, instead, the escape is controlled by the slow diffusion in energy, and the rate scales linearly with γ:

$$k_{\mathsf{under}} = C\,\gamma\,\exp\!\left(-\frac{\Delta U}{T}\right), \tag{2.5.23}$$

where C is a prefactor determined by the local properties of the potential and the energy-diffusion coefficient.

The physical meaning of the escape rate k is directly related to the probability of remaining inside the potential well. The average survival time τ_{s} is the inverse of the rate,

$$\tau_{\mathsf{s}} = \frac{1}{k}\,, \tag{2.5.24}$$

and represents the typical time scale over which a particle escapes the well due to stochastic fluctuations. Consequently, the survival probability decays exponentially in time as $P(t) = \exp(-kt)$ in the stationary regime. The *trapping efficiency* can thus be expressed as the fraction of trajectories that remain confined over a given time, which, for slowly varying parameters, can be approximated by

$$\eta \simeq \exp\!\left(-\int k(t)\,\mathrm{d}t\right)\,. \tag{2.5.25}$$

When two potential wells are present, the exchange of probability between them can be described by a two-state kinetic model:

$$\dot{N}_{\mathsf{a}} = -k_{\mathsf{a}\to\mathsf{b}}N_{\mathsf{a}} + k_{\mathsf{b}\to\mathsf{a}}N_{\mathsf{b}}\,, \qquad \dot{N}_{\mathsf{b}} = -k_{\mathsf{b}\to\mathsf{a}}N_{\mathsf{b}} + k_{\mathsf{a}\to\mathsf{b}}N_{\mathsf{a}}\,, \tag{2.5.26}$$

where $k_{\mathsf{a}\to\mathsf{b}}$ and $k_{\mathsf{b}\to\mathsf{a}}$ are the forward and backward transition rates. The stationary current between the two states reads

$$J = k_{\mathsf{a}\to\mathsf{b}}N_{\mathsf{a}} - k_{\mathsf{b}\to\mathsf{a}}N_{\mathsf{b}}\,. \tag{2.5.27}$$

In thermodynamic equilibrium, detailed balance implies $J = 0$, and the ratio of the transition rates satisfies

$$\frac{k_{\mathsf{a}\to\mathsf{b}}}{k_{\mathsf{b}\to\mathsf{a}}} = \exp\!\left(-\frac{U(q_{\mathsf{b}}) - U(q_{\mathsf{a}})}{T}\right)\,, \tag{2.5.28}$$

in analogy with the MB distribution obtained previously.

Chapter 3

The model

3.1 Motivation

The manipulation of longitudinal beam distributions has become an increasingly important topic in accelerator physics. Controlling beam stability requires achieving specific distribution shapes, managing the spread in energy and time, and modulating the transport of particles between stable regions of phase space. These operations are particularly critical in lepton colliders, where dissipative effects and stochastic perturbations complicate the beam dynamics and require advanced theoretical and numerical approaches.

This work focuses on the adiabatic manipulation of longitudinal distributions in systems subject to these effects. Non-linear beam manipulation techniques have been extensively developed for hadron accelerators, exploiting phenomena such as resonance trapping and phase-space transport. However, extending these methods to lepton colliders requires a rigorous adiabatic framework for stochastically perturbed Hamiltonian systems, which is still lacking.

The first part of this study recovers the equations of motion for a Hamiltonian model with external phase modulation, introduced in Chap. 1.4, analysing its deterministic dynamics and comparing the analytical results with the predictions of standard Hamiltonian theory. This approach is particularly suited for simulating phenomena in hadron accelerators, where damping and stochastic effects from synchrotron radiation can be neglected.

In contrast, in lepton accelerators, the small particle mass makes damping and random fluctuations significant. To account for this, the model is extended to include these effects, allowing the study of their impact on beam stability with respect to the hadron case. This is achieved by modelling the longitudinal motion as the one of a particle interacting with a thermal bath: energy damping corresponds to friction-like forces, while stochastic fluctuations are represented as random collisions with the bath particles.

Within this framework, the interplay of fluctuation and dissipation naturally leads to an isothermal process. The following sections are organised to reflect this logical construction, moving from the deterministic hadron-like model to the stochastic framework.

3.2 Theoretical aspects

Let us now introduce the standard Hamiltonian model for synchrotron motion, which is essentially the one already presented in Sects. 1.4.1 and 1.4.2. Then, the damping term and the random noise expressions are derived and included in the equations, representing the complete equations of motion for the stochastic model.

Recall that the motion of particles in the longitudinal plane is determined by how the beam interacts with the RF cavities, which provides the electric field to accelerate them. The synchronous particle is perfectly tuned to the RF frequency, gaining the energy required to keep circulating. Instead, all the other particles produce *synchrotron oscillations* back and forth with respect to the synchronous one.

For a sinusoidal electric field $\mathcal{E} = \mathcal{E}_0 \sin(h\omega_{\mathsf{rev}} t + \phi_{\mathsf{s}})$, the corresponding synchrotron equations of motion read:

$$\dot{\phi} = h\omega_{\mathsf{rev}}\eta_{\mathsf{s}}\,\delta + a\omega_{\mathrm{m}}\cos(\omega_{\mathrm{m}}t + \psi_0) \qquad \dot{\delta} = \frac{\omega_{\mathsf{rev}} eV}{2\pi E_{\mathsf{s}}\beta_{\mathsf{s}}^2}\left(\sin\phi - \sin\phi_{\mathsf{s}}\right)\,. \tag{3.2.1}$$

From now on, we will stick to the case of a stationary bucket, namely $\phi_{\mathsf{s}} = \pi$. This corresponds to the situation where the RF cavities simply restore the exact amount of energy lost due to damping.

3.2.1 Derivation of the stochastic synchrotron equations

In order to derive the damping contribution, the rate of change of the energy deviation must now take into account both the energy provided by the RF cavity and the energy radiated by the particle. The general expression reads:

$$\frac{\mathrm{d}E}{\mathrm{d}t} = \frac{U_{\mathsf{RF}}(\tau) - U(E)}{T_{\mathsf{rev}}}\,, \tag{3.2.2}$$

where T_{rev} is the revolution period, $U_{\mathsf{RF}}(\tau)$ is the energy gained from the RF system, and $U(E)$ is the energy lost through radiation. τ denotes the particle arrival–time deviation with respect to the synchronous particle, i.e. the time delay such that a particle arriving later has $\tau > 0$.

For small oscillations, both quantities can be expanded to first order as:

$$U_{\mathsf{RF}}(\tau) \simeq U_0 + e\dot{V}(\pi)\,\tau, \qquad U(E) = U_0 + W\,\Delta E\,, \tag{3.2.3}$$

where $\dot{V}(\pi) = -h\omega_{\text{rev}}V_{\text{s}}$ and $W = \frac{\mathrm{d}U}{\mathrm{d}E}\big|_{E_{\text{s}}}$.
Substituting these expansions into Eq. (3.2.2) gives:

$$\frac{\mathrm{d}E}{\mathrm{d}t} = -\frac{eh\omega_{\text{rev}}V_{\text{s}}}{T_{\text{rev}}}\,\tau - \frac{W}{T_{\text{rev}}}\,\Delta E\,. \tag{3.2.4}$$

Recalling that $\delta = \frac{\omega_{\text{rev}}}{E_{\text{s}}\beta_{\text{s}}^2}\left(\frac{\Delta E}{\omega_{\text{rev}}}\right)$ and differentiating with respect to time, Eq. (3.2.2) becomes

$$\dot{\delta} = -\frac{eh\omega_{\text{rev}}V_{\text{s}}}{E_{\text{s}}\beta_{\text{s}}^2T_{\text{rev}}}\,\tau - \frac{W}{E_{\text{s}}\beta_{\text{s}}^2T_{\text{rev}}}\,\Delta E\,. \tag{3.2.5}$$

From this last expression, the following quantity can be defined:

$$\alpha_{\text{E}} = \frac{W}{2T_{\text{rev}}}\,. \tag{3.2.6}$$

We refer to α_{E} as the *damping rate*, i.e. the quantity which measures how quickly energy oscillations are damped due to synchrotron radiation losses. Thus, we arrive at the compact form:

$$\dot{\delta} = -\frac{h\,eV_{\text{s}}\omega_{\text{rev}}}{E_{\text{s}}\beta_{\text{s}}^2T_{\text{rev}}}\,\tau - 2\frac{\alpha_E}{\beta_{\text{s}}^2}\,\delta\,. \tag{3.2.7}$$

Note that in storage rings, we can find the explicit expression for α_{E} as:

$$\alpha_{\text{E}} = \frac{U_0}{2T_{\text{rev}}E_{\text{s}}}\,(2+\mathcal{D}) \qquad \mathcal{D} = \frac{1}{2\pi}\oint \mathrm{d}s\,D(s)\left[\frac{1}{\rho^2} + 2K(s)\right]_{\text{dipoles}}\,, \tag{3.2.8}$$

where $\mathcal{D}$ is the damping partition number, $D(s)$ is the dispersion function, and the integral is calculated only over the dipoles. Therefore, Eq. (3.2.7) shows that the energy oscillations are now subject to a damping term proportional to δ, meaning that larger energy deviations with respect to the synchronous particle lead to higher losses for synchrotron emission.

Eq. (3.2.7) can be recast in order to highlight the dependence on the angular variable ϕ. Since the RF field oscillates with frequency $h\omega_{\text{rev}}$, during this delay the field phase advances by $h\omega_{\text{rev}}\tau$. Therefore, the late particle "sees" the field at a phase

$$\phi = \phi_{\text{s}} + \Delta\phi = \pi + h\omega_{\text{rev}}\tau\,, \tag{3.2.9}$$

or equivalently:

$$\tau = \frac{\phi - \pi}{h\omega_{\text{rev}}}\,. \tag{3.2.10}$$

Substituting this expression into Eq. (3.2.7) gives

$$\dot{\delta} = -\frac{eV_s\omega_{rev}}{2\pi E_s\beta_s^2}(\phi - \pi) - 2\frac{\alpha_E}{\beta_s^2}\,\delta\,. \tag{3.2.11}$$

In Sect. 1.4.1, we saw that the particles oscillate around the synchronous particle with frequency

$$\omega_s = \omega_{rev}\sqrt{\frac{h\,eV\eta_s}{2\pi E_s\beta_s^2}}\,, \tag{3.2.12}$$

and since

$$\frac{h\,eV_s\omega_{rev}^2}{2\pi E_s\beta_s^2} = \frac{\omega_s^2}{\eta_s}\,, \tag{3.2.13}$$

Eq. (3.2.7) can equivalently be written as:

$$\dot{\delta} = -\frac{\omega_s^2}{h\eta_s\omega_{rev}}\,\tau - 2\frac{\alpha_E}{\beta_s^2}\,\delta\,. \tag{3.2.14}$$

Alternatively, one can approximate Eq. (3.2.11) as:

$$\dot{\delta} = \omega_s\sqrt{\frac{eV}{2\pi E_s\beta_s^2\eta_s}}\,\sin\phi - 2\frac{\alpha_E}{\beta_s^2}\,\delta\,. \tag{3.2.15}$$

Indeed, for small oscillations around the synchronous phase $\phi_s = \pi$ the two forms are approximately equivalent, since $\sin\phi \approx -(\phi - \pi)$.

Lastly, let us find the expression for stochastic fluctuations due to the discrete quantum nature of photon emission. Noise is modelled as a term of white-noise with amplitude determined by the diffusion coefficient, as we saw in (1.4.39). From the Einstein condition, we can write the diffusion coefficient in the general form

$$D \;=\; \sqrt{2\,T\gamma\,m} = \sqrt{\frac{4\,\alpha_E}{\beta_s^2 h\eta_s\omega_{rev}}\,T}\,. \tag{3.2.16}$$

where T is the effective temperature of the system, $\gamma = 2\alpha_E/\beta_s^2$ is the damping coefficient and $m = 1/(h\eta_s\omega_{rev})$ is the effective mass.

We can now express the effective temperature T in terms of the equilibrium variance of the variable δ. In stationary conditions:

$$T \;=\; \frac{\langle\delta^2\rangle}{2m} \;=\; \frac{h\eta_s\,\omega_{rev}}{2}\,\langle\delta^2\rangle\,, \tag{3.2.17}$$

and using

$$\langle \delta^2 \rangle \;=\; \left(\frac{\sigma_E}{E_\mathrm{s}\,\beta_\mathrm{s}^2}\right)^2 \;=\; \frac{\gamma_\mathrm{s}^2}{2\beta_\mathrm{s}^4}\,\frac{C_q}{\rho}\,, \tag{3.2.18}$$

we obtain the explicit expression

$$T \;=\; \frac{\gamma_\mathrm{s}^2\, h\eta_\mathrm{s}\,\omega_\mathrm{rev}}{4\,\beta_\mathrm{s}^4}\;\frac{C_\mathrm{q}}{\rho}\,. \tag{3.2.19}$$

where $C_\mathrm{q} = 3.83 \times 10^{-13}\,\mathrm{m}$.

We can finally bring together all the obtained results to write the equations of motion for the stochastic system, as:

$$\begin{aligned}
\dot{\phi} \;&=\; h\eta_\mathrm{s}\omega_\mathrm{rev}\,\delta + a\omega_\mathrm{m}\cos(\omega_\mathrm{m}t+\psi_0)\,,\\
\dot{\delta} \;&=\; \omega_\mathrm{s}\sqrt{\frac{eV}{2\pi E_\mathrm{s}\beta_\mathrm{s}^2\eta_\mathrm{s}}}\,\sin\phi - 2\frac{\alpha_E}{\beta_\mathrm{s}^2}\,\delta + \frac{\gamma_\mathrm{s}}{\beta_\mathrm{s}^3}\sqrt{\frac{\alpha_\mathrm{E}C_q}{\rho}}\,\xi(t)\,.
\end{aligned} \tag{3.2.20}$$

From the deterministic part of Eqs. (3.2.20), we can read the Hamiltonian whose canonical equations reproduce the conservative dynamics. Indeed, the time-dependent Hamiltonian

$$\mathcal{H}(\phi,\delta,t) = \frac{1}{2}\,h\eta_\mathrm{s}\omega_\mathrm{rev}\,\delta^2 + \;\frac{\omega_\mathrm{rev}eV_\mathrm{s}}{2\pi E_\mathrm{s}\beta_\mathrm{s}^2}\cos\phi + a\omega_\mathrm{m}\,\delta\cos(\omega_\mathrm{m}t+\psi_0) \tag{3.2.21}$$

yields the deterministic terms of the equations of motion through Hamilton's equations.

3.3 Adiabatic capture into resonance

In the present section, we apply to our model the analytical framework for the description of adiabatic resonance crossing in a nonlinear Hamiltonian system. When a slowly varying external parameter drives the system through a 1:1 resonance, the phase–space structure changes, i.e. a stable island where particles can be trapped is formed. By tuning the modulation parameters, the island size and shape can be varied and different trapping probabilities are obtained. To this end, the derivation is inspired by the work of A. Neishtadt in Ref. [26].

Consider the one-dimensional Hamiltonian of our system given by Eq. (3.2.21). The following change of variable can be made

$$P = \zeta\,\delta\,, \qquad Q = \frac{\phi+\pi}{\zeta}\,, \qquad\qquad \zeta^2 = h\eta_\mathrm{s}\omega_\mathrm{rev}\,, \tag{3.3.1}$$

and the Hamiltonian becomes

$$\mathcal{H}(P,Q) = \frac{P^2}{2} - A^2\cos(\zeta Q) + \frac{a\omega_{\rm m}}{\zeta}P\cos(\psi+\psi_0)\,, \qquad A = \frac{\omega_{\rm s}}{\zeta}\,, \tag{3.3.2}$$

with $\psi = \omega_{\rm m}t$.

Let us now focus on the unpertubed Hamiltonian:

$$\mathcal{H}_0(Q,P) = \frac{P^2}{2} - A^2\cos(\zeta Q)\,. \tag{3.3.3}$$

Since the system has one degree of freedom, it is automatically integrable and the energy $h_0 = \mathcal{H}_0(Q,P)$ is a first integral. This means that trajectories on the (Q,P) plane can be parametrised through the action-angle variables.

Let us define the following parameter:

$$\kappa^2 = \frac{1}{2}\left(1 + \frac{h_0}{A^2}\right), \tag{3.3.4}$$

which defines the different domains in phase-space. Indeed, $\kappa^2 = 1$ identifies the separatrix, which divides the phase-space regions of bounded oscillations for $0 \leq \kappa^2 < 1$, and the region of rotations for $\kappa > 1$, as it can be seen in Fig. 3.1. We will stick to the case of $0 \leq \kappa^2 < 1$.

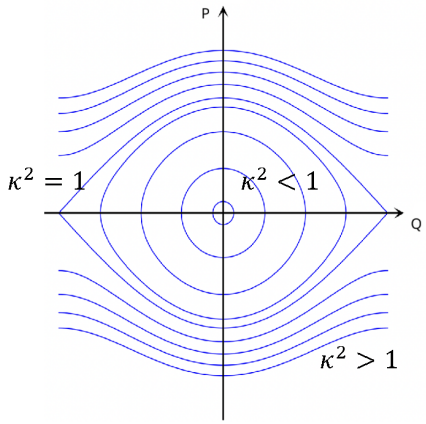

Figure 3.1: Phase-space for the non-linear pendulum in (Q,P) coordinates (from [4]).

The action variable, as a function of the energy h_0 of the unperturbed pendulum, can be found as:

$$I(h_0) = \frac{8A}{\pi}\left[E(\kappa) - (1-\kappa^2)K(\kappa)\right]\,, \tag{3.3.5}$$

where $E(\kappa)$ and $K(\kappa)$ are the complete elliptic integrals of the second and the first kind, respectively:

$$E(\kappa) = \int_0^{\frac{\pi}{2}} \mathrm{d}u \, \sqrt{1 - \kappa^2 \sin^2 u}\,, \tag{3.3.6}$$

$$K(\kappa) = \int_0^{\frac{\pi}{2}} \mathrm{d}u \, \frac{1}{\sqrt{1 - \kappa^2 \sin^2 u}}\,. \tag{3.3.7}$$

Then, the angle variable θ can be obtained by inverting one of the two following expressions for Q and P:

$$\begin{aligned} Q &= \frac{2}{\zeta} \arccos\left(\mathsf{dn}\left(\frac{A}{\Omega(\kappa)}\theta, \kappa\right)\right)\,, \\ P &= 2\kappa A \,\mathsf{cn}\left(\frac{A}{\Omega(\kappa)}\theta, \kappa\right)\,, \end{aligned} \tag{3.3.8}$$

where cn and dn are Jacobi elliptic functions and

$$\Omega(\kappa) = \frac{\pi}{2}\frac{A}{K(\kappa)} \tag{3.3.9}$$

is the frequency of the unperturbed pendulum outside the small-oscillation approximation. We can obtain a Cartesian representation through the action-angle coordinates as:

$$\begin{aligned} X &= \sqrt{2I}\cos\theta \\ Y &= -\sqrt{2I}\sin\theta\,. \end{aligned} \tag{3.3.10}$$

The Jacobi elliptic function $\mathsf{cn}\left(\frac{A}{\Omega(\kappa)}\theta, \kappa\right)$ can then be expanded (see Ref. [5]) as:

$$\mathsf{cn}\left(\frac{A}{\Omega(\kappa)}\theta, \kappa\right) = \frac{2\pi}{\kappa K(\kappa)} \sum_{n=0}^{\infty} \frac{q^{n+\frac{1}{2}}}{1+q^{2n+1}} \cos\left[(2n+1)\frac{\pi A}{2K\Omega(\kappa)}\theta\right]\,. \tag{3.3.11}$$

where $q = \mathsf{exp}\left(-\pi\frac{K(1-\kappa^2)}{K(\kappa)}\right)$.

Substituting Eqs. (3.3.9) and (3.3.11) into Eq. (3.3.8) leads to the following:

$$P = 2A\frac{2\pi}{K(\kappa)} \sum_{n=0}^{\infty} \frac{q^{n+\frac{1}{2}}}{1+q^{2n+1}} \cos[(2n+1)\theta]\,. \tag{3.3.12}$$

It is useful to introduce a new set of coordinates $(\tilde{I}, \gamma)$, where $\gamma = \theta - \psi$ is a slow variable, through the following generating function:

$$W(\tilde{I}, \theta) = \tilde{I}(\theta - \psi)\,, \tag{3.3.13}$$

from which we immediately find the new action as

$$I = \frac{\partial W(\tilde{I}, \theta)}{\partial \theta} = \tilde{I}\,. \tag{3.3.14}$$

Close to the resonance, we have $\dot{\gamma} = 0$, that is, $\dot{\theta} = \omega_{\mathrm{m}}$. Since $\dot{\theta} = \Omega$, we get the expression of the resonant condition, namely

$$\Omega = \omega_{\mathrm{m}} \tag{3.3.15}$$

for a resonance $1:1$ between the unperturbed pendulum and the external modulation. The new expression for the Hamiltonian reads:

$$\tilde{\mathcal{H}}(\tilde{I}, \gamma) = \mathcal{H}(\tilde{I}, \gamma) + \frac{\partial W(\tilde{I}, \theta)}{\partial t} = \mathcal{H}(\tilde{I}, \gamma) - \tilde{I}\omega_{\mathrm{m}}\,. \tag{3.3.16}$$

From now on, the tildes will be omitted.

Regarding $Q = Q(\theta)$, its Fourier expansion can be found to be the primitive of (3.3.12). Since:

$$\dot{Q} = \frac{\partial \mathcal{H}_0}{\partial P} = P\,, \tag{3.3.17}$$

the relation between the two coordinates is given by

$$\dot{Q} = \frac{\mathrm{d}Q}{\mathrm{d}t} = \frac{\partial Q}{\partial \theta}\frac{\partial \theta}{\partial t} = \frac{\partial Q}{\partial \theta}\Omega = P\,. \tag{3.3.18}$$

This leads to

$$Q = \frac{1}{\Omega(\kappa)}\int \mathrm{d}\theta\, P(\theta) = 8\int \mathrm{d}\theta \sum_{n=0}^{\infty} \frac{q^{n+\frac{1}{2}}}{1+q^{2n+1}}\cos[(2n+1)\theta]\,, \tag{3.3.19}$$

where we substituted expression (3.3.9).

It can be shown that the series is uniformly convergent for $0 < q < 1$, so we can switch sum and integral positions. Eventually, we get

$$Q = \sum_{n=0}^{\infty} \frac{8}{2n+1}\frac{q^{n+\frac{1}{2}}}{1+q^{2n+1}}\sin[(2n+1)(\gamma+\psi)]\,, \tag{3.3.20}$$

where the constant term has been neglected.

Since we will average the system near the resonance, we keep only the $n = 0$ term of the sum, for both Q and P. The resulting expressions read:

$$Q_{\mathsf{r}} = 8\frac{q^{\frac{1}{2}}}{1+q}\sin(\gamma+\psi)\,, \tag{3.3.21}$$

$$P_{\mathsf{r}} = \frac{4\pi A}{K(\kappa)}\frac{q^{\frac{1}{2}}}{1+q}\cos(\gamma+\psi)\,. \tag{3.3.22}$$

By substituting P_{r} in place of P in $\mathcal{H}_1$, we obtain the following:

$$\mathcal{H}_1(\gamma,\psi) = \frac{4\pi A a\omega_{\mathrm{m}}}{K(\kappa)\,\zeta}\frac{q^{\frac{1}{2}}}{1+q}\cos(\gamma+\psi)\cos\psi\,,$$

where we set $\psi_0 = 0$.

If we now rewrite the cosines product using trigonometric identities and then average over ψ, we obtain:

$$\mathcal{H}_1(\gamma) = \frac{2\pi A a\omega_{\mathrm{m}}}{K(\kappa)\zeta}\frac{q^{\frac{1}{2}}}{1+q}\cos\gamma\,. \tag{3.3.23}$$

Since the phase $\psi = \omega_{\mathrm{m}} t$ evolves much faster than the intrinsic motion of the unperturbed system ($\omega_{\mathrm{m}} \gg \Omega$), it can be treated as a fast variable. Therefore, the averaging method can be applied, replacing the Hamiltonian by its mean over a period of ψ, so that only the slow dynamics of the resonant variables (I,γ) is retained. The full Hamiltonian as a function of the action-angle coordinates reads:

$$\begin{aligned}\mathcal{H}(I,\gamma) &= \mathcal{H}(I,\gamma) - I\omega_{\mathrm{m}} = \\ &= \mathcal{H}_0(I) + \varepsilon G(I)\cos\gamma - I\omega_{\mathrm{m}}\,,\end{aligned} \tag{3.3.24}$$

where $\varepsilon = a\,\omega_{\mathrm{m}}$ and

$$G(I) = \frac{2\pi A}{K(\kappa)\,\zeta}\frac{q^{\frac{1}{2}}}{1+q}\,. \tag{3.3.25}$$

We now introduce the resonant action I_{res} defined by the resonance condition

$$\Omega(I_{\mathsf{res}}) \equiv \left.\frac{\partial\mathcal{H}_0}{\partial I}\right|_{I=I_{\mathsf{res}}} = \omega_{\mathrm{m}}\,. \tag{3.3.26}$$

If we now expand $\mathcal{H}_0(I) - I\omega_{\mathrm{m}}$ using the Taylor series about I_{res}, we get:

$$\mathcal{H}_0(I) - I\omega_m = \mathcal{H}_0(I_{\mathsf{res}}) - I_{\mathsf{res}}\omega_{\mathrm{m}} + \tfrac{1}{2}\,\alpha\,(I - I_{\mathsf{res}})^2 + \mathcal{O}\left((I-I_{\mathsf{res}})^3\right)\,, \tag{3.3.27}$$

where

$$\alpha \equiv \left.\frac{\mathrm{d}\Omega}{\mathrm{d}I}\right|_{I_{\mathrm{res}}} = \left.\frac{\mathrm{d}^2\mathcal{H}_0}{\mathrm{d}I^2}\right|_{I_{\mathrm{res}}} . \tag{3.3.28}$$

The averaged Hamiltonian then reads:

$$\mathcal{H} = \mathcal{H}_0(I_{\mathrm{res}}) + \frac{1}{2}\alpha(I - I_{\mathrm{res}})^2 + \varepsilon G(I_{\mathrm{res}})\cos\gamma - I_{\mathrm{res}}\omega_{\mathrm{m}} \tag{3.3.29}$$

Now, the coordinate transformation $(I, \gamma) \to (\mathcal{J}, \tilde{\gamma})$ can be performed, whose generating function $\mathcal{G}(I,\, \tilde{\gamma}) = (I - I_{\mathrm{res}})\,\tilde{\gamma}$ gives:

$$\mathcal{J} = \frac{\partial \mathcal{G}}{\partial \tilde{\gamma}}\,, \qquad \gamma = \frac{\partial \mathcal{G}}{\partial I} = \tilde{\gamma}\,, \qquad \tilde{\mathcal{H}} = \mathcal{H} + \frac{\partial \mathcal{G}}{\partial t} = \mathcal{H} - \dot{I}_{\mathrm{res}}\tilde{\gamma}\,. \tag{3.3.30}$$

Omitting tildes and setting $b = -\dot{I}_{\mathrm{res}}$, we get to the pendulum-like form with an external torque:

$$\mathcal{H}_{\mathrm{eff}}(\mathcal{J}, \gamma,\, t) = \frac{p^2}{2} + \varepsilon G(I_{\mathrm{res}})\cos\gamma + b\,\gamma\,. \tag{3.3.31}$$

where $p = \sqrt{\alpha}\,\mathcal{J}$.

We want now to find an expression to evaluate the area $\mathcal{A}$ of the resonant island, since the probability of trapping a particle that crosses the separatrix is a function of $\mathcal{A}$ itself. Taking into account only pendulum terms, the area within the separatrix (Ref. [8]) in the (p, γ) plane is:

$$\mathcal{A}_{p\gamma}(t) = 16\sqrt{\varepsilon G(I_{\mathrm{res}})}\,. \tag{3.3.32}$$

Thus, in the $(\mathcal{J}, \gamma)$ variables the area is

$$S(t) = \int_{\mathrm{sep}} \mathrm{d}\mathcal{J}\,\mathrm{d}\gamma = \frac{1}{\sqrt{\alpha}}\,\mathcal{A}_{p\gamma}(t) = 16\,\sqrt{\frac{\varepsilon G(I_{\mathrm{res}})}{\alpha}}\,. \tag{3.3.33}$$

Lastly, we have to find an explicit expression for α. Since $\alpha = \left.\frac{\mathrm{d}\Omega}{\mathrm{d}I}\right|_{I_{\mathrm{res}}}$, we can write

$$\left.\frac{\mathrm{d}\Omega}{\mathrm{d}I}\right|_{I_{\mathrm{res}}} = \frac{\mathrm{d}\Omega/\mathrm{d}\kappa}{\mathrm{d}I/\mathrm{d}\kappa} = \frac{-\dfrac{\pi}{2}A\,\dfrac{K'(\kappa)}{[K(\kappa)]^2}}{\dfrac{8A}{\pi}(E'(\kappa) + 2\kappa K(\kappa) - (1-\kappa^2)K'(\kappa))}\,. \tag{3.3.34}$$

Using the definitions (3.3.4) and (3.3.9) and formulas for derivatives of elliptic integrals (Ref. [5]), we get to the explicit form:

$$\alpha = -\frac{\pi^2}{16\,\kappa^2(1-\kappa^2)}\,\frac{E(\kappa)-(1-\kappa^2)K(\kappa)}{[K(\kappa)]^3}\Big|_{I=I_{\text{res}}}. \tag{3.3.35}$$

We can now move on to find the expression for trapping probability inside the resonant island. By differentiating the area $S(t)$ within the separatrix, we get:

$$\dot{S}(t) = \frac{8}{\sqrt{\alpha}}\left[\sqrt{\frac{G}{\varepsilon}}\,\dot{\varepsilon} + \sqrt{\frac{\varepsilon}{G}}\,\dot{G}\right]. \tag{3.3.36}$$

In the same way, we differentiate the resonance condition $\Omega(I_{\text{res}}(t)) = \omega_{\text{m}}(t)$, which gives

$$\alpha\,\dot{I}_{\text{res}}(t) \;=\; \dot{\omega}_m(t) \quad\rightarrow\quad b \;=\; -\,\frac{\dot{\omega}_m(t)}{\alpha}\,. \tag{3.3.37}$$

Finally, the general expression for the capture probability (Ref. [27]) reads:

$$\Pr(t_*) \;=\; \frac{\dot{S}(t_*)}{2\pi\,|b(t_*)|}\,, \tag{3.3.38}$$

where t_* denotes the moment of separation crossing. Substituting $\dot{S}$ and b yields

$$\Pr(t_*) = \frac{4\sqrt{|\alpha|}}{\pi\,|\dot{\omega}_{\text{m}}|}\left[\sqrt{\frac{G}{\varepsilon}}\,\dot{\varepsilon} + \sqrt{\frac{\varepsilon}{G}}\,\dot{G}\right]. \tag{3.3.39}$$

where all quantities should be calculated at $t = t_*$.

Using $\varepsilon = a(t)\,\omega_{\text{m}}(t)$ and the product rule, one finds the full time derivatives

$$\dot{\varepsilon} = \dot{a}\omega_{\text{m}} + a\dot{\omega}_{\text{m}} \qquad \dot{G} = G'(I_{\text{res}})\,\dot{I}_{\text{res}}\,, \tag{3.3.40}$$

with $\dot{I}_{\text{res}} = \dot{\omega}_{\text{m}}/\alpha$, and if the slow variation of $G(I_{\text{res}}(t))$ can be neglected, the expression simplifies to

$$\Pr(t_*) = \frac{4\sqrt{|\alpha|}}{\pi\,|\dot{\omega}_{\text{m}}|}\,\dot{\varepsilon}\,\sqrt{\frac{G}{\varepsilon}}\,. \tag{3.3.41}$$

The formula (3.3.41) then represents the probability that the single particle that encounters the separatrix at time t_* is trapped on the resonance island. For a distribution, since

each particle crosses the separatrix at a different time t_*, we have to average the probabilities over the total number of particles considered. The total trapping probability is obtained as:

$$\mathrm{Pr}_{\mathrm{tot}} = \frac{1}{N} \sum_{i=0}^{N} \mathrm{Pr}_i(t_*) \tag{3.3.42}$$

Chapter 4

Numerical simulations and results

In this chapter, we present the numerical results obtained from the simulations of the model introduced in the previous sections. All computations have been performed in `Python`.

Following the same logical structure of the entire thesis, the first part of the chapter is dedicated to the Hamiltonian model. Here we consider the equations of motion including only the conservative terms and the RF phase modulation. The results in this section constitute the reference framework against which the stochastic simulations are compared.

In the second part, we turn to the full stochastic model, where the equations of motion include both linear damping and noise. The purpose of this analysis is to determine how the additional stochastic terms modify the Hamiltonian structure and to quantify their effect on the stability of the resonance island and on the efficiency of trapping the escape rates. By comparing the stochastic simulations with the Hamiltonian results, we identify the regimes in which damping and noise provide negligible corrections, as well as those where their influence becomes significant.

To compare results in different, but realistic working conditions, all the simulations were conducted using the machine parameters of the two lepton accelerators presented in the introduction, i.e. ALS and FCC-ee, the latter considered in its first proposed optical configuration (Z optics). The model considered is inspired by that proposed in Ref. [10].

Before delving into the simulations, let us show the accelerator parameters considered in Table 4.1 (data from [21], [18], [9]). For completeness, the table contains the machine parameters for all four configurations of the FCC-*ee*, although the numerical simulations are performed using the data related to the Z configuration.

Table 4.1: Machine parameters for the ALS and the FCC-*ee* in the four designed optics.

Parameter	Unit	ALS	FCC-ee (Z)	FCC-ee (WW)	FCC-ee (ZH)	FCC-ee ($t\bar{t}$)
Beam energy E_s	GeV	1.5	45.6	80	120	182.5
RF voltage V_{rf}	GV	0.0015	0.09	1.0	2.1	2.1–9.2
Harmonic number h	–	328	130000	130000	130000	130000
Momentum compaction α_c	–	1.6e-3	14.8e-6	14.8e-6	7.3e-6	7.3e-6
Synchrotron tune ν_s	–	0.0075	0.025	0.0506	0.0358	0.0872
Revolution period T_{rev}	s	4.13e-6	303.03e-6	303.03e-6	303.03e-6	303.03e-6
Bending radius ρ	m	4.01	10760	10760	10760	10760
Energy lost per turn U_0	GeV	0.00011	0.039	0.369	1.86	9.94
Effective temperature T	s^{-1}	1.63e-1	2.83e-3	8.68e-3	9.66e-3	2.24e-2
Damping rate γ	s^{-1}	36.26	5.65	30.44	102.24	359.82

4.1 Algorithms

4.1.1 Symplectic integration

To investigate the long-term dynamics of the system described by Eqs. (3.2.20), separately for the pure Hamiltonian part and for the full stochastic model, we will make use of numerical integrators of the equations of motion. However, the choice of the suitable numerical method has to be carefully addressed.

Standard explicit integrators, such as the family of Runge–Kutta methods, while robust for general differential equations, often introduce numerical dissipation and fail to preserve the fundamental geometric structure of Hamiltonian phase space.

For this study, the most appropriate choice is represented by *symplectic integrators*, which preserve the symplectic 2-form of Hamiltonian systems in the (q, p) phase space, namely

$$\omega_2 = \mathrm{d}p \wedge \mathrm{d}q \,. \tag{4.1.1}$$

This property ensures that the numerical flow exactly conserves phase-space volume and, more importantly, retains the full geometric character of autonomous Hamiltonian systems. Hence, the discrete map produced at each time-step is itself a canonical transformation.

In our system, however, the Hamiltonian function contains a slow time-dependent phase modulation, which can be treated as a small perturbative term. In this regime, the symplectic structure is approximately conserved, and the evolution is stable in the long-term.

In the stochastic model, the flow is further modified by the presence of noise and damping, which explicitly break the symplecticity. Even in this case, the same symplec-

tic scheme for the deterministic Hamiltonian part is retained, and the stochastic and dissipative contributions are directly added to the equations of motion. Since these additional terms enter as small corrections as well, the numerical evolution preserves the conservative geometry at leading order, while the noise and damping act as perturbations superimposed on the underlying Hamiltonian structure.

Mathematical formulation

Consider a separable Hamiltonian of the form

$$\mathcal{H}(q,p,t) = T(p) + V(q) + U(q,t)\,, \tag{4.1.2}$$

where $U(q,t)$ represents the time-dependent modulation term. The evolution of any phase–space observable $f(q,p)$ is governed by the Lie operator

$$D_{\mathcal{H}} f = \{f, \mathcal{H}\}\,, \tag{4.1.3}$$

so that the exact Hamiltonian flow over a time step h is formally written as the exponential map

$$f(t+h) = e^{\,hD_{\mathcal{H}}} f(t)\,. \tag{4.1.4}$$

For a separable Hamiltonian with time-dependent perturbation, the Lie operator is split into

$$D_{\mathcal{H}} = D_T + D_V + D_U\,, \tag{4.1.5}$$

where each term is the Lie operator applied to the correspondent contribution in Eq. (4.1.2). We can then identify three separated exponential maps, respectively, associated to the kinetic, potential, and modulation terms as:

$$\begin{aligned} e^{hD_T} &: \ (q,p) \mapsto (q + h\,\frac{\partial T(p)}{\partial p},\ p) \\ e^{hD_V} &: \ (q,p) \mapsto (q,\ p - h\,\frac{\partial V(q)}{\partial q}) \\ e^{hD_U} &: \ (q,p) \mapsto (q,\ p - h\,\frac{\partial U(q,t)}{\partial q})\,. \end{aligned} \tag{4.1.6}$$

A second-order symplectic integrator is obtained using the Strang composition

$$e^{hD_{\mathcal{H}}} = e^{\frac{h}{2}D_T}\, e^{\frac{h}{2}D_U}\, e^{hD_V}\, e^{\frac{h}{2}D_U}\, e^{\frac{h}{2}D_T} + \mathcal{O}(h^3)\,. \tag{4.1.7}$$

Each exponential map in (4.1.7) is an exact canonical transformation, and therefore their composition is also canonical. This implies that the discrete-time flow preserves the symplectic 2-form of Eq. (4.1.1), and hence the phase-space volume.

In terms of numerical simulation, this is equivalent to updating the canonical coordinates accordingly to the equations of motion.

If we recover Eqs. (3.2.20) and temporarily neglect the damping and noise terms, by integrating with respect to time we obtain:

$$\phi(t) = \phi(t_0) + h\eta_{\mathrm{s}}\omega_{\mathrm{rev}} \int_{t_0}^{t} \delta(t')\,\mathrm{d}t' + a \int_{t_0}^{t} \cos(\omega_m t' + \psi_0)\,\mathrm{d}t'\,, \tag{4.1.8}$$

$$\delta(t) = \delta(t_0) + \frac{\omega_{\mathrm{rev}} e V_{\mathrm{s}}}{2\pi E_{\mathrm{s}} \beta_{\mathrm{s}}^2} \int_{t_0}^{t} \sin\phi(t')\,\mathrm{d}t'\,. \tag{4.1.9}$$

The logic of symplectic integrators is to evaluate the canonical variables at different times. For a second-order symplectic integrator, ϕ is evaluated at half-integer steps $(t + \Delta t/2)$ and δ at integer steps $(t + \Delta t)$.

Therefore, the overall integration scheme from step n to step $n+1$ is the following:

$$\phi_{n+1/2} = \phi_n + \left(h\eta_{\mathrm{s}}\omega_{\mathrm{rev}}\delta_n + a\,\omega_{\mathrm{m}}\cos(\omega_{\mathrm{m}}t + \psi_0)\right)\frac{\Delta t}{2}\,, \tag{4.1.10}$$

$$\delta_{n+1} = \delta_n + \frac{\omega_{\mathrm{rev}} e V_{\mathrm{s}}}{2\pi E_{\mathrm{s}} \beta_{\mathrm{s}}^2} \sin\big(\phi_{n+1/2}\big)\Delta t\,, \tag{4.1.11}$$

$$\phi_{n+1} = \phi_{n+1/2} + \left(h\eta_{\mathrm{s}}\omega_{\mathrm{rev}}\delta_n + a\,\omega_{\mathrm{m}}\cos(\omega_{\mathrm{m}}t + \psi_0)\right)\frac{\Delta t}{2} \tag{4.1.12}$$

Stochastic case

In the full stochastic model, Eq. (3.2.20) contains a damping force and a stochastic momentum kick generated by Gaussian white noise. We can model the equation for $\dot{\delta}$ as

$$\dot{q} = f(q,p) + s(q)\,\xi(t)\,, \tag{4.1.13}$$

where the damping term is included in the deterministic function $f(q,p)$ and $\xi(t)$ is a white noise in the Stratonovich interpretation. The evolution over a step Δt is then approximated as

$$q(t+\Delta t) = \exp\big(\sqrt{\Delta t}\;\xi_n\,D_s\big)\;\exp\big(\Delta t\,D_f\big)\,q(t) + O(\Delta t^{3/2})\,, \tag{4.1.14}$$

where the weight $\sqrt{\Delta t}$ corresponds to the request that the variance of the stochastic fluctuations be $\propto \Delta t^{-1}$ in the continuous limit. We now obtain the relation:

$$\begin{aligned} q(t+\Delta t) - q(t) &= \int_t^{t+\Delta t} \left[f(q(t'), p(t')) + s(q(t'))\, \xi(t') \right] \, \mathrm{d}t' \\ &\simeq f(q,p)\, \Delta t + s(q(t+\Delta t/2)) \int_t^{t+\Delta t} \xi(t')\, \mathrm{d}t' + \mathcal{O}(\Delta t^{3/2}) \,, \end{aligned} \tag{4.1.15}$$

where the second term has been evaluated at half the time-step value following the Stratonovich interpretation. The following Taylor expansion can be performed:

$$s(q(t+\Delta t/2)) \simeq s(q(t)) + \frac{\partial s}{\partial q} \left(q(t+\Delta t/2) - q(t) \right) , \tag{4.1.16}$$

where

$$q(t+\Delta t/2) - q(t) = \int_t^{t+\Delta t/2} \left[f(q(t'), p(t')) + s(q(t'))\, \xi(t') \right] \mathrm{d}t' \,. \tag{4.1.17}$$

Since the deterministic term is $\mathcal{O}(\Delta t)$ while the stochastic term is $\mathcal{O}(\sqrt{\Delta t})$, we can neglect the contribution by $f(q,p)$ and write:

$$q(t+\Delta t/2) - q(t) \simeq \int_t^{t+\Delta t/2} s(q(t'))\, \xi(t')\, \mathrm{d}t' \;\simeq\; s(q(t)) \int_t^{t+\Delta t/2} \xi(t')\, \mathrm{d}t' \,, \tag{4.1.18}$$

and substituting this into the Taylor expansion of $s(q(t+\Delta t/2))$, we obtain the following

$$s(q(t+\Delta t/2)) \simeq s(q(t)) + \frac{\partial s}{\partial q}\, s(q(t)) \int_t^{t+\Delta t/2} \xi(t') \mathrm{d}t' + \mathcal{O}(\Delta t) \,. \tag{4.1.19}$$

Using this approximation of the stochastic coefficient in the second term of Eq. (4.1.15) yields:

$$\begin{aligned} & s(q(t+\Delta t/2)) \int_t^{t+\Delta t} \xi(t')\, \mathrm{d}t' \simeq \\ & \simeq \left[s(q(t)) + s(q(t)) \frac{\partial s}{\partial q} \int_t^{t+\Delta t/2} \xi(t') \mathrm{d}t' \right] \int_t^{t+\Delta t} \xi(t'')\, \mathrm{d}t'' + \mathcal{O}(\Delta t^{3/2}) \,. \end{aligned} \tag{4.1.20}$$

Performing the multiplication yields the linear stochastic term and the quadratic term. By mapping the stochastic integrals to the discrete variable ξ_n such that $\int_t^{t+\Delta t} \xi(t')\, \mathrm{d}t' \equiv$

$\sqrt{\Delta t}\,\xi_n$ (where $\mathbb{E}[\xi_n^2] = 1$), and utilising the Stratonovich property that the product of integrals $\left(\int_t^{t+\Delta t/2} \xi(t')\mathrm{d}t'\right)\left(\int_t^{t+\Delta t} \xi(t'')\,\mathrm{d}t''\right)$ contributes $\frac{\Delta t}{2}$ to the deterministic part, the full stochastic term expansion becomes:

$$\begin{aligned} & s(q(t+\Delta t/2)) \int_t^{t+\Delta t} \xi(t')\,\mathrm{d}t' \simeq \\ & \simeq s(q(t))\sqrt{\Delta t}\,\xi_n + \frac{\Delta t}{2} s(q(t)) \frac{\partial s}{\partial q} + \mathcal{O}(\Delta t^{3/2})\,. \end{aligned} \tag{4.1.21}$$

Substituting this result along with the deterministic term $f(q,p)$ into the total increment (Eq. (4.1.15)), we obtain:

$$\begin{aligned} & q(t+\Delta t) - q(t) \simeq \\ & \simeq f(q,p)\,\Delta t + s(q(t))\sqrt{\Delta t}\,\xi_n + \frac{\Delta t}{2} s(q(t)) \frac{\partial s}{\partial q} + \mathcal{O}(\Delta t^{3/2})\,, \end{aligned} \tag{4.1.22}$$

and this expansion matches the result obtained in the scheme of Eq. (4.1.14)), where the term with $\Delta t/2$ is absorbed into the stochastic exponential and where ξ_n^2 has been replaced by its expected value of 1. This equivalence confirms the validity of the chosen Lie splitting integrator for the Stratonovich stochastic differential equation. This geometric approach ensures that the numerical scheme preserves the intrinsic structure of the underlying Hamiltonian dynamics, including the dissipation and fluctuation effects, thus providing a second-order convergence in the strong sense for the deterministic part and the correct scaling for the noise.

Eventually, in the simulation, the final equation for the particle energy deviation δ (using $q = \delta$ and $t = n\Delta t$) is implemented as

$$\begin{aligned} \delta_{n+1} = \delta_n + \omega_\mathrm{s}\sqrt{\frac{eV}{2\pi E_\mathrm{s}\beta_\mathrm{s}^2\eta_\mathrm{s}}}\,\sin\!\big(\phi_{n+1/2}\big)\,\Delta t - 2\frac{\alpha_E}{\beta_\mathrm{s}^2}\,\delta_n\,\Delta t + \\ + \frac{\gamma_\mathrm{s}}{\beta_\mathrm{s}^3}\sqrt{\frac{\alpha_E C_q}{\rho}}\,\sqrt{\Delta t}\,\xi_n\,, \end{aligned} \tag{4.1.23}$$

where $\xi_n \sim \mathcal{N}(0,1)$.

4.1.2 Detail of the numerical simulations

In order to present the mechanism of the numerical simulations, let us first introduce the parameters of the model, shown in Table 4.2.

In the table, the value of the total integration time, which is a function of $\Delta\omega_\mathrm{m} = \omega_{\mathrm{m,\,f}} - \omega_{\mathrm{m,\,i}}$ through the adiabatic parameter and the number of steps (see Sect. 4.1.2),

Table 4.2: Model parameters for the case of the ALS and the FCC-*ee* (Z).

Parameter	Unit	ALS	FCC-ee (Z)
Particles N	-	10'000	10'000
Adiabatic parameter μ	-	0.005	0.005
Final modulation frequency $\nu_{\mathrm{m,f}}$	-	0.83	0.83
Total integration time T_{tot}	s	29.22	29.21
Time interval $\mathrm{d}t$	s	4.5e-6	1.2e-4

is chosen for a value of $\omega_{\mathrm{m,i}}$ such that it corresponds to an intermediate value of the trapping probability. In the following, we will refer to the modulation frequency both as ν_{m} and $\omega_{\mathrm{m}} = \nu_{\mathrm{m}}\,\omega_{\mathrm{s}}$. When dealing with the actual values, to better understand the relationship of the modulation frequency as a fraction of the synchrotron frequency ω_{s}, the variable ν_{m} is preferred.

In the numerical simulations, a stroboscopic map is used to save the particle trajectories. Indeed, it is convenient to synchronise the system with the modulation period, to avoid the combined effect of the modulation frequency and the natural frequency ω_{s}. In this way, we study the system in the rotating frame of reference, which is the only way through which the island structure is visible.

Regarding the choice of model parameters, the time interval and the total integration time are obtained as follows. Taking into account the period of the synchrotron oscillations as $T_{\mathrm{s}} = 2\pi/\omega_{\mathrm{s}}$, we define the time-step $\mathrm{d}t$ to be a certain fraction of T_{s}. To obtain a high temporal resolution and be conservative enough for the symplectic integrator to work properly, we choose $M = 100$ and define $\mathrm{d}t = T_{\mathrm{s}}/M$. Now, setting $T_{\mathrm{mod}} = 2\pi/\omega_{\mathrm{m,f}}$, we find the number of steps within a modulation period as $N_{\mathrm{mod}} = T_{\mathrm{mod}}/\mathrm{d}t$. Then, we choose a sufficient number of total Poincaré sections that we want to obtain as N_{sec}, and determine the total number of integration steps performed by the integrator as $N_{\mathrm{steps}} = N_{\mathrm{mod}} \cdot N_{\mathrm{sec}}$. In particular, the quantity N_{sec} is chosen according to the value of the adiabatic parameter μ, to perform the simulations under adiabatic conditions. The formula used to find N_{sec} as a function of μ follows directly from the previous definitions:

$$N_{\mathrm{sec}} = \frac{|\omega_{m,f} - \omega_{m,i}| \cdot M}{2\pi \cdot \mu \cdot N_{\mathrm{mod}}} \tag{4.1.24}$$

where the result has to be rounded up to the closest integer. The total integration time T_{tot} is then found as $T_{\mathrm{tot}} = N_{\mathrm{steps}} \cdot \mathrm{d}t$.

The initial frequency $\nu_{\mathrm{m,i}}$, which is not specified in the table above, is varied within a different range of values for ALS and FCC-ee, corresponding to the intervals for which there is a probability of trapping different from 0 and 1. The amplitude of the external modulation is determined by $\varepsilon = a\,\omega_{\mathrm{m}}$. The sweep is thought to provide a varying

amplitude and constant frequency in the first 10% of the steps (ω_{m} is constant while a varies). This generates a slow variation of the position of the fixed point at the origin of the phase space; then, in the remaining 90% steps, the modulation strength still increases while the frequency ω_{m} varies from $\omega_{\mathrm{m,\,i}}$ to $\omega_{\mathrm{m,\,f}}$. A graphical representation of this sweep is shown in Fig. 4.1 using ν_{m} instead of ω_{m} for clarity.

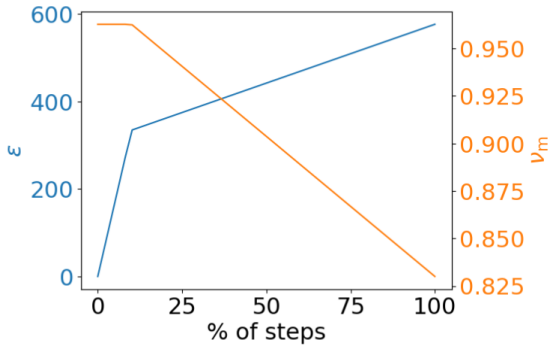

Figure 4.1: Evolution of the modulation parameters with respect to the percentage of steps of the symplectic integrator, for a representative value $\nu_{\mathrm{m,\,i}} = 0.961$ for the ALS.

4.1.3 Average phase-advance

The *tune* is defined as the 1-turn phase advance, namely the number of synchrotron oscillations performed by a particle in one revolution of the reference frame. In the longitudinal case, the motion around the stable fixed point is harmonic with synchrotron angular frequency ω_{s} and

$$\nu_{\mathrm{s}} = \frac{\omega_{\mathrm{s}}}{2\pi} \,. \tag{4.1.25}$$

To extract ν_{s} from numerical trajectories, one can track the phase variable associated with the synchrotron oscillation, namely, the canonical coordinate ϕ. By computing the average of the phase advance of a particle at each evolution step:

$$\langle \Delta\phi \rangle_N = \frac{1}{N} \sum_{n=0}^{N} (\phi_n - \phi_{n-1}) \,, \tag{4.1.26}$$

where N is the number of points of the particle trajectory, one obtains the particle *primary tune*. In addition, if we consider the stroboscopic map of the trajectory, i.e. if we use Poincaré sections to track the particle at each external modulation period T_{mod}, we find the *secondary tune*. This represents the motion of the particles in the rotating frame.

4.2 Results for the Hamiltonian model

4.2.1 Phase spaces

In the following, the Cartesian representation given by Eqs. (3.3.10) will be adopted.

To investigate the evolution of the system in the range of frequencies considered, Figs. 4.2 and 4.3 contain the phase-space evolution at fixed modulation frequency ω_{m} and varying amplitude $\varepsilon = a\,\omega_{\mathrm{m}}$ (first row, corresponding to the first 10% of the modulation sweep), and the evolution for a varying frequency (second row, remaining 90%):

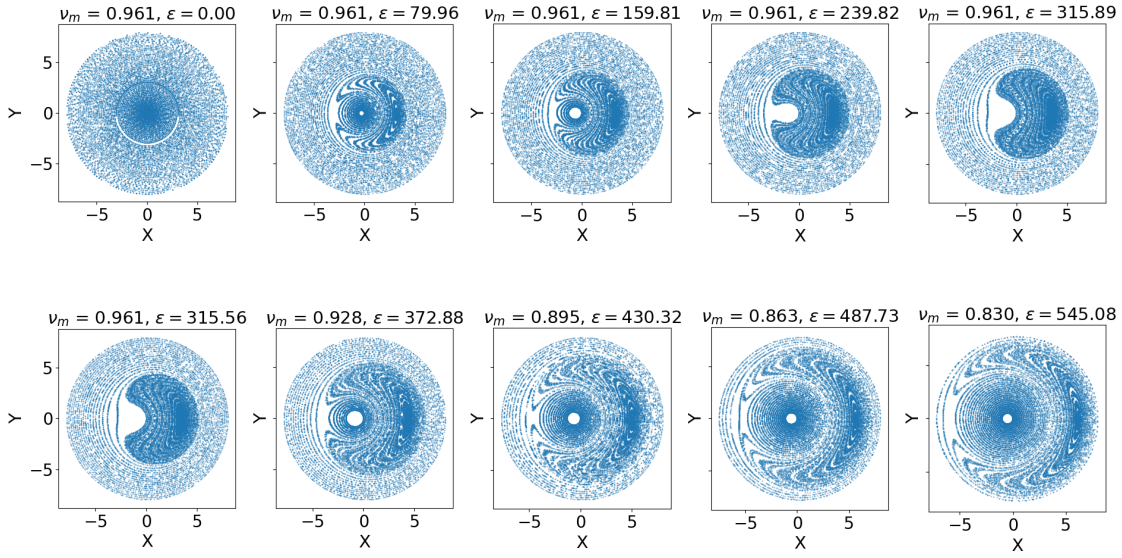

Figure 4.2: Related to the ALS. *Top row*: phase-space portrait for fixed frequency ω_{m} and varying amplitude. *Bottom row*: phase-space portrait for varying frequency ω_{m}.

The primary tune associated with each particle can be computed, which represents a useful quantity to identify the particle trajectories. In particular, the tune for trapped particles turns out to be equal to the frequency of the external modulation. This gives a tool to classify particles that end up in the resonance island, that is, indeed, how trapped particles are counted in the later simulations. The alignment between the primary tunes of the particles ν and the modulation frequency ν_{m} is known as *a tune lock*. The plots in Fig. 4.4 show the phase space at the final frequency $\nu_{\mathrm{m}} = 0.83$ for each accelerator, where each trajectory is coloured based on its associated tune. This becomes more clear by plotting the tune values versus the initial action of each particle, as in Fig. 4.5, which highlight the tune-locking phenomenon.

We can clearly see how the trajectories that make up the resonance island share the same tune, which is equivalent to the modulation frequency $\nu_{\mathrm{m}} = 0.83$.

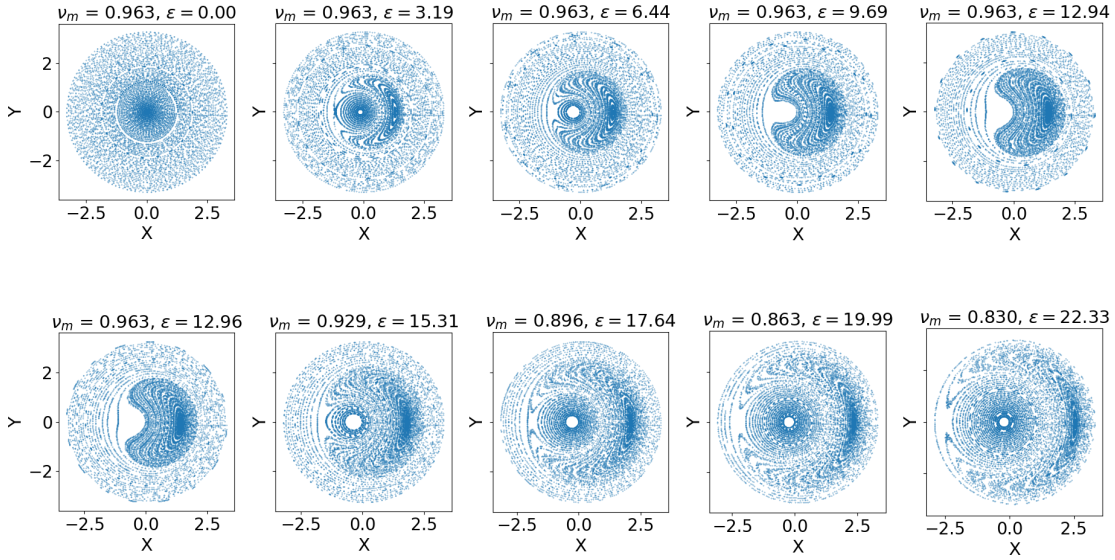

Figure 4.3: Related to the FCC. *Top row*: phase-space portrait for fixed frequency ω_{m} and varying amplitude. *Bottom row*: phase-space portrait for varying frequency ω_{m}.

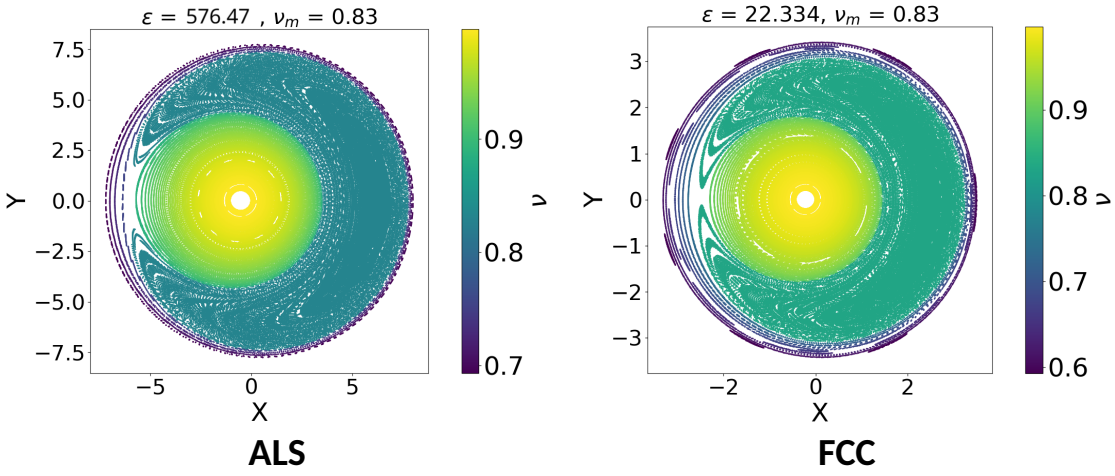

Figure 4.4: Phase-spaces at the final value of ν_{m} coloured by particles' tune for the ALS and the FCC-*ee*.

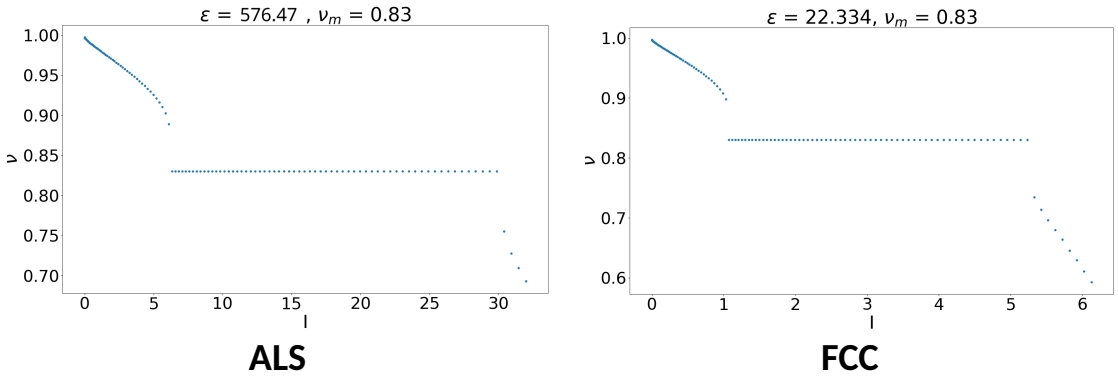

Figure 4.5: Tune lock at final ν_{m} for the ALS and the FCC-*ee*. Particles trapped into the resonance island have $\nu = \nu_{\mathrm{m}}$.

4.2.2 Trajectories and adiabatic jump

Particles which are trapped in the resonance island display a peculiar trajectory in the phase-space, where the different regions can be distinguished. Fig. 4.6 represents the evolution of the orbit of such a kind of particle both for ALS and FCC-ee, together with the evolution of the action for the same particle. The sudden variation of the value of the action highlights the behaviour of the orbit: we can see that on the first steps of the trajectory, the particle starting in the vicinity of the origin creates spirals of constant amplitude before changing position drastically. This is the behaviour that we expect when the initial time interval of the modulation changes only the amplitude ϵ of the external exciter, while maintaining a fixed value of its frequency ω_{m}. Indeed, in this window, the fixed point in the centre is slowly pulled towards its intermediate position corresponding to 10% of the sweep, and the particle follows its displacement. Then, as soon as it encounters the separatrix, it gets trapped in the resonant island and stabilises on a new orbit. The action is here computed as $I = \mathcal{A}/2\pi = \frac{1}{2\pi}\oint Y \mathrm{d}X$, where $\mathcal{A}$ is the area within a closed trajectory, obtained by performing an evolution at each time-step t_i with $\varepsilon(t_i)$ and $\omega_{\mathrm{m}}(t_i)$ fixed.

4.3 Results for the stochastic model

As we saw before, Eq. (3.2.20) represents the equations of motion related to the Hamiltonian system of Eq. (3.2.21) extended to the stochastic case. The presence of the damping term and the stochastic noise introduces additional effects to the trapping process, which can be measured to see their influence on the Hamiltonian model of reference.

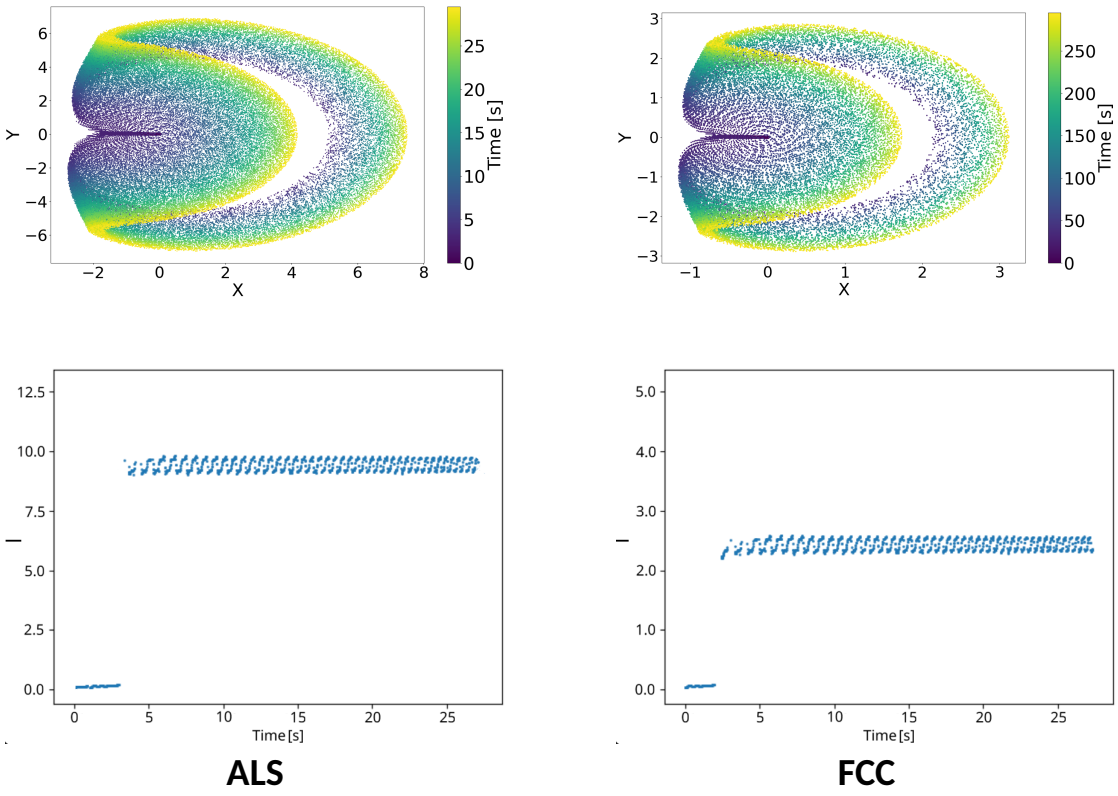

Figure 4.6: *Above*: evolution of the orbit of a trapped particle coloured by time-step (note that, for the FCC plot, the number of steps has been increased by a factor of 10 to get a higher number of points). *Below*: evolution of the action for the same particle; the sudden jump corresponds to the moment of separatrix crossing.

4.3.1 Relaxation

First, to validate the model and quantify the approach to an equilibrium condition, we investigate the relaxation of a distribution initially placed at the centre of phase space in the absence of the resonant island. When the modulation is switched off, the dynamics is governed by the damping and stochastic noise. Indeed, according to Sect. 2.5, the competition between dissipation and fluctuations drives the system towards equilibrium, represented by the Maxwell-Boltzmann distribution, which maximises the Gibbs entropy and satisfies the fluctuation-dissipation relation.

The relaxation time τ_{rel} extracted from the evolution of the action distribution can be directly compared with the modulation time T_{tot}. Indeed, if $\tau_{\text{rel}} \ll T_{\text{mod}}$, we can consider that the system reaches equilibrium in much less time than the time required for sweep. This allows one to assume that the system is always in equilibrium during modulation. To this end, Figs. 4.7 and 4.8 contain the histogram of the initial distribution and the final distribution of the action $\rho(I)$ using 100 bins, compared to the MB distribution ρ_{MB} for both the ALS and the FCC-*ee*. To measure the error between the two curves, we use the L2-norm normalised with respect to ρ_{MB}. The formula reads:

$$\|\rho(I) - \rho_{\text{MB}}\|_2 = \sqrt{\sum_{i=1}^{N} \left(\frac{\rho_i(I) - \rho_{\text{MB}}}{\rho_{\text{MB}}} \right)^2} \tag{4.3.1}$$

For the histogram of the actions, the centre of each bin is considered. The initial distribution is a Gaussian having an emittance that is 50% larger than the equilibrium emittance.

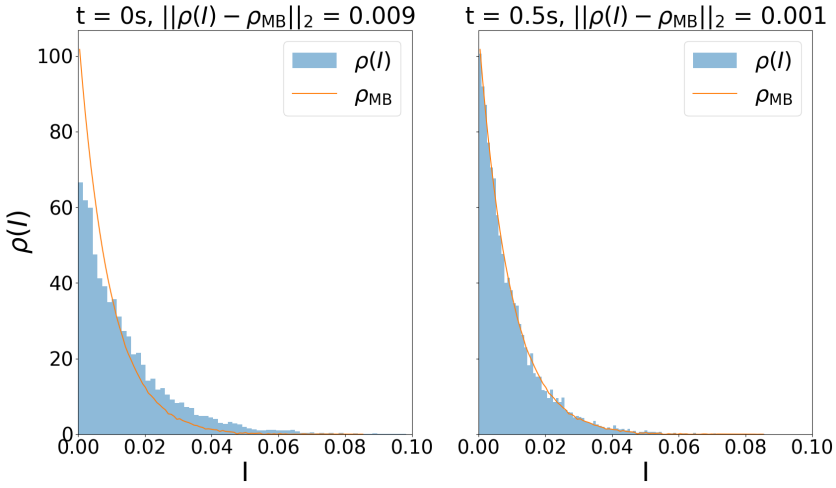

Figure 4.7: Comparison between the distribution of actions $\rho(I)$ and the MB distribution ρ_{MB} at the initial and final instant for the ALS.

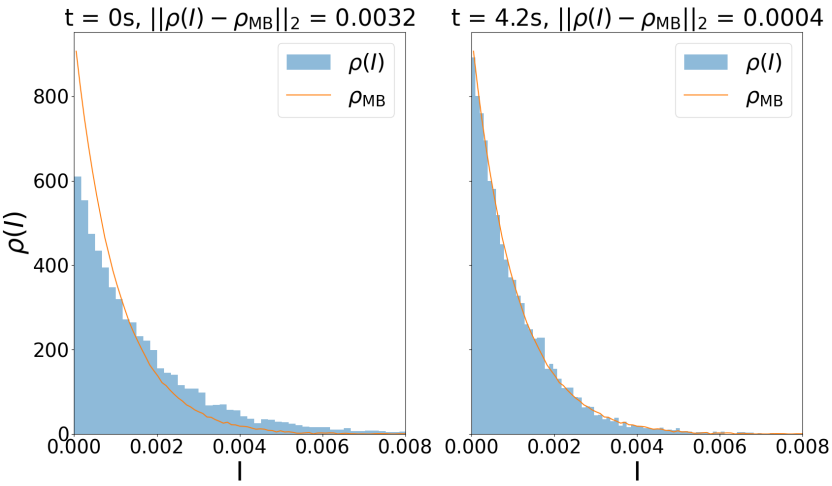

Figure 4.8: Comparison between the distribution of actions $\rho(I)$ and the MB distribution ρ_{MB} at the initial and final instant for the FCC-ee

To obtain the relaxation time, the L2-norm between the curves is computed at each step of the evolution. Then, since we expect the error to drop exponentially, we compute the slope m of the exponential in logarithmic scale, i.e. of the straight line obtained before the plateau region. The relaxation time is then given by $\tau_{\text{rel}} = -1/m$. The plot is in Fig. 4.9.

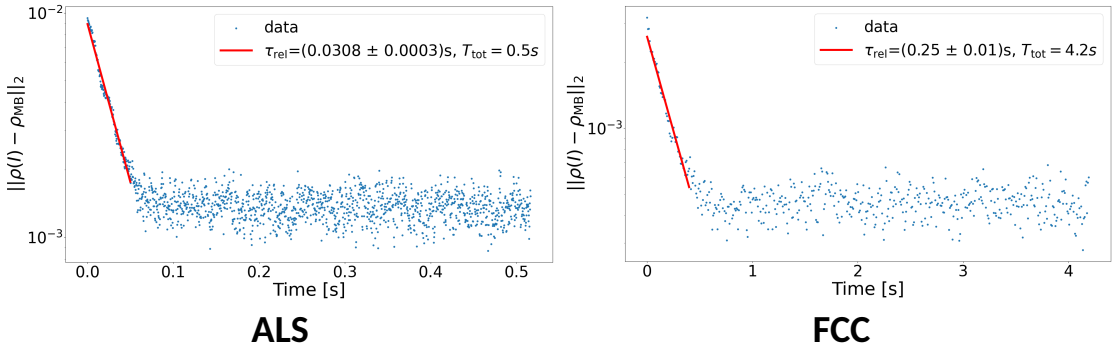

Figure 4.9: L2-norm vs. Time with the norm computed between $\rho(I)$ and ρ_{MB}. The linear part allows one to find the decay time, which is compared with the modulation time T_{mod}.

As can be seen in the legends, the condition $\tau_{\text{rel}} \ll T_{\text{mod}}$ holds and the system can then be considered relaxed during the sweep.

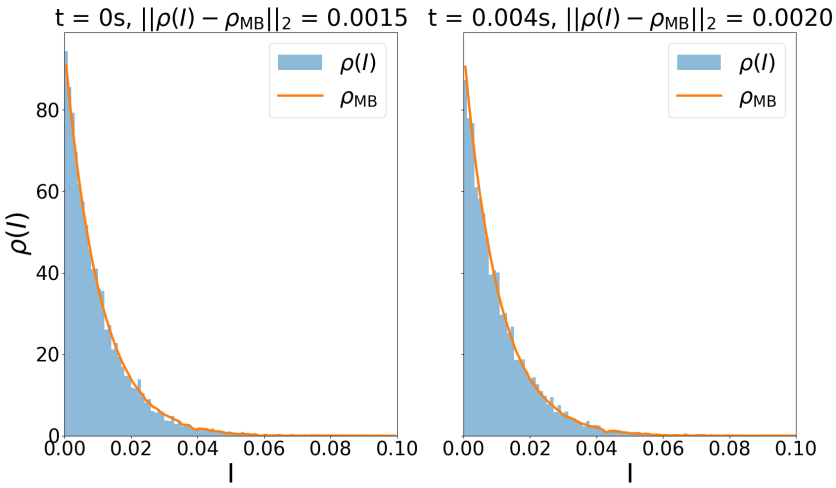

Figure 4.10: Comparison between the distribution of actions $\rho(I)$ and the MB distribution ρ_{MB} at the initial and final instant for the ALS, for an adiabatic modulation far from the resonance ($\nu_{\text{m}} = 0.5$).

4.3.2 Effect on adiabatic invariants

As we saw in Hamiltonian theory, the action I of a particle is an adiabatic invariant. The only exception is when a particle that encounters the separatrix gets trapped into the resonant island, where a sudden variation of the action occurs, but the new value on which the action stabilises remains constant again. In the stochastic case, because of the kicks imparted by the noise, it is clear that the action cannot be conserved in the same way. However, if the distribution of particles is relaxed in the MB distribution as soon as the adiabatic ramp begins, the interplay between damping and noise should cause the distribution of the action $\rho(I)$ to vary by a negligible amount during the modulation sweep. Thus, $\rho(I)$ is an adiabatic invariant in the first approximation. In order to verify this fact, we consider a distribution at the centre of the phase space that is relaxed at its equilibrium emittance, so $\rho(I) \simeq \rho_{\text{MB}}$. Then, we can start the sweep by keeping the modulation frequency far from the resonance at a constant value of $\nu_{\text{m}} = 0.5$ and let the amplitude ϵ evolve in the usual way. Then, we can compute the L2-norm between $\rho(I)$ and ρ_{MB} through Eq. (4.3.1) and compare it to the error at the starting point, to obtain the relative variation of the distribution of actions. Figures 4.10 and 4.11 display this comparison for both the ALS and the FCC-ee, where 100 bins are used.

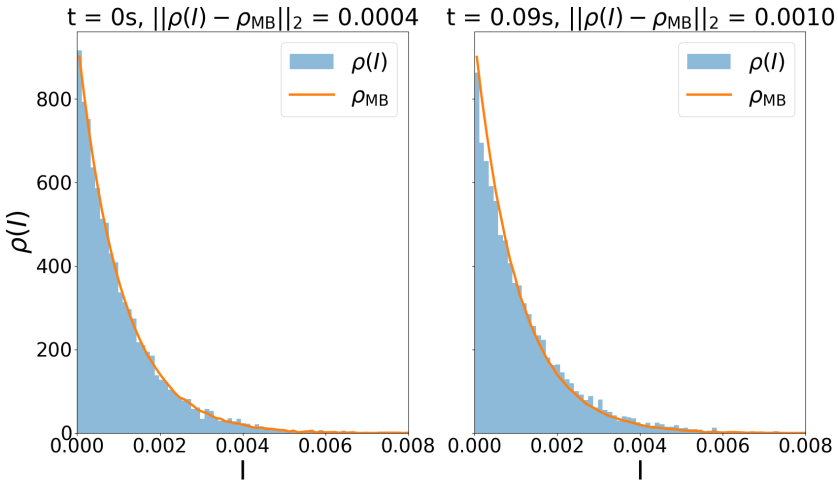

Figure 4.11: Comparison between the distribution of actions $\rho(I)$ and the MB distribution ρ_{MB} at the initial and final instant for the FCC-*ee*, for an adiabatic modulation far from the resonance ($\nu_{\text{m}} = 0.5$).

4.4 Trapping process

In Sect. 2.4, the theory of separatrix crossing in the presence of a slow modulation is presented, developing a general formulation for the trapping process of a general system composed of two inner regions and an external one. Then, in Sect. 3.3, we presented the theory of adiabatic trapping in a resonance, where we used the model under study to obtain a Hamiltonian formulation to evaluate the trapping probability. In particular, we have seen that the probability of trapping is related to the area of the resonance island through its time derivative, as shown in Eq. (3.3.38). In the second instance, we considered the case of a stochastically perturbed model, which is obtained by adding damping and random noise contribution to the equations of motion. We expect that these two contributions provide significant effects: the presence of a damping might hinder the trapping efficiency, since it pushes the particles towards the local fixed point; on the other hand, stochastic kicks might provide a sudden increase of the energy of the particles and make them jump across the separatrix earlier than in the Hamiltonian case. In order to visualise the evolution of the process with respect to time in the stochastic system, we can plot the position of particles and the phase-space portrait at time t_i for some i, which corresponds to a specific value of the modulation frequency ω_{m} and of its strength ε. In particular, the initial time instant is the one for which the frequency ω_{m} starts to vary, namely the first step after the initial ramp within 10% of the total. The last plot corresponds to the moment in which the system has stabilised and the number of particles in the different regions does not change any more. The

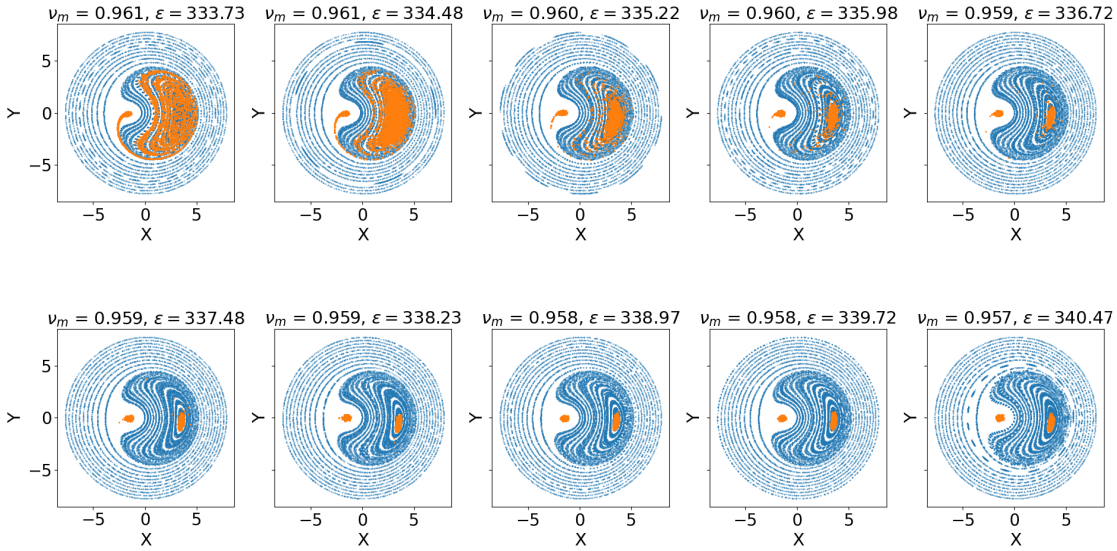

Figure 4.12: Evolution of the phase-space portrait and position of the particles for different time-steps for the ALS.

initial frequency $\omega_{\text{m,i}}$ is chosen in order to obtain an intermediate probability of trapping for the cases, namely $\nu_{\text{m,i}} = 0.961$ for the ALS and $\nu_{\text{m,i}} = 0.975$ for the FCC. The corresponding plots are shown in Figs. 4.12 and 4.13.

Some interesting behaviours are visible. First of all, we can see that the capture into the resonance island occurs in a very narrow range of times. Indeed, the entirety of the plots corresponds to instants of time which are understood between the 10% and the 12.5% of evolution in the case of ALS and between the 10% and 17% in the case of FCC. In addition, in the case of the ALS, we can see that the filling up of the island is almost instantaneous, since the first plot is the very first integration step after the frequency has started to change. Moreover, the positions of the particles in the second half of the plots is already well-established, which means that the whole transfer inside the resonant island occurs in even less time. In the case of the FCC, instead, the trapping keeps happening even when the island has moved by a non-negligible amount, and the relaxation on the island's basin of attraction is much slower. These results may be used as practical hints on how to perform the trapping, for example, by considering that after a while the modulation does not affect the position of particles any more, so the variation of the parameters can cease. However, the adiabaticity of the process must be taken into account anyway, since it might change the trapping efficiency considerably. As a follow up, within this context, an interesting study could be the analysis of the trapping efficiency as a function of the adiabatic parameter. In addition, it can also be interesting to investigate the properties of particles that foster their trapping, for example by studying the evolution of the distribution of actions $\rho(I)$ in the initial moments when

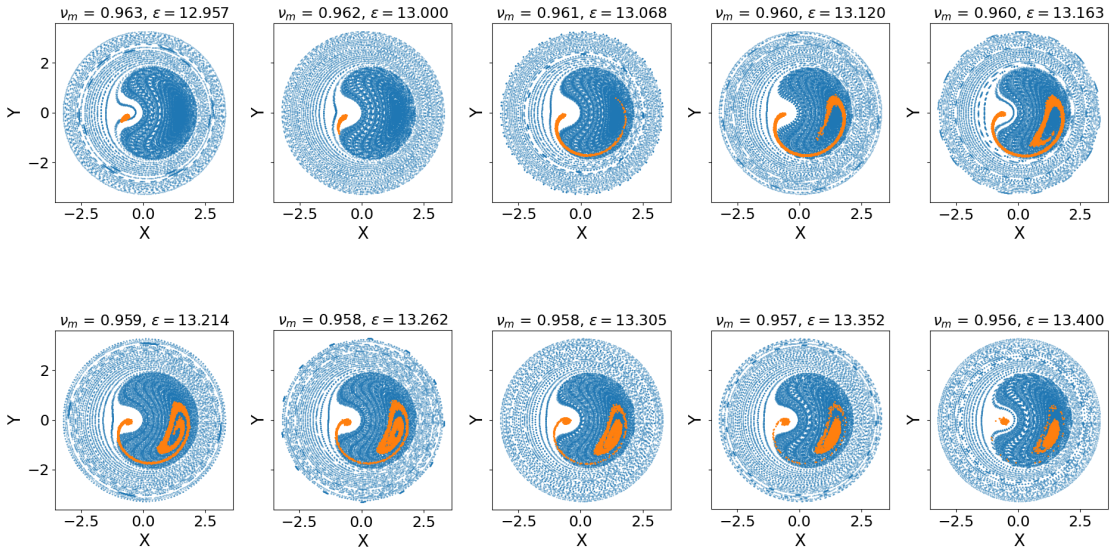

Figure 4.13: Evolution of the phase-space portrait and position of the particles for different time-steps for the FCC.

trapping occurs. We expect that the separatrix can catch a certain fraction of particles, in particular those whose action I is the largest up to a certain value. The possibility of trapping more or less particles would then be a consequence of the choice of the modulation parameters.

Following this last claim, as our final analysis, we measured the trapping probability as a function of the initial frequency $\omega_{\mathrm{m,\,i}}$, maintaining a fixed final frequency $\omega_{\mathrm{m,\,f}}$. Here, we considered the trapping probability both for the Hamiltonian and the stochastic case, in order to compare them and try to draw the leading mechanisms that guide the trapping process. The initial distribution is the equilibrium distribution of the stochastic case at the centre of the phase-space, namely the one for which $\rho(I) \simeq \rho_{\mathrm{MB}}$. These plots are those in Fig. 4.14, where we used ν_{m} instead of ω_{m} for clarity (recall that $\omega_{\mathrm{m}} = \nu_{\mathrm{m}}\omega_{\mathrm{s}}$).

We note that the behaviour for the two machines is significantly different. First of all, note that a higher value of $\nu_{\mathrm{m,\,i}}$ implies that the island starts closer to the centre, i.e. the starting distribution of particles is more in the nearby of the island. Keeping this claim in mind, we can notice that in the case of the ALS, the trapping for the Hamiltonian case starts before that in the stochastic case when the island is closer to the centre. This could be addressed to the different contributions of the damping and the noise, i.e. in the stochastic system the damping dominates over the fluctuations, therefore the particles are pulled towards the centre and get trapped later. In contrast, for the FCC, the trapping starts much earlier in the stochastic case: differently from before, the noise might provide a more significant contribution with respect to the damping. Thus,

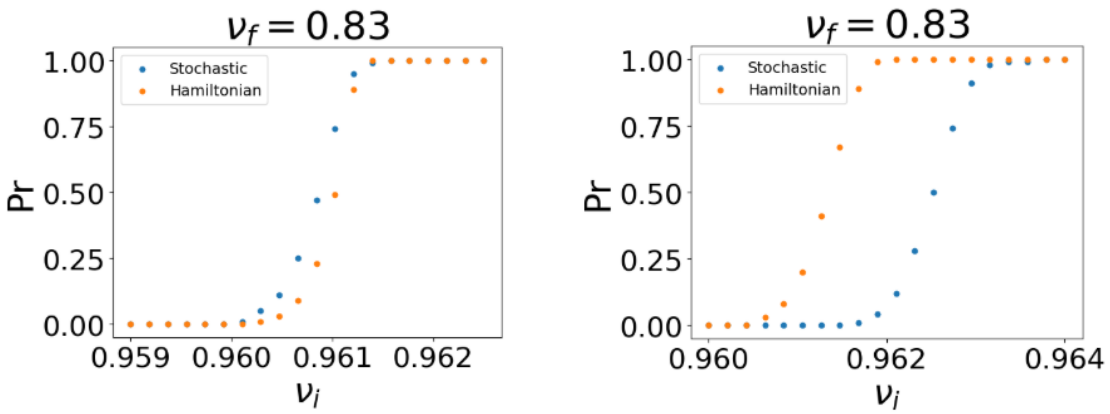

Figure 4.14: Comparison between the trapping probability in the Hamiltonian case and stochastic case. The probability is computed as the fraction of particles which are found in the island by the end of the integration process.

particles start earlier to become trapped because of the fluctuations.

Nevertheless, in order to compare the two cases in the same exact conditions, one should ensure that the distance between the two fixed points[1] (the one in the centre and the one in the island) are the same at the initial and at the final stages of the modulation. In this situation, one can compare the trapping efficiency as a consequence of the contributions of the different terms in the equations of motion, including damping and noise. That being said, further investigations for the comparison could move in this direction.

[1]Actually, in the presence of noise and damping, the term ”fixed point” is not the right one to use, since this concept belongs to Hamiltonian systems. In the stochastic case, they should be considered more as basins of attraction.

Conclusions and Outlook

In this thesis, we conducted a study of a simplified model developed to investigate longitudinal beam manipulation techniques in circular accelerators. The work followed a clear and logical progression that can be summarised as follows.

We began with an introduction to beam dynamics, outlining the main aspects of transverse motion and providing a more detailed analysis of longitudinal dynamics. In this framework, we derived the equations governing synchrotron motion and discussed their extensions in the presence of external modulation, radiation damping, and stochastic noise.

The second chapter presented the fundamental concepts of Dynamical Systems theory, with particular emphasis on Hamiltonian mechanics and stochastic dynamics. We examined the application of perturbation theory and discussed adiabatic theory in relation to separatrix crossing.

On these physical and mathematical basis, we introduced the model analysed throughout the thesis, considering both its Hamiltonian formulation and its stochastic extension.

Finally, through extensive `Python` simulations, we presented the main results obtained from the two models, focusing in particular on the mechanism of particle trapping induced by resonance phenomena.

Below, we summarise the main results of the thesis for both the Hamiltonian and stochastic descriptions.

- **Hamiltonian model:**
  - We analysed the phase-space structure in the presence of a 1:1 resonance and examined its evolution for representative values of the modulation parameters.
  - We studied the behaviour of particles trapped inside the resonant island, characterising their orbits, and the evolution of the corresponding action variables.
- **Stochastic model:**

  - We investigated the dynamics of particles under the combined effects of damping and noise, such as how they guide the distribution of particles towards an equilibrium condition.
  - We verified and quantified the preservation of adiabatic invariance for the action distribution in off–resonance conditions, extending the analogous behaviour observed in the Hamiltonian case at the level of single–particle action.
  - We analysed the key time intervals of particle trapping, providing insight that may guide future studies on the mechanisms underlying the trapping process.

- **Overall comparison:** We compared the trapping efficiency of the Hamiltonian and stochastic models, identified the origin of the differences between them, and outlined possible directions for further investigation.

Beyond the scientific results, the preparation of this thesis required a significant effort in gaining a deep understanding of the topics involved. Describing beam dynamics through the classical theory of Mechanics allowed us to exploit well-established results while engaging with more niche aspects, such as the adiabatic theory for Hamiltonian and stochastic systems. The implementation of these concepts in `Python` also involved several technical challenges, including the management of large amount of data and the optimisation of simulation performance.

As stated in the introduction, this work is intended not only as a theoretical analysis but also as a contribution to the optimisation of top–up injection for the FCC–*ee*. The considerable energy loss experienced by leptons during acceleration requires continuous particle injection to maintain stable luminosity conditions. Achieving this goal requires precise control of beam properties and finely tuned manipulation of phase-space. Within this context, the results and methodologies developed in the present thesis aim to contribute in this direction.

Acknowledgement

After a long and challenging journey, I am finally approaching the end. Throughout these years I have met incredible people, outstanding minds, and gained unique experiences. The most incredible of these has been spending three months at CERN to prepare this thesis. I chose to pursue Physics exclusively because of CERN, after my school trip in the fifth year of high school, and the only thought in my mind has been to come back, not as a visiting student, but to live the life of a researcher.

For this incredible opportunity, I must thank my professor and supervisor, Prof. Armando Bazzani, and my co-supervisor, Dr. Massimo Giovannozzi, who gave me the opportunity to realise this small dream. I also want to thank them for their patience and the immense knowledge they shared with me. I am also extremely grateful to Dr. Federico Capoani, with whom I spent most of the time. He is slightly older than me, but he has already proven himself to be an excellent mentor in addition to becoming a friend. I want to thank all the people I met at CERN, the Italians, the Spanish colleagues, the Argentinians, and others. They were crucial to making my time at CERN enjoyable and fun.

I also want to thank my family and friends, who I thanked the same two years ago. My amazing girlfriend Alice, my parents and brother, and my dog Leo, who are my number one fans. I also thank my grandma Raffaella, all my uncles and aunts, my cousins, and my friends from Gambettola. You have been and continue to be essential in my life, I hope nothing changes.

I would also like to remember my grandma Rosina and my grandpas Guido and Gino. I hope you can see me in all times, I made it.

And last but not least, I have to thank myself for never giving up.

Bibliography

[1] About the ALS. https://als.lbl.gov/about/about-the-als/.

[2] Advanced light source. https://en.wikipedia.org/wiki/Advanced_Light_Source.

[3] The pendulum - additional aspects. http://physique.unice.fr/sem6/2011-2012/PagesWeb/PT/Pendule/En/more3.html, 2012.

[4] Simple pendulum with phase space flow. https://www.physicswithelliot.com/simple-pendulum-with-phase-space, 2023.

[5] M. Abramowitz. *Handbook of Mathematical Functions, With Formulas, Graphs, and Mathematical Tables,*. Dover Publications, Inc., USA, 1974.

[6] M. Aiba, B. Goddard, K. Oide, Y. Papaphilippou, Á. Saá Hernández, D. Shwartz, S. White, and F. Zimmermann. Top-up injection schemes for future circular lepton collider. *Nuclear Instruments and Methods in Physics Research Section A: Accelerators, Spectrometers, Detectors and Associated Equipment*, 880:98–106, 2018.

[7] V.I. Arnol'd. Small denominators and problems of stability of motion in classical and celestial mechanics. *Russian Mathematical Surveys*, 18(6):85, dec 1963.

[8] V.I. Arnold. *Mathematical methods of classical mechanics*, volume 60. Springer, 1989.

[9] W. Bartmann, J. Burnet, C. Carli, A. Chance, P. Craievich, M. Giovannozzi, C. Grojean, J. Gutleber, K. Hanke, A. Henriques, P. Janot, C. Lourenco, M. Mangano, T. Otto, J. H. Poole, S. Rajagopalan, T. Raubenheimer, E. Todesco, T. P. Watson, and G. Wilkinson. Future circular collider feasibility study report volume 1: Physics and experiments, 2025.

[10] J. M. Byrd, W.-H. Cheng, and F. Zimmermann. Nonlinear effects of phase modulation in an electron storage ring. *Phys. Rev. E*, 57:4706–4712, Apr 1998.

[11] F. Capoani. *Shaping transverse beam distributions by means of adiabatic crossing of resonances*. PhD thesis, alma, Giugno 2022.

[12] R. Cappi and M. Giovannozzi. Novel method for multiturn extraction: Trapping charged particles in islands of phase space. *Phys. Rev. Lett.*, 88:104801, Feb 2002.

[13] European Southern Observatory (ESO). CERN Aerial View. `https://supernova.eso.org/exhibition/images/cern-aerial-cc/`, 2024.

[14] A. Franchi and M. Giovannozzi. Split or unsplit electron beams?, 2022.

[15] R Garoby. Bunch merging and splitting techniques in the injectors for high energy hadron colliders. 1998.

[16] P. Hänggi, P. Talkner, and M. Borkovec. Reaction-rate theory: fifty years after kramers. *Rev. Mod. Phys.*, 62:251–341, Apr 1990.

[17] J. Henrard. *The Adiabatic Invariant in Classical Mechanics*, pages 117–235. Springer Berlin Heidelberg, Berlin, Heidelberg, 1993.

[18] C. Kim, A. Jackson, and A. Warwick. Beam lifetime and beam brightness in als. In *Proceedings Particle Accelerator Conference*, volume 1, pages 198–200 vol.1, 1995.

[19] H.A. Kramers. Brownian motion in a field of force and the diffusion model of chemical reactions. *Physica*, 7(4):284–304, 1940.

[20] L. D. Landau and E. M. Lifšic. *1 : Meccanica / Lev D. Landau, Evgeneij M. Lifsits*. Editori riuniti Mir, Roma, 1976.

[21] S. Lee. *Accelerator Physics (Fourth Edition)*. World Scientific Publishing Company, 2018.

[22] D. Mitoli, M. Petrov, J. Maul, W. B. Stoll, M. T. Ruggiero, and A. Erba. Anharmonic vibrational states of double-well potentials in the solid state from dft calculations. *Journal of Chemical Theory and Computation*, 21(11):5365–5371, March 2025.

[23] C. E. Montanari. *Diffusive models and chaos indicators for non-linear betatron motion in circular hadron accelerators*. PhD thesis, alma, Giugno 2023.

[24] A. I. Neishtadt. Probability phenomena due to separatrix crossing. *Chaos: An Interdisciplinary Journal of Nonlinear Science*, 1(1):42–48, 07 1991.

[25] A. I. Neishtadt and A. A. Vasiliev. Change of the adiabatic invariant at a separatrix in a volume-preserving 3d system. *Nonlinearity*, 12(2):303, feb 1999.

[26] A. I. Neishtadt, A. A. Vasiliev, and A. V. Artemyev. Capture into resonance and escape from it in a forced nonlinear pendulum. *Regular and Chaotic Dynamics*, 18(6):686–696, November 2013.

[27] A.I. Neishtadt. Passage through a separatrix in a resonance problem with a slowly-varying parameter. *Journal of Applied Mathematics and Mechanics*, 39(4):594–605, 1975.

[28] J. T. Seeman. Injection issues of electron - positron storage rings. In *B Factories: the State of the Art in Accelerators, Detectors, and Physics*, 9 1992.

[29] U. Seifert. Stochastic thermodynamics: principles and perspectives. *Eur. Phys. J. B*, 64:423–431, 2008.

[30] U. Wienands. Lepton collider operation with constant currents. *Conf. Proc. C*, 0505161:149, 2005.

[31] Wikipedia contributors. Discovery of neptune — Wikipedia, the free encyclopedia. `https://en.wikipedia.org/wiki/Discovery_of_Neptune`, 2024.